1987

Interaction of long waves and nearshore barred topography--a mechanism of bar migration

Chang-Shik Kim
College of William and Mary - Virginia Institute of Marine Science

Order Number 8805970

Interaction of long waves and nearshore barred topography—a mechanism of bar migration

Kim, Chang Shik, Ph.D.

The College of William and Mary, 1987

U·M·I
300 N. Zeeb Rd.
Ann Arbor, MI 48106

PLEASE NOTE:

In all cases this material has been filmed in the best possible way from the available copy. Problems encountered with this document have been identified here with a check mark ✓.

1. Glossy photographs or pages _____
2. Colored illustrations, paper or print _____
3. Photographs with dark background _____
4. Illustrations are poor copy _____
5. Pages with black marks, not original copy ✓
6. Print shows through as there is text on both sides of page _____
7. Indistinct, broken or small print on several pages ✓
8. Print exceeds margin requirements _____
9. Tightly bound copy with print lost in spine _____
10. Computer printout pages with indistinct print _____
11. Page(s) _____ lacking when material received, and not available from school or author.
12. Page(s) _____ seem to be missing in numbering only as text follows.
13. Two pages numbered _____. Text follows.
14. Curling and wrinkled pages _____
15. Dissertation contains pages with print at a slant, filmed as received _____
16. Other Many Pages Contain Correction Fluid.

Best Copy Available. Photoed As Received.

University Microfilms International

INTERACTION OF LONG WAVES AND NEARSHORE BARRED TOPOGRAPHY

- A Mechanism of Bar Migration

A Dissertation

Presented to

The Faculty of the School of Marine Science

The College of William and Mary in Virginia

In Partial Fulfillment

Of the Requirements for the Degree of

Doctor of Philosophy

---

by

Chang Shik Kim

1987

APPROVAL SHEET

This dissertation is submitted in partial fulfillment of

Doctor of Philosophy

Chang Shik Kim

Approved, November 1987

L. Donelson Wright, Ph.D.
Committee Chairman/Advisor

John D. Boon, III, Ph.D.

Robert J. Diaz, Ph.D.

John M. Brubaker, Ph.D.

Anthony J. Bowen, Ph.D.
Dalhousie University
Halifax, Nova Scotia, Canada

TABLE OF CONTENTS

TABLE OF CONTENTS (cont.)

ACKNOWLEDGEMENTS

It would not have been possible for me to complete this dissertation without the support and guidance provided by my supervisor, Professor L. Don Wright. His warm humanism and scientific criticism throughout the course of this research have enabled me to publish many parts of this work.

I also would like to thank the rest of my thesis committee: Professor John D. Boon III, Drs. Robert J. Diaz and John M. Brubaker. A special pleasure to thank is due to Professor Anthony B. Bowen at Dalhousie University in Canada, who participated in my thesis defense as the external examiner. To all I gratefully acknowledge their constructive criticism, support and reviews of the manuscript.

I thank Ms. Cynthia Gaskins for her expert typing the mathematical notations.

Numerous friends have cheered me through my studies. Among them, Cheol Mo and Sung Kim who shared cheerful time in an Korean fashion, Jeff List for many scientific discussions on coastal processes, Mal Green through co-working research projects, and many more in the Reed Hall family, VIMS.

Special thanks are due to the Peninsula Korean Catholic Communities for their love, faith and friendship, especially to the Club members.

Finally, I thank my family who have supported, both morally and financially, and waited this day with patience.

This thesis is dedicated with love to my wife, Inja J. Kim, and to my daughter, Curie R. Kim, and my son, Cuejin J. Kim.

LIST OF TABLES

LIST OF FIGURES

LIST OF FIGURES (cont.)

Page

LIST OF FIGURES (cont.)

LIST OF FIGURES (cont.)

Page

LIST OF PRINCIPAL SYMBOLS

a	wave amplitude
a_n	shoreline amplitude of a mode n edge wave
Ao	free stream particle semi-excursion amplitude
b_i	crest height of the ith bar
C	phase velocity
Cg	group velocity
D	$(= 2m\sigma (X/g \tan \beta)^{1/2})$ a nondimensional offshore distance
E	local energy density
f	frequency (Hz)
$f_n(x)$	offshore structure of a mode n edge wave
g	gravitational acceleration
h(x)	water depth
ho(x)	local still water depth
δh	depth perturbation of barred profile from a plane beach
H(x)	incident wave height
Ho	deepwater wave height
i	$\sqrt{-1}$
J_j	jth order Bessel function of the first kind
k	radian wave number
k_b	equivalent Nikuradse roughness
k_s	hydraulic roughness
k_y	longshore component of wave number
ℓ	total boundary layer thickness
L	wave length
L_i	offshore distance of ith bar from the shoreline
Lm(x)	Laguerre polynomial of order m
m	(=1, 2, 3...) index for the fundamental and harmonics
n	edge wave mode number
p	pressure
R	reflection coefficient
R^v	vertical runup excursion
Sxx	onshore component of radiation stress in the direction of x

T	wave period
$u(x,z,t)$	horizontal component of the velocity inside the boundary layer
$\bar{u}(x,z,t)$	depth integrated velocity outside the boundary layer
u'	turbulent velocity fluctuation of u
$u_i(x,z,t)$	ith term in an expansion of u in power of ka
$\bar{u}_E$	horizontal component of Eulerian streaming velocity
$\bar{u}_S$	horizontal component of Stokes drift
u^*	bed friction velocity ($= (\tau_o/\rho)^{1/2}$)
$U(x,t)$	water particle velocity in the interior of water column
$\bar{U}$	total mass transport velocity ($= \bar{U}_L + \bar{U}_w$)
$Uo(x)$	complex amplitude of velocity in the inviscid field
$U_1(x,t)$	horizontal component of Uo outside the boundary layer
$\bar{U}_L$	mass transport velocity ($= \bar{u}_E + \bar{u}_S$) due to long wave
$\bar{U}_w$	mass transport velocity due to wind wave
w	vertical component of the velocity in the boundary layer
w'	turbulent velocity fluctuation of w
w_i	ith term in an expansion of w inpowers of ka
$\bar{W}$	vertical component of the mass transport velocity
x	offshore coordinate
y	alongshore coordinate
Y_j	jth order Bessel function of the second kind
z	vertical coordinate
z'	distance above the bottom
zo	value of z at which the no-slip condition is applied
Δx	offshore increment between the grid points
$\overline{uw}$	Reynolds stress due to the turbulent fluctuations in u and w
α	constant in the exponential beach profile
β	local beach slope
$\bar{\beta}$	mean beach slope of a variable profile
γ	$-(\sigma/2\nu)^{1/2} - 1/\delta$

δ	Stokes boundary layer thickness (= $(2\nu/\sigma)^{1/2}$)
δ_*	displacement thickness
ε	small parameter on the order of ka
ζ	displacement of mean water level from the still water level
η	displacement of free surface
$\eta_{(0)}$	η at the shoreline
$\eta_{(1)}$	η at $1\Delta x$ from the shoreline
θ	phase difference between incoming and outgoing waves
ν	molecular kinematic viscosity
ν_t	eddy viscosity (turbulent kinematic viscosity)
ν_m	effective eddy viscosity (= $\tau/(\partial u/\partial z)$)
ξ	nondimensional vertical length (= z/δ)
ρ	water density
σ	radian frequency
τ	shear stress
τ_o	bed shear stress at $z = z_o$
ϕ	velocity potential
χ	nondimensional offshore distance = $2\sigma(x/g\beta)^{1/2}$
ψ	nondimensional mass transport velocity = $\bar{U}/(a^2\sigma^3/4g\beta^3\chi^3)$

Subscript

os	value of oscillatory boundary layer
E	component of Eulerian streaming
L	long wave
w	wind wave
s	significant value
S	component of Stokes drift
in	component of incoming wave
out	component of outgoing wave
std	component of standing wave
∞	value in deep water

ABSTRACT

It has been widely observed in nature that longshore bar topography changes profile in the onshore-offshore direction. It is common for some bars to migrate onshore during post-storm phases and offshore during storms. Although the behavior of submarine bars has been widely reported, its mechanisms and forcings are far less clear.

To determine the mechanism for bar migration or for the persistence of bar systems, a numerical model is developed, which accounts for the mass transport velocities in the bottom boundary layer induced by a family of combined long waves at surf-beat frequencies and wind waves. The present approach simulates the structures of the streaming velocities near the bed on mild and steep beaches under different wave conditions. The results from the numerical investigation show that the beach slope and the relative stength of the mass transport velocities between wind wave and infragravity wave appear to be the most important causes of the bar behavior. The influence of bars on modification of long waves is also considered. The long wave profiles on a barred topography show the trapping of antinodes toward bar crests with amplitude increased.

The numerical approach is tested against field data obtained during the DUCK82 experiment. The model allows for long waves to be in broad-band frequencies, which is advantageous over existing approaches. The numerical results are consistent with observed data for bar formation, migration offshore, migration onshore, and even for bar maintenance.

INTERACTION OF LONG WAVES AND NEARSHORE BARRED TOPOGRAPHY

- A Mechanism of Bar Migration

CHAPTER 1

INTRODUCTION

The dynamics of the coastal area in many ways are distinct from the dynamics of the deep ocean. The primary causes of this distinction are due to the presence of the shoreline and the variable topography. A shallow, sloping bottom and the constraint of the coastline lead to steepening and breaking of incident gravity waves and the development of the surf zone. Consequent results are the temporal and spatial variability of geomorphology due to the active sediment transport associated with complex hydrodynamic processes in the nearshore. The coastal processes including morphodynamic as well as hydrodynamic variability change the scales in space and in time.

Horikawa (1981) classified coastal phenomena into three categories as macroscale, mesoscale and microscale. The macroscale phenomena with geologic time scales and space scale of several kilometers would predict long-term coastal changes by taking account of the historical sea-level change, ground-level change due to crustal movement as well as man-made effects. The microscale phenomena on the order of seconds in time and millimeters in space provide the fundamental details of our knowledge of larger scale processes such as wave transformation, wave-current interaction, boundary-layer processes, grain-fluid interaction and numerous processes in this category. Changes in shoreline and sea-bottom topography, bar and cusp formation, and nearshore currents fall in the category of mesoscale phenomena with time and space scales on the order of hours and meters respectively. These mesoscale phenomena are involved in the potential for causing loss of life and property damage by erosion and flooding associated with the

waves and coastal storm events. For this reason, numerous investigations have been carried out, but the actual coastal processes have not been sufficiently understood due to the complexity of nearshore hydrodynamics and its correlation with the sediment transport process.

Figure 1.1 schematizes the interactions among the various elements such as waves, wave-induced and nearshore currents, sediment transport and topography, etc. Sediment particles will be transported by fluid motion. The fluid motion in the nearshore is dominated by waves. Waves are, in turn be modified through feedback processes due to the topography. Therefore the wave field and associated currents in the nearshore, which affect the topographical variability, should be precisely understood.

Natural beaches change profile on both short and long time scales. Common features in regions with an abundant supply of sand-size sediment are longshore bars parallel to the shoreline. The submarine bars exposed to a constant wave action for a long duration remain very stable while some bars migrate onshore during post-storm phase and offshore during storms with migration rate up to 2.1 m/hr (Sallenger et al., 1985). The dynamic aspects of bar migration shoreward or seaward have direct implication to the sediment transport process via erosion and deposition of sediments in the nearshore. The signature of the two cycles of erosional and depositional (recovery) profiles on a given beach is usually characterized by the presence of longshore bars. Bars provide a natural protection to the beach by causing incoming waves to break farther offshore reducing the energy reaching the beach. Offshore bars also provide a mechanism for the temporary storage of eroded sediments as part of the cycle toward beach recovery

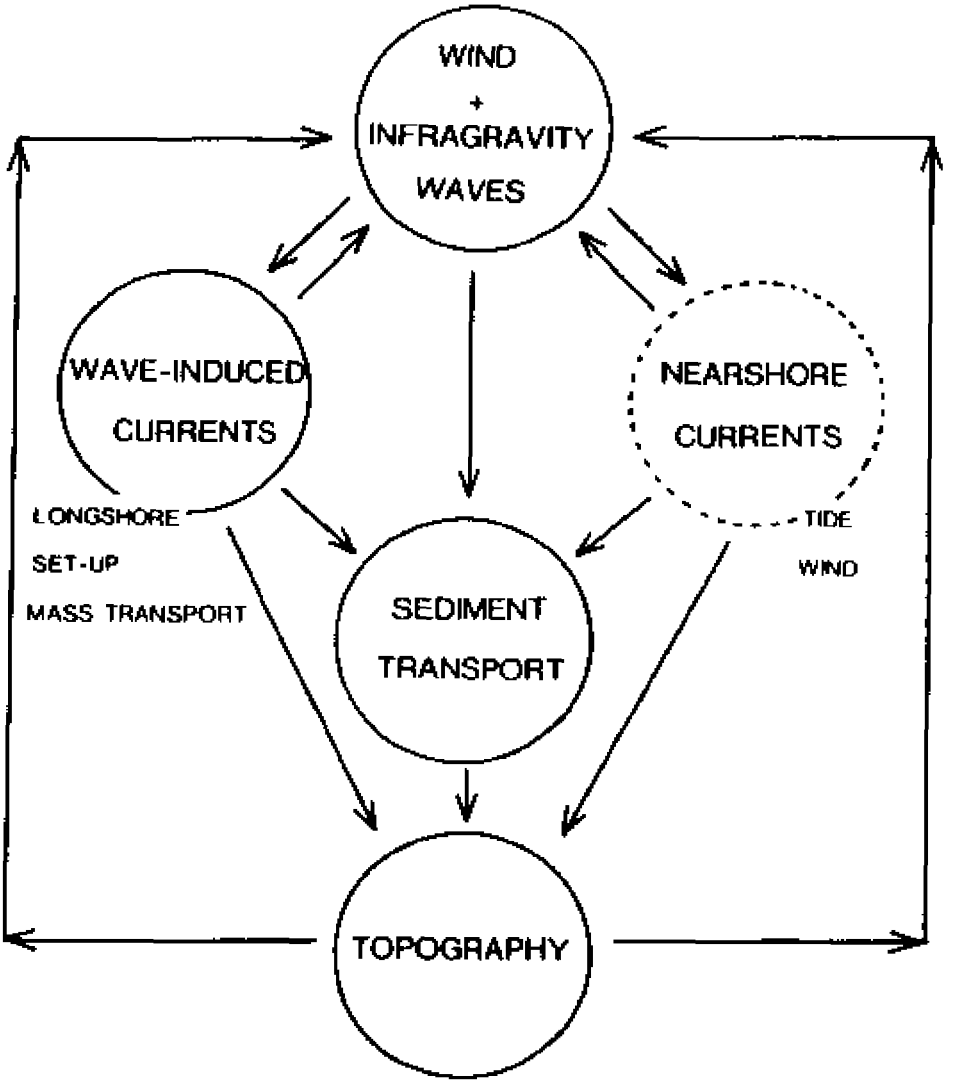

Figure 1.1: Schematic diagram showing interactions among the various elements in the nearshore. Waves and currents provide forcing to the sediment transport while the growing topography would modify the wave field through energy dissipation or resonance, etc..

(Birkemeier et al., 1987), or a coupling agent to exchange the sediments between the surf zone and the inner shelf (Wright et al., 1984).

Previous observations of self-maintaining or rapidly migrating offshore bar system suggest the importance of the interaction of topography and nearshore hydrodynamics. The mechanisms controlling longshore bar formation and migration are not well understood, presumably due to the complexity of the wave field and its relation to the morphodynamics.

On sloping beaches, it is clear from recent field observations that wave energy at frequencies much lower than incident waves increases shoreward (Bowen and Huntley, 1984; Guza and Thornton, 1985; Wright, 1982; and many others). These low-frequency motions, particularly with periods of 30 - 300 s (surf beats) have been extensively investigated to link with the potential roles in erosion, transport and deposition of sediment in the nearshore, provide a source energy for controlling topographic features such as beach cusps and nearshore bars (e.g. Bowen and Huntley, 1984 for review). These long period motions (infragravity waves) with relatively long wavelength and low amplitude in the nearshore are associated with different motions identified through the dispersion relationship between frequency and longshore wave number. The low-frequency motion in the nearshore is characterized by a combination of different forms such as forced waves (Longuet-Higgins and Stewart, 1962), edge waves (Bowen and Inman, 1969), standing waves (Suhayda, 1974) and seagoing waves (Tucker, 1950; Symonds et al., 1982). Numerous field observations confirmed that the infragravity motions are, in fact, of standing waves in the cross-shore, either leaky modes or high-mode edge waves (Guza and Thornton, 1985; Huntley, 1976; Suhayda, 1974; Wright et al., 1982). The cross-shore structure of high-mode edge waves is very similar to that of leaky modes. The energy level at surf beat

periods has been observed to be closely comparable with that of incident waves (Guza and Thornton, 1985; Wright et al., 1982).

Previous studies of topographic features in the nearshore revealed the important role of low-frequency wave activity. The approaches to explain bar formation in response of breaking process or tidal variation have not been satisfactory (Bowen, 1980; Mason et al., 1984). Under many circumstances, the bars are observed well inside the surf zone and in tideless lakes. Bowen and Inman (1971) suggested that large, crescentic bar systems might be formed by the drift velocities assoiated with low-frequency, standing edge waves. Short (1975) identified low-frequency, infragravity waves as a possible cause for the parallel bars observed off Alaska. Recently Holman and Bowen (1982) demonstrated that any two infragravity waves of the same frequency but different modes could produce complex patterns of drift velocities, which resembled the topographic patterns. For a self-maintaining bar-system, Kirby et al. (1981) suggested that bars formed at antinodes of standing waves tend to trap the antinode of resonant edge wave modes, leading to the maintenance of the bar.

However some bar systems persist virtually year-round (Wright et al., 1982) while some bars undergo appreciable and rapid shoreward and seaward migration at speed up to 2.1 m/hr (Sallenger et al., 1985). Also the offshore bar system may modify the wave field. None of the existing approaches provides the mechanism for bar migration under varying wave conditions, and accounts for the feedback between the growing topography and long waves. Moreover, low-frequency waves observed in nature consist of wide-banded energy instead of a single predominant frequency which conventionally provides the positions of nodes and antinodes of infragravity waves.

The purpose of the present study is to examine, by way of a numerical model, longshore bar formation and migration due to the mass transport velocities induced by the waves, and to verify the model results using field data observed during a major storm event. The nearshore wave fields consist of the energetic wind waves and relatively high energy-level of infragravity waves. A close link between this complicated hydrodynamic field and the sea-bed is through the bottom boundary layer. Considering the temporal and spatial scales of the bar system, the mass transport velocity (drift velocity) of the wave field can play an important role in perturbing the beach profile (Bowen, 1980). By setting up a wave field comprised of wind waves and infragravity waves, the present study investigates the consequent distributions of mass transport velocities and boundary-layer parameters on arbitrary barred-topography under varying wave conditions. To consider the interaction of waves and the barred topography in the nearshore, it is necessary to know (1) natu of the steady flows in the bottom boundary laye: induced by the nearshore wave field, and (2) the effect of the barred topography on the wave field through dissipation of wave energy and /or frequency selection between the resonant conditions of the barred topography and the preferred wave modes.

In the following chapter, known characteristics of long waves and topography feedback are described in more detail. Kinematics and generation mechanisms of infragravity waves and observational evidence are provided to propose a wave field in the model. Also in Chapter 2, the basic concept of the mass transport velocity in the bottom boundary layer is introduced and its application to simple cases are given. Observational evidence based on previous studies to link the interaction between the wave field and topographic features is

referenced to address the topic on the processes of bar formation/migration.

In Chapter 3 a wave field combined with transforming wind waves and infragravity waves is proposed for numerical investigation to examine longshore bar formation on plane beaches. The wind wave field is predicted using the algorithm developed by Ebersole et al. (1986) in and outside the surf zone. A simple boundary layer model accounting for steady bottom-flows arising from two-frequency waves, which is different from the conventional oscillatory wave or wave-current boundary layers, is developed. Consequently mass transport velocity induced by the modeled wave field is derived. This approach provides a basis for examining the sensitivity of bar formation to beach slope and wave conditions through numerical experiment.

Examination of the bar migration on a given barred-topography which is designed based on the general profiles observed in nature, is the subject of Chapter 4. Under varying wave conditions, the basic model developed in Chapter 3, is run to estimate the distributions of mass transport velocities and boundary-layer parameters such as shear stresses and bed friction velocities which are critical to determine the direction and magnitude of the sediment transport. The present method is somewhat limited in covering all possible aspects of environmental conditions, particularly of extremely high waves such as hurricanes with wave height of 5 - 6 m, and of variable alongshore topography or wave conditions. Nevertheless, the analysis provides an opportunity to examine the insight of mechanism for bar migration under varying wave condition on arbitrary beach topography, and to narrow the gap of discrepancy between the previous studies and field observations.

When the bar system persists even under varying wave conditions, the wave field is expected to be in equilibrium with the bar system. The influence of a bar on the modification of long waves is considered in Chapter 5. Using the finite difference scheme for a steady state, the long wave equation is solved to examine the behavior of the long wave structure over the bar topography. The general results of Chapter 5 show that, in fact, the bar crest tends to trap the antinodes of standing waves as suggested by Kirby et al. (1981) and Symonds and Bowen (1984).

Chapter 6 deals with observational verification of the model. Data collected at Duck, North Carolina during a 3-day storm in October (DUCK82) provide an opportunity to examine the model. Test runs are selected as 4 distinct events; pre- , developing, fully developed and post- stages of a storm. For each test run, input wave parameters for model run are given by observed data and implemented on the precedent topography. The predicted distribution of bed friction velocity along the shore-normal line is compared with the profile observed on the day of wave input. To test the applicability to a persisting bar system, the model is run on the persisting profile with assumed steady-state wave conditions. The results of numerical experiments show an excellent agreement with observations of the behavior of bar system during different stages of a storm.

Finally, Chapter 7 summarizes the results and discuss the limitations, and offers suggestions for further research.

CHAPTER 2

A REVIEW OF LONG WAVES AND TOPOGRAPHIC FEEDBACK

2.1. Long Waves in the Nearshore Zone

When water waves approach a sloping beach they usually increase in amplitude and break. In the nearshore field where the sediment transport is very active by the wave-induced currents, the incident waves transfer their energy to lower frequencies by nonlinear interaction, resulting in wave motion at periods substantially longer than the incident waves. Recent field measurements on beaches confirm the existance of different types of long-period waves close to the shore. Possible long-wave motions are in the form of progressive or standing edge waves, forced wave motion and free leaking waves propagating away from the shoreline. In this section the generation mechanism and characteristics of each type of long wave are described.

2.1.1. Edge Waves

Edge waves, which are generated by resonant interaction with the incident wind waves and trapped against the shoreline by refraction, propagate alongshore with surface elevation maximum at shoreline and decaying exponentially in the offshore direction.

The edge wave solutions to the shallow water equation have been found for simple profiles, a linear slope (Ursell, 1952; Eckart, 1951) and an exponential profile (Ball, 1967).

For a beach of linear slope angle, β, Eckart (1951) described the edge waves in terms of the velocity potential ϕ such as;

$$\phi = \frac{a_n g}{\sigma} f_n(x) \cos(k_y y - \sigma t) \qquad (2.1)$$

: for a progressive edge wave

and

$$\phi = \frac{a_n g}{\sigma} f_n(x) \cos k_y y \cos \sigma t \qquad (2.2)$$

: for a standing edge wave

, where a_n is the shoreline amplitude of the edge wave of mode number n, which is the number of zero crossings of the profile across the mean water level, g is the gravitational acceleration, σ is the angular frequency, k_y is the longshore wave number and t is time. The offshore structure $f_n(x)$ is given by

$$f_n(x) = \exp(-k_y x) \, Ln(2k_y x) \qquad (2.3)$$

where Ln is the Laguerre polynomial of order n and its values for n=0, 1 and 2 are

$$\begin{aligned} L0\ (2k_y x) &= 1 \\ L1\ (2k_y x) &= 1 - 2k_y x \\ L2\ (2k_y x) &= 1 - 4k_y x + 2(k_y x)^2. \end{aligned} \qquad (2.4)$$

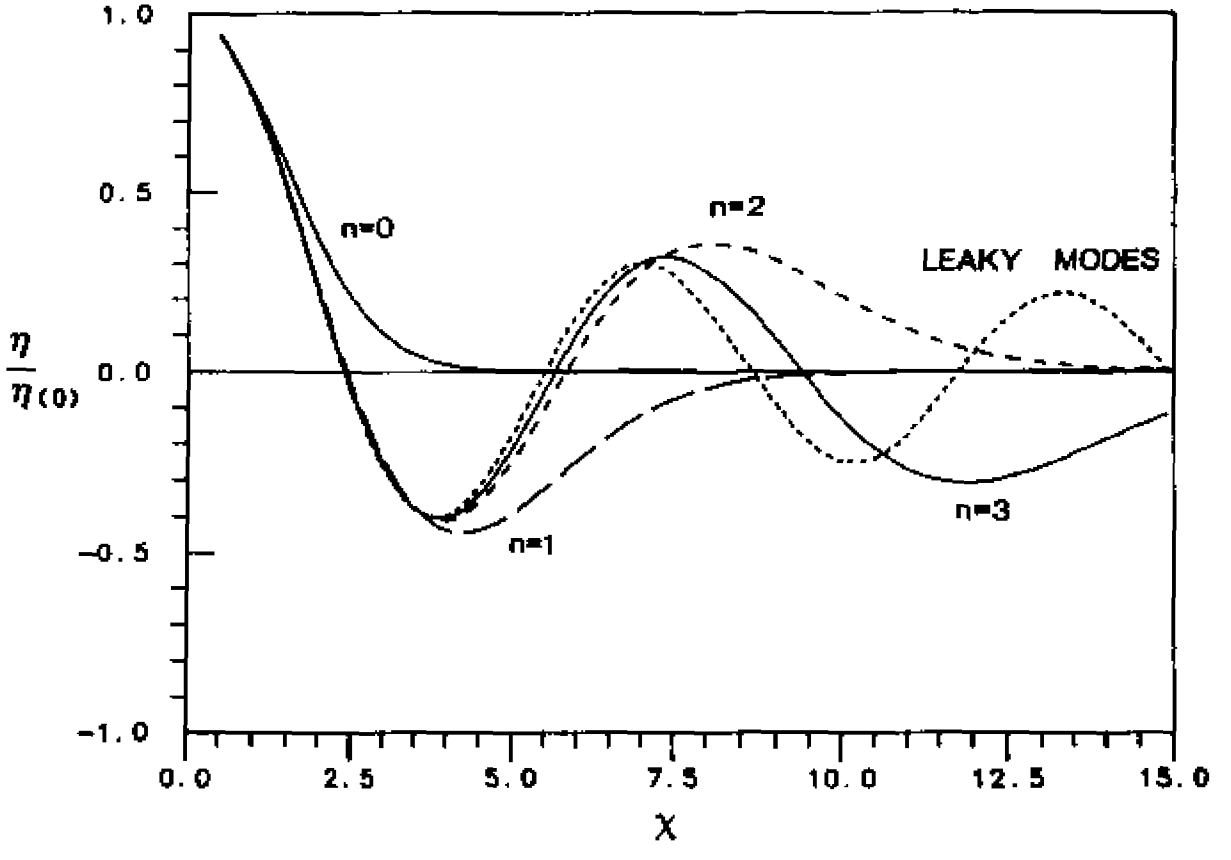

Figure 2.1: Cross-shore structure of the surface elevation of edge waves (modes 0-3) and leaky modes plotted along a nondimensional offshore distance $\chi = 2\sigma(x/g\beta)^{1/2}$. The behavior of high mode edge waves ($n \geq 3$) appears in the same form with that of leaky modes.

Figure 2.1 is a plot of $f_n(\chi)$ against the nondimensional offshore distance $\chi = \sqrt{4\sigma^2 x/g\beta}$ for the first four modes with the simple dispersion relation as $\sigma^2 = gk_y(2n+1)\tan\beta$. The velocity u (u,v) and the elevation η are given by

$$u = (u,v) = \nabla \phi$$

$$\eta = -\frac{1}{g}\frac{\partial \phi}{\partial t} \qquad (2.5)$$

where ∇ is the horizontal gradient as $\nabla = (\partial/\partial x, \partial/\partial y)$.

The beach profiles in nature are more commonly concave profiles (Dean, 1977). An analytical solution for an exponential profile of the form

$$h = h_\infty [1 - \exp(-\alpha x)] \qquad (2.6)$$

was given by Ball (1967), where h is the water depth, h_∞ is the water depth at $x = \infty$, and α is a constant. Ball's solution for standing and progressive edge waves shows a similar solution to Eckart's. An interesting feature of Ball's theory is the prediction of the condition for trapped edge waves, which is

$$\sigma^2 > n(n+1)\,\sigma^2\, gh_\infty \quad \text{or equivalently} \quad k_y^2 > n(n+1)\,\alpha^2 \ . \qquad (2.7)$$

Physically, the cutoff period of an edge wave mode occurs when the longshore wave number of a free wave, k_y, becomes equal to the wave number of a free gravity wave, k_∞ , at $x = \infty$. When $k_y < k_\infty$, the nearshore solution can be matched to a free 'leaky' wave which carries energy away from the shoreline; When $k_y > k_\infty$, no such matching is possible and the only free waves which can exist are edge waves trapped

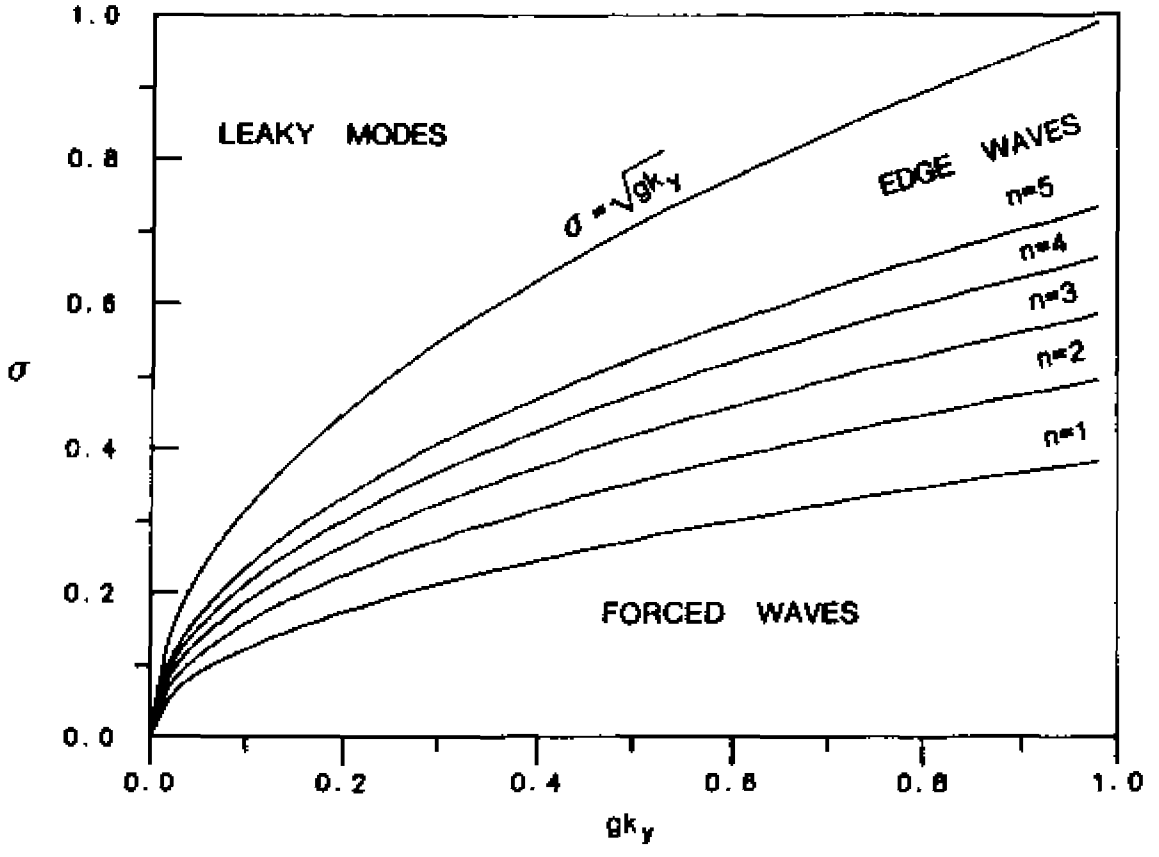

Figure 2.2: Plot of dispersion relations of nearshore wave motion in frequency (σ) - longshore wave number (k_y) space. The trapped modes of edge waves are shown for mode 1 to 5. Forced waves take positions between the edge waves when $\sigma^2 < gk_y$ while leaky modes occupy in a space of $\sigma^2 > gk_y$.

against the shoreline. At the cutoff period itself the edge wave solution matches to a free wave travelling parallel to the shoreline. The dispersion relations of leaky and edge waves in k_y-σ space are shown in Figure 2.2.

Edge waves are most likely generated through a nonlinear interaction with an incident wave field. On a shallow, sloping beach, nonlinear interaction occurs at second order in the form of resonant triads, e.g., $\sigma_1 = \sigma_2 \pm \sigma_3$. Gallagher (1971) showed that the interaction between two incoming waves may result in the resonant excitation of edge waves at the beat frequency. Guza and Davis (1974) showed the way in which edge waves at the subharmonic, $\sigma/2$, of the incoming wave frequency, σ, grow resonantly, and Guza and Bowen (1974) extended edge wave growth to include the limiting conditions such as dissipation of energy by friction, energy radiation and demodulation.

In addition to the wave-wave interaction, there are other possible nearshore interactions involving the topographic effects which will follow in later section of this chapter.

2.1.2 Forced Wave

Progressive wind waves in weakly nonlinear dispersive systems are unstable to modulation perturbations (Benjamin and Feir, 1967) resulting in wave groups with new length and time scales which are much larger than the length and period of the carrier waves (Yuen and Lake, 1980). The wave groups with slowly varying amplitude (wave envelope) in shallow water have been the subject of many investigations due to its possible energy source to the infragravity energy (energy beats) and to harbor resonance.

Longuet-Higgins and Stewart (1962) introduced the concept of radiation stress, S, which is defined as an excess momentum flux due to the presence of waves. The stress, Sxx, representing the flux of horizontal momentum parallel to the direction of wave propagation is given by;

$$Sxx = E \left(\frac{2kh}{\sinh 2kh} + \frac{1}{2} \right) \quad : \text{for progressive waves} \qquad (2.8)$$

$$Sxx = 2E \left(\frac{2kh}{\sinh 2kh} + \frac{1}{2} \right) \quad : \text{for standing waves} \qquad (2.9)$$

,where the wave energy $E = (1/2)\ \rho g a^2$, a is the wave amplitude, k is the wave number, and h is the water depth.

It is noted that the radiation stress is proportional to the square of wave amplitude. Since the wave group contains the carrier waves of varying amplitude, there exists a spatial gradient of Sxx along the wave ray.

The momentum balance on a sloping beach leads to

$$\frac{d\,Sxx}{d\,x} + g(\bar{\zeta} + h)\frac{d\,\bar{\zeta}}{d\,x} = 0 \qquad (2.10)$$

, where $\bar{\zeta}$ is the mean water level. Integration of Equation (2.10) with the aid of $\bar{\zeta} \ll h$ yields the fluctuation of mean water level due to the varying Sxx such as

$$\bar{\zeta} = -\frac{Sxx}{\rho(gh - C_g^2)} + \text{const} \qquad (2.11)$$

, where C_g is the group velocity. The radiation stress in the wave groups produces a bound, low frequency long wave that is 180^o out of phase with the envelope of the carrier waves (Fig. 2.3). Equation (2.11) states that as the water depth diminishes and the group velocity C_g approaches $(gh)^{1/2}$, the response of the surface to the applied stress will increase. Although the validity of the formula is violated by wave breaking and large Ursell number $ak/(kh)^3$, the driving mechanism of forced wave due to the fluctuation of in wave groups remains sound.

Munk (1949) and Tucker (1950) observed low frequency wave motion and they interpreted the seagoing long waves as a release of a forced long wave under shoreward propagating wave groups. Recently Huntley and Kim (1984) and Guza et al. (1984) observed unambiguously the presence of forced long wave bounded under the incident wave groups in shallow waters.

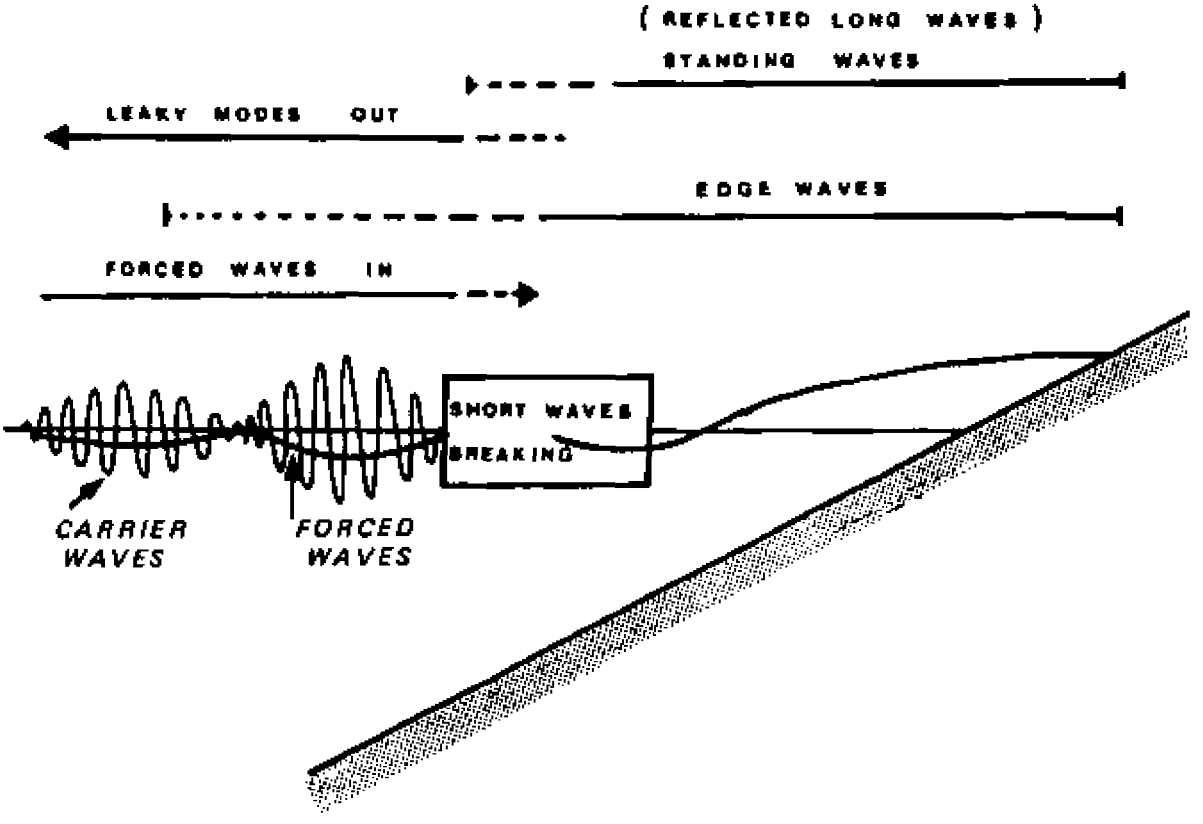

Figure 2.3: Possible wave motions in the nearshore. Wind waves break near the shoreline while forced waves bounded in the wind-wave groups are amplified. Nonlinear interaction and/or reflection could generate edge waves and/or standing waves. Leaky modes radiate their energy offshore beyond the surf zone.

Although the detailed mechanism of the forced wave behavior in the surf zone where the groupiness disappears, has not yet been determined, it is generally accepted that the low-frequency oscillation in the surf zone is dominated by a standing wave (Guza and Thornton, 1985; Kim and Huntley, 1985; Suhayda, 1974; Wright et al., 1982). This fact implies that the long wave incoming from offshore is reflected back at the shoreline to form a standing wave in the surf zone or some part of its energy radiates seaward by a mechanism suggested by Symonds et al. (1982) which is discussed in the next section.

2.1.3. Leaky Modes

Leaky modes of wave motion in shallow water include any free wave motions which do not satisfy the dispersion relation of trapped edge waves, e.g., when $\sigma^2 > gk_y$ (Fig. 2.2). These leaky modes carries energy shoreward (e.g., incident wind waves) or away from the shoreline such as the seagoing waves reflected at the shoreline.

When waves run up a gently sloping beach, the short gravity waves break and loose much of their energy in turbulence. However low frequency waves with long wave length and small amplitude are expected to be reflected at the shoreline or at a chaotic discontinuity of dynamics such as break point.

Although the observations of seagoing free long waves are not new (examples: Munk, 1949; Tucker, 1950), their generation mechanism has not been understood until Symonds et al. (1982) proposed a mechanism of long wave generation accounting for time-varying break points. It is clear from the observation of standing waves dominantly in the surf zone (Suhayda, 1974; Guza et al., 1984, Kim and Huntley, 1985, Wright et al., 1986) that a portion of incoming long wave reaching the shoreline is

reflected back to couple with the incident long waves. Alternatively surf beats observed by Munk (1949) and Tucker (1950) may be a form of the reflected long wave which appears to take place in the zone of breaking waves (Peregrine, 1967).

Symonds et al. (1982) parameterize the setup (Longuet-Higgins and Stewart, 1964) within the surf zone with a time-dependent breakpoint. Since the setup is proportional to the square of wave amplitude, the wave-induced setup and the width of the surf zone will vary as wave height varies in the incident wave groups. The forcing of the sinusoidally varying breakpoint on a plane beach results in free long waves at group period and its harmonics. Shoreward of the breakpoint, standing waves (ζ_m) are found in form of

$$\zeta_m = A_1 J_0(Dx^{1/2}) \sin(m\sigma t) + A_2 J_0(Dx^{1/2}) \cos(m\sigma t) \qquad (2.12)$$

where m=1,2,3 ... (index for the fundamental and harmonics), J_0 is the zero-order Bessel function of the first kind, A_i (i=1,2) are the constants, $D^2 = 4m^2\sigma^2 X/g \tan\beta$ and X is the mean position of the breakpoint. Outside the breakpoint, a seagoing progressive wave is obtained such as

$$\zeta_m = A_1 [J_0(Dx^{1/2}) \sin(m\sigma t) + Y_0(Dx^{1/2}) \cos(m\sigma t)] \qquad (2.13)$$

where Y_0 is the zero-order Bessel function of the second kind. The velocity field can be obtained by mass conservation (Phillips, 1966) as

$$\frac{\partial \zeta}{\partial t} + \frac{\partial (h\bar{u})}{\partial x} = 0 \qquad (2.14)$$

where $\bar{u}$ is the depth averaged velocity. The amplitude of the outgoing wave depends on the relative phase between the standing wave in the surf zone and outgoing wave radiating from the forcing region.

Although the results of several field experiments attempting to verify the Symonds et al.'s model (Kim, 1985; Guza et al., 1984) show a qualitative agreement in terms of frequency and strong indication of seagoing waves by the cross-correlation study, the difficulties in determining the seagoing waves generated at breakpoints lie in the accurate measurement of time-varying breaking points and breaking height, and parameterization of the groupiness. However an accurately controlled laboratory experiment carried by Kostense (1984) shows good agreement with the model of Symonds et al. (1982), showing low correlation between the incident bound waves and the seagoing free waves as suggested by Symonds et al.(1982). Kostense (1984) concluded that two-dimensional surf beat outside the surf zone induced by incident wave groups should be considered as the result of two wave systems, i.e., incident bound (forced) waves propagating shoreward at group velocity, and outgoing free waves which are generated in the surf zone. His conclusion is apparently in accordance with the field observations by Elgar and Guza (1985) and Kim and Huntley (1985).

2.2. Mass Transport Induced by Oscillatory Flow

2.2.1. Frame Works on Horizontal Bottoms

Small-amplitude surface gravity waves are known to induce mean drift velocities in the direction of wave propagation. A knowledge of the steady streaming (mass transport) velocity distribution close to the sea bed is of considerable importance to sediment transport and pollutant dispersion in the coastal area. The most fundamental past study of wave-induced mass transport is due to Longuet-Higgins (1953).

Water particle motion due to wave propagation is not simply circular or oscillatory. Although its first-order mean value is zero, its second-order value is non-zero quantity because of a slow mean drift of the fluid elements (Stokes drift). In water of finite depth, the friction of the water induces second-order mean velocity (Eulerian streaming velocity) near the bottom. Eulerian streaming velocity arises as a consequence of the Reynolds stress set up by the velocity gradient across the first-order boundary layer. The total mass transport velocity ($\tilde{U}$) near the bottom is (correct to the second order) the sum of the Stokes drift ($\tilde{u}_S$) and the Eulerian streaming velocity ($\tilde{u}_E$),

$$\epsilon^2 \tilde{U} = \epsilon^2(\tilde{u}_E + \tilde{u}_S) = \epsilon^2 \left(\tilde{u}_E + \overline{\int (u_1 \, dt \cdot \nabla) \, u_1} \right) \qquad (2.15)$$

Lagrange = Euler + Stokes

, where ϵ is a small quantity such as wave steepness (a/L) and u_1 is the wave orbital velocity at the first order.

A wave whose surface displacement in the form of

$$\eta = a \cos(kx - \sigma t) \tag{2.16}$$

has non-zero second-order quantity given as (Longuet-Higgins, 1953)

$$\bar{u}_s = \frac{\sigma k a^2 \cosh 2k(\eta + h)}{2 \sinh^2 kh} \tag{2.17}$$

which is the Stokes drift arising from the incomplete closure of the particle paths of wind waves.

The mean momentum equation in the bottom boundary layer satisfies the balance between viscous and Reynolds stresses;

$$\frac{\partial}{\partial z} \overline{uw} = \nu \frac{\partial^2 \bar{u}_E}{\partial z^2} \tag{2.18}$$

, where ν is the molecular kinematic viscosity.

An integration with the expression of Reynolds stress in terms of wave parameter gives the Eulerian drift such as (Phillips, 1966)

$$\bar{u}_E = \frac{a^2 k \sigma}{4 \sinh^2 kh} \{ 3 - 2(\gamma z'+2) e^{-\gamma z'} \cos \gamma z' - 2(\gamma z'-1) e^{-\gamma z'} \sin \gamma z' + e^{-2\gamma z'} \tag{2.19}$$

where $z' = z+h$ is the distance above the bottom, $\gamma = (\sigma / 2\nu)^{1/2}$, and the thickness of boundary layer $\delta = (1/\gamma) = (2\nu / \sigma)^{1/2}$. Thus just beyond the boundary layer ($\gamma z' \longrightarrow \infty$), the mass transport is

$$\bar{U} = \bar{u}_E + \bar{u}_S = \frac{5 \sigma a^2 k}{4 \sinh^2 kh} \tag{2.20}$$

$\bar{W} = 0$ (vertical component).

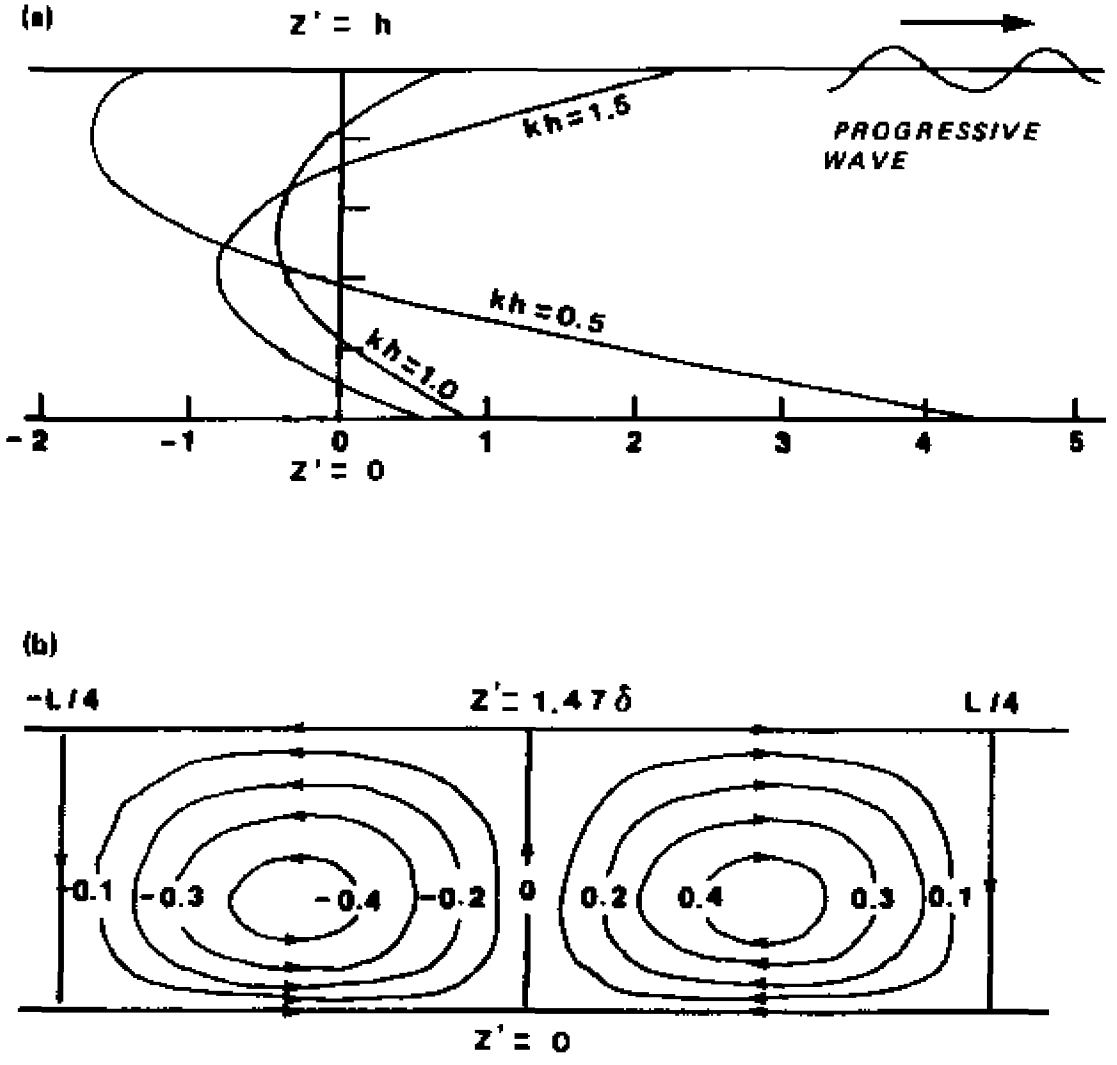

Figure 2.4: Drift of fluid in the water column for progressive waves and in the boundary layer at the bottom for standing waves. The positive value is in the same direction while the negative value is in the opposite direction with the wave propagation. (a) Drift of fluid near the bottom has the same direction with the progressive waves propagating from left to right. (b) Drift of fluid in the bottom boundary layer ($0 \leq z' \leq 1.47\,\delta$) for a standing wave with antinodes at $\pm$ L/4 and kh = 1.0, showing convection cells with alternation of convergence and divergence at every quarter wave length (L/4). The values along the abscissa in the plot (a) and contours in the plot (b) are the relative magnitudes of the drift intensity at different positions.

A graph representing the typical profile in the water column for the progressive wave is given in Figure 2.4a which shows a drift of fluid in the direction of wave propagation near the bottom.

For a standing wave $\eta = 2a \cos kx \cos \sigma t$, the mass transport is given as

$$\bar{U} = \frac{a^2 k \sigma}{2 \sinh^2 kh} \sin 2kx \left(-3 + 8 e^{-\gamma z'} \sin \gamma z' + 3 e^{-\gamma z'} \right) \quad (2.21)$$

which is shown in Figure 2.4b for $0 \leq z' \leq 1.47\ \delta$. The horizontal mass-transport velocity varies with sin 2kx which is the harmonic frequency of the standing wave. The particles very close to the bottom tend to move towards the planes of greatest horizontal first-order motion and away from the planes where the motion is purely vertical, but for larger values of $\gamma z'$, the particles drift in the reversed sense. Hence there is a circulation in the boundary layer itself, in cells with length scale of (1/4)L. The vertical velocity is given by

$$\bar{W} = \frac{a^2 k^2 \sigma}{\gamma \sinh^2 kh} \cos 2kx \int_0^{\gamma z'} \left(-3 + 8e^{-\gamma z'} \sin \gamma z' + 3e^{-2\gamma z'}\right) d(\gamma z')$$

$$= \frac{a^2 k^2 \sigma}{\gamma \sinh^2 kh} \cos 2kx \left[-3\mu + \frac{8}{2} e^{-\mu} (-\sin \mu - \cos \mu) - \frac{3}{2} e^{-2\mu} \right]_0^{\mu}$$

$$= \frac{a^2 k^2 \sigma}{\gamma \sinh^2 kh} \cos 2kx \left[-3\mu - 4e^{-\mu} (\sin \mu + \cos \mu) - \frac{3}{2} e^{-2\mu} + \frac{11}{2} \right]$$

(2.22)

, where $\mu = \gamma z'$, and $\bar{W}$ vanishes when $\gamma z' = 0$ and 1.47 for ν = constant.

2.2.2 Application to sloping and rough bottoms

The theoretical contributions by Longuet-Higgins (1953) are within the framework of laminar flow on horizontal bottoms. The sea beds are frequently rippled and the hydrodynamic conditions in shallow water are rough. The presence of bed roughness, growing ripples or bars and hydrodynamic complexity are expected to affect and modify the mass-transport velocity distribution predicted by Longuet-Higgins. The possible relevance of Longuet-Higgins' idea in connection with the wave-induced sediment transport in nature has been pointed out and extended by several authors. Amongst these, Russel and Osorio (1958) conducted experiments to determine wave-induced drift in the turbulent channel flow and observed the mass transport velocities in agreement with the prediction of Longuet-Higgins' laminar theory. For progressive waves, Russel and Osorio showed the mass transport velocity at the outer edge of a turbulent boundary layer is independent of the functional form of the eddy viscosity. Hunt and Johns (1963) computed the mass transport velocities in both rotating and non-rotating systems. The results are consistent with the formation of a series of sand-bars or long sand ripples offshore, dependent on the wave length and the angle of incident waves. However Hunt and Johns did not take account for the effect of the variable depth. Johns (1970) used a coefficient of eddy viscosity which is a function of distance from a fixed boundary to calculate the mass transport velocity within a turbulent boundary layer. He found that the mass transport velocity induced at the outer edge of the layer by a progressive wave is the same in both laminar and turbulent system, which is in accordance with Longuet-Higgins (1953).

For standing waves the mass transport velocity induced at the outer edge of the layer is substantially less in the turbulent case than in the laminar case. At the same time, the turbulent boundary layer leads to a strong drift within the lower most 25% of the layer in a direction that is opposite to the drift well outside the boundary layer. Then it is possible that the direction of the net sediment movement beneath a standing wave will be different in the laminar and turbulent cases.

Applications of theoretical formula for the mass-transport velocity distribution to the realistic sea beds and wave fields have been obtained by several authors. Lau and Travis (1973) investigated the mass transport velocity in the bottom boundary layer due to slowly varying Stokes waves impinging on and reflecting from a plane-sloping beach. The result is interpreted to indicate the possible locations of submarine longshore bar formation. Carter et al. (1973) studied the mass transport velocity due to the wave field combined with a progressive and a standing waves which are reflected from a vertical wall in a constant depth. A striking feature is such that the magnitude and the direction of mass transport vary with the reflection coefficients ($0 \leq R \leq 1$) which would be function of the beach slope, wave steepness, grain size and ripple steepness, etc.. Bijker et al. (1974) measured mass transport profiles produced by waves propagating over a gently sloping bottom. Their theoretical considerations based on linear wave theory applied outside the breaker zone show a significant influence of the slope on the mass transport velocities for relatively long waves and steep slopes.

Over a rippled bed of small height to length ratio in a constant depth, the bed roughness appeared to increase the mass transport velocity for small waves but decrease it for large waves (Brebner et al., 1966; Bijker et al., 1974; Sleath, 1974). The flow at the bottom boundary layer is determined by the bed shear stress (τ_o). For rough surface the bed roughness length z_o is defined by $z_o = k_b/30$, where k_b is the equivalent Nikuradse roughness. Trowbridge and Madsen (1984) claimed, using time-varying eddy viscosity coefficient, that there is a reversal of the Stokes drift at small values of kh, corresponding to relatively long waves. However their results are inconclusive due to the sensitivity of the assumed vertical structure of the time-varying part of the viscosity. Also they just considered the steady streaming of Stokes drift induced by a monochromatic wave, which is not readily applicable to the nearshore wave field in nature.

2.3. The Influence of Long Waves on the Nearshore Geomorphology

2.3.1. Edge waves and rhythmic longshore features

The rhythmic longshore perturbations on the beach system such as beach cusps and crescentic bars are very common on natural beach. Their longshore spacing ranges from a few centimeters to several kilometers. Many attempts to link the nearshore processes with the rhythmic topography have been done due to the important implication to the on/offshore sediment transport.

Many mechanisms have been suggested to explain the existence of beach cusps but the most plausible is that they are the response of the beach sediment to the presence of edge waves (Bowen and Inman, 1969, 1971; Guza and Inman, 1975). According to Bowen and Inman (1971 standing edge waves formed by two progressive edge waves propagating in opposite directions might form beach cusps having a spacing of half the edge wave length. Bowen and Inman (1971) also showed that the drift velocities associated with standing edge waves may generate offshore crescentic bars. Huntley (1980) identified the presence of low-frequency edge waves and suggested the possible role of the observed edge waves to form the crescentic bars based on relatively large drift velocities estimated for the edge waves.

Although the possible role of edge waves for formation of rhythmic topography in the nearshore zone has been well recognized, it has been questionable whether edge waves of very narrow-banded frequencies could exist in the natural system (Wright, 1982) which is so complex itself. Moreover edge wave amplitudes are limited by energy radiation, finite

amplitude demodulation and viscosity (Guza and Bowen, 1976). The nearshore morphology does not grow continuosly along with the water motion. The size of the waves are limited by many processes and a candidate is the damping effect by the changing topography. Little published theoretical work on edge wave generation has considered the importance of topographic effects, though some laboratory experiments (Guza and Inman, 1975) appear to suggest a negative feedback between subharmonic edge waves and a growing beach cusps.

2.3.2 Long waves and linear bars

The velocities dominating the motion in the inner surf zone are often those at surf-beat frequencies rather than incident wave frequencies. Even farther seawards in the surf zone it has been widely reported that a significant long wave field in various forms is formed by several generation mechanisms (Longuet-Higgins and Stewart, 1962; Suhayda, 1974; Munk, 1949; Symonds et al., 1982). Among the possible form of long waves in the nearshore zone, the standing waves (leaky or edge) which are generated by the superposition of two progressive waves travelling in opposite directions have been highlighted as a dominant energy source responsible for the nearshore bars.

Steady drift velocities arise from the second order solution of progressive wave (Fig. 2.4a) and standing wave (Fig. 2.4b) (Longuet-Higgins, 1953). The drift velocity field of the standing wave in the bottom boundary layer illustrates the convection-cell type at every quarter wave length.

showing the convergence and divergence of drifting mass. Supporting the theoretical work of Longuet-Higgins, Carter et al. (1973) showed the laboratory experiments that the drift velocity associated with a standing wave tends to rework sediment into a series of bars. Theoretically, zeros in the drift velocity occur under both nodes and antinodes of the standing wave; material should converge at either nodes or antinodes depending on whether bed load or suspended load dominates.

Noda (1968) demonstrated the movement of suspended sediment towards the antinodal position and Bowen (1975) also predicted sediment accumulation under either the nodes or antinodes of standing waves, leading to the formation of linear offshore bars. Short (1975) identified low-frequency standing waves as a possible cause for the parallel bars observed off Alaska and demonstrated the similarity of offshore spacings between the bars and the standing wave antinodes.

There are numerous observations of the 'standingness' in water motion in the surf zone (Wright et al., 1982). More recently Symonds and Bowen (1984) theoretically obtained a standing wave solution in inner-bar area with the antinode over the bar crest and seagoing wave solution generated by time-varying break points. Clearly the formation of offshore bars is initially associated with the standing waves over the topography.

However many bar-systems persist virtually year round (Wright et al., 1982) while some bars may undergo appreciable and rapid shoreward and seaward migration at speed of 2.1 m/hr (Sallenger et al., 1985). The offshore bar system may influence but also respond to the wave field. As shown in Holman and Bowen (1982), any two waves of the same frequency at different modes could produce complex patterns of drift velocity above the sea bed. A small change in beach slope can produce 100% error in prediction of the edge wave mode (Holman and Bowen, 1979).

Under the varying wave conditions, the beach profile tends to change towards the state of equilibrium condition (Dean, 1977). When a particular wave field generates a bar system which is in equilibrium with the exerting wave field, the dredging of a bar will break the stability of the shoreline. Importance of the wave-topography interaction should be addressed to protect the nearshore environment.

2.4. Modification of Long Waves by Nearshore Topography

As waves move toward the coast, they undergo a transformation in wave characteristics by the influence of sloping bottom and undulating sea bed. The incident gravity wave feels the bottom during its shoaling and eventually breaks when the surface water at the crest is moving at the same speed as the phase speed (Phillips, 1966). However a long wave with relatively small amplitude is easily reflected by the uneven bottom rather than breaking.

A close interaction between the water motion and sea bed is through bed-friction. The changing sea bed may provide different resistance to the flow above the boundary layer. The friction factor on the bed is a function of the shear stress which is determined by the bed-form geometry (Jonsson, 1963). An addition of bar topography to plane beach profile is considered as a remarkable change in the profile, hence provides a significant effect to the flow field. On real beaches, strong topographic constraints may be obvious. However our understanding of influence of the barred topography to the wave field is far less clear.

On edge wave growth, Guza and Bowen (1976) addressed the important role of offshore energy radiation in the form of an outgoing progressive wave. Huntley (1980) suggested that the edge waves are generated as a result of the interaction between incident waves and a pre-existing topography which provided appropriate length scale to meet the resonant conditions.

Using the drift velocities derived by Hunt and Johns (1963), Holman and Bowen (1982) introduced a simple sediment transport model to estimate the new topography that would be in equilibrium with the theoretical drift patterns of two edge wave modes. However they did not

include the feedback between the growing topography and the edge wave field.

For a self-maintaining bar-system, Kirby et al. (1981) presented a numerical model of the interaction between the pre-existing bars and edge waves. They suggested that bars formed at antinodes of normal standing waves tend to trap the antinodes of resonant edge wave modes, leading to maintenance of bar. Also they found that amplification of the edge wave profiles in the offshore region increased with increasing wave period and with distance offshore, suggesting the favorable energy radiation seawards for long-period waves. Although Kirby et al. (1981) provide an approach toward a closer link between sea bed - wave interaction on persisting bar system, their model is not readily applicable the mobile bar system migrating at speed of up to 2.1 m/hr.

The long wave field in the nearshore zone is characterized by a combination of different forms such as forced waves, edge waves, standing waves and seagoing wes. Although complete identification of these long period waves has not yet been achieved, several field observations confirm the presence of standing waves in the surf zone and forced or seagoing waves outside the surf zone (Wright et al., 1982; Symonds et al., 1982; Elgar and Guza, 1985; Huntley and Kim, 1984). Symonds and Bowen (1984) developed a model to predict the resonant conditions for a standing wave solution over the existing topography. Their results show that an amplification in the long wave response occurs when the standing wave has an antinode at the bar crest, providing a mechanism for maintaining the bar under a broad spectrum of forcing by grouped waves. However their results can only apply to a steady state bar system used, rather than examining the response of the barred topography to different wave conditions.

2.5 Discussion

This chapter has reviewed the previous studies on the nearshore wave field and its possible implications for the geomorphologic processes. It is generally observed in nature that the long wave energy takes a significant portion of the total wave energy. Although the long wave field is complex itself in the nearshore, it is characterized by a combination of different forms such as forced waves, edge waves, standing waves and seagoing waves depending upon the main interest of each investigation and the data availability to explore the nature of the wave field. One mode observed clearly and commonly in field experiments is the presence of standing waves, either edge waves or leaky modes, at periods longer than that of incident wind waves.

In a series of attempts to link the characteristic nearshore waves and the nearshore geomorphology, most of investigations have inferred the possible role of the edge waves to the persisting geomorphology instead of providing the fundamental mechanism for the migration processes.

There have been numerous observations of the bar migration in the on-offshore direction. However there are few attempts to explain the mechanisms for that process. With varying wave conditions, the bar profile responds in different way. The approaches to explain the bar formation as a response to breaking process or tidal variation have not been satisfactory. Under many circumstances, the bars are observed well inside the surf zone and even observed in tideless lakes. The approach only using standing edge waves seems to be appropriate in some cases when the nodes or antinodes of specific mode coincide with the bar positions observed in nature. However it has been difficult to confirm

whether a specific mode of edge wave would persist under varying wave conditions as a predominant source of energy responsible for bar formation. Usually the low frequency waves consist of wide-banded energy instead of a single frequency. In this case it might be very difficult to point out the nodes or antinodes responsible for the bar system due to the different positions of nodes of waves at multi-banded frequencies.

Because the temporal and spatial scales of the bar system are larger than those of the incident wind waves, it might be sensible to consider a steady flow such as the streaming velocity induced by the waves as a source energy to move the sediment shoreward or seaward depending on the wave structure. Visually the wind waves are dominant in the nearshore. So the total wave field could be a combination of the wind wave and long wave with different structure across the shore-normal line.

In this study, a numerical investigation to elucidate the mechanism of bar migration under varying wave conditions is presented by using the mass transport velocity in the bottom boundary layer induced by the combination of long waves and wind waves. Also the effect of barred topography on modification of long waves is examined. It has been felt that a fundamental understanding of the mechanism of bar migration is needed urgently rather than setting up a morphological model based on a sort of 'guess work' on spurious coefficients, particularly in the nearshore where the hydrodynamic system is so complex.

CHAPTER 3

INFLUENCE OF NEARSHORE WAVES ON LONGSHORE BAR FORMATION

3.1 Introduction

To consider the interaction of waves and the barred topography in the nearshore, it is necessary to know (1) the nature of the steady flows induced by the nearshore wave field, and (2) the effects of the barred topography on the wave field through dissipation of wave energy and/or frequency selection to fit the resonant conditions of the barred topography and the preferred wave modes. Chapter 2 has provided a general description of the nearshore wave field and its morphologic implications. However, detailed mechanisms for the generation of barred topography and the feedback from the topography to the waves have been very scare, so that there is little in the way of a direct prediction for the behavior of the longshore bars in connection with the wave climate.

The purpose of the present chapter is to examine the mechanism of the longshore bar formation by the mass transport induced by the nearshore wave field, addressing the wave field on plane sloping beaches and consequent distribution of mass transport velocities in the bottom boundary layer. Based on the wave field combined with long waves at surf-beat frequencies and wind waves, the mass transport has been determined on gently sloping bottoms. The present approach is different from the previous investigations which are described in Chapter 2 by taking into account the wave field including the effects of long waves

and breaking waves based on field observations and laboratory experiments in and outside the surf zone. Hence the considerations are not limited to the offshore region.

To provide an understanding of the bar migration it is necessary to consider the effects of the barred topography on the wave-flows. The investigation of the bar formation due to the nearshore waves will provide a basic idea to examine the bar migration and the feedback which will be addressed in later chapters.

In this chapter, (1) the mass transport velocity induced by waves in the bottom boundary layer is defined, (2) the nearshore waves are modeled, (3) the mass transport velocities of each wave mode in the bottom boundary layer are derived and finally (4) the distributions of mass transport and shear stresses in the near-bottom across a shore-normal line are predicted and their implications for the longshore bar formation are discussed.

3.2 Definitions and Basic Concepts

This section predicts the behavior of wave-induced mass transport in the bottom boundary layer. We will adopt a local coordinate system (x,z) with x in the direction of wind wave propagation and z pointing upward normal to the surface. For small bottom slopes, z is nearly in the vertical direction. Water depth is variable only in the x-direction. Thus all of the physical quantities are assumed uniform in the y-direction (horizontally normal to the x-direction).

Under these idealized conditions, the boundary layer approximation of the horizontal momentum equation takes the form

$$\frac{\partial u}{\partial t} + u \frac{\partial u}{\partial x} + w \frac{\partial u}{\partial z} = -\frac{1}{\rho} \frac{\partial p}{\partial x} + \nu_m \frac{\partial^2 u}{\partial z^2} \qquad (3.1)$$

and the continuity requires

$$\frac{\partial u}{\partial x} + \frac{\partial w}{\partial z} = 0 \tag{3.2}$$

where u and w are the horizontal and vertical velocities in the bottom boundary layer respectively, and p is the pressure. The vertical eddy viscosity ν_m that is contributed by the molecular kinematic viscosity (ν) mainly near the bottom and the eddy viscosity (ν_t) away from the bottom, is assumed to be constant to yield a constant total stress such that $\tau = (\nu + \nu_t) \frac{\partial u}{\partial z} = \nu_m \frac{\partial u}{\partial z}$. This means that the viscous stress close to the bed must match up with the Reynolds stress further out. The pressure gradient in the thin boundary layer at the bottom is assumed to be the same as the pressure gradient just outside the boundary layer. Consequently

$$-\frac{1}{\rho}\frac{\partial p}{\partial x} = -\frac{\partial U_1}{\partial t} + U_1 \frac{\partial U_1}{\partial x} \tag{3.3}$$

where U_1 is the tangential component of the inviscid velocity field.

When the wave steepness ka is sufficiently small, we can expand a variable into a power series;

$$u = \epsilon u_1 + \epsilon^2 u_2 + \ldots\ldots \tag{3.4}$$

where ϵ =ka, k wave number and a is the wave amplitude. The first-order term corresponds to the basic oscillatory component and the second-order term consists of the steady residual and the second-harmonics.

At the first order, equations (3.1) and(3.2) with equation (3.3) give

$$\frac{\partial u_1}{\partial t} = \frac{\partial U_1}{\partial t} + \nu_m \frac{\partial^2 u_1}{\partial z^2} \tag{3.5}$$

$$\frac{\partial u_1}{\partial x} + \frac{\partial w_1}{\partial z} = 0 \qquad (3.6)$$

The boundary conditions are

$$u_1 = w_1 = 0 \quad \text{on } z=0$$

$$u_1 = U_1 \quad \text{when } z \gg \delta$$

where the Stokes boundary layer $\delta = \sqrt{2\ \nu_m/\sigma}$ and σ is the radian frequency.

The mainstream is taken to be a small-amplitude oscillatory flow and represented by the real part of

$$U_1(x,t) = \text{REAL}\ [\ U_o(x)\ e^{-i\sigma t}\ ]. \qquad (3.7)$$

At the first order, the u_1 of equation (3.5) in the bottom boundary layer is given as

$$u_1(x,z,t) = \text{REAL}\ [U_o(x)\ F(\zeta)\ e^{-i\sigma t}] \qquad (3.8)$$

where $F(\zeta) = 1 - e^{-(1-i)\zeta},\ \zeta = z/\delta$. (3.9)

At the next order, the momentum equation is

$$\frac{\partial u_2}{\partial t} - \frac{\partial^2 u_2}{\partial z^2} = U_1 \frac{\partial U_1}{\partial x} - \left(u_1 \frac{\partial u_1}{\partial x} + w_1 \frac{\partial u_1}{\partial z}\right) \qquad (3.10)$$

Inspection of the equation (3.10) leads to the second-order velocity u_2 into

$$u_2(x,z,t) = \bar{u}_E + \text{REAL}\ [\tilde{u}_2 e^{-2i\sigma t}] \qquad (3.11)$$

where $\bar{u}_E$ is the induced-streaming velocity and $\tilde{u}_2$ is the oscillatory flow which is overshadowed by u_1.

Substituting (3.11) into (3.10) and taking the average over the period give

$$-\nu_m \frac{\partial^2 \tilde{u}_E}{\partial z^2} = \overline{U_1 \frac{\partial U_1}{\partial x}} - \left(\overline{u_1 \frac{\partial u_1}{\partial x}} + \overline{w_1 \frac{\partial u_1}{\partial z}} \right)$$

$$- \overline{U_1 \frac{\partial U_1}{\partial x}} - \left(\frac{\partial}{\partial x} \overline{u_1 u_1} + \frac{\partial}{\partial z} \overline{u_1 w_1} \right) \qquad (3.12)$$

Equation (3.12) describes that the steady streaming $\tilde{u}_E$ arises because a mean shear-stress field must be present in order to balance the dynamic pressure field and the Reynolds stress field.

The boundary conditions are

$$\tilde{u}_E = 0 \quad \text{at } z = 0$$

$$\frac{\partial}{\partial z} (\tilde{u}_E) \longrightarrow 0 \quad \text{as } z/\delta \longrightarrow \infty \ . \qquad (3.13)$$

By means of substitution, one can obtain the solution of u_2 as

$$u_2(x,z) = \tilde{u}_E(x,z) = -\frac{1}{\sigma} \text{REAL} \left[F_2(\xi)\, U_o(x) \frac{\partial U_o^*}{\partial x} \right] \qquad (3.14)$$

where $F_2(\xi) = -\frac{1}{2}(1-3i)e^{(-1+i)\xi} - \frac{i}{2} e^{-(1+i)\xi}$

$$- \frac{1+i}{4} e^{-2\xi} + \frac{1}{2}(1+i)\,\xi e^{(-1+i)\xi} + \frac{3}{4}(1-i) \qquad (3.15)$$

and * denotes the complex conjugate.

The solution (3.14) represents the Eulerian streaming velocity which has been derived at the outer edge of the boundary by Hunt and Johns (1963).

It is well understood that the mass transport velocity consists of the Eulerian streaming velocity and the Stokes drift arising from the uncloseness of the water particle path. The Stokes' drift is given as

$$\int \left[\overline{u_1 (x,t)\, dt} \right] \cdot \nabla u_1 (x,t) \qquad (3.16)$$

With the aid of Equation (3.8), the Stokes' component is

$$\tilde{u}_S = \text{REAL}\left[\frac{i}{2\sigma}\left[Uo\,\frac{\partial\, Uo^*}{\partial\, x}\left(1 - e^{-(1-i)\xi} - e^{-(1+i)\xi} + e^{-2\xi}\right)\right]\right] \quad (3.17)$$

The Lagrangian mass transport velocity with the alongshore homogeneity throughout the boundary layer is

$$\tilde{U} = \tilde{u}_E + \tilde{u}_S$$

$$= \frac{1}{4\sigma}\,\text{REAL}\left[\,F_5(\xi)\,Uo\,\frac{\partial\, Uo^*}{\partial\, x}\,\right] \quad (3.18)$$

where $F_5(\xi) = -8i\,e^{-(1-i)\xi} + 3(1+i)\,e^{-2\xi} - 3 + 5i$ (3.19)

which is due to Carter et al. (1973).

The function $F_5(\xi)$ describes the momentum transfer process through the boundary layer. The real and imaginary parts of $F_5(\xi)$ are shown in Figure 3.1. It is noticeable that the mass transport velocity in the bottom boundary layer depends on the nondimensional vertical length scale $\xi = z/\delta$, where $\delta = \sqrt{2\ \nu_m/\sigma}$. In reality, the thickness of the Stokes boundary layer δ is a function of the vertical viscosity ν_m and the wave frequency σ . The mean value of eddy viscosity in turbulent flow suggested by Kajiura (1968) in the outer layer is $\nu_m = 0.05\ \kappa\ u^{*2}/\sigma$, which yields ν_m on the order of 1 cm^2/s with $\kappa = 0.4$, typical $u^* = 5$ cm/s and $\sigma = 0.52$ rad. For the case of turbulent flow with eddy viscosity $\nu_m = 100\ \nu_{laminar} = 1\ cm^2/sec$ (Carter et al., 1973) and $\sigma = 0.125$ rad (infragravity wave), $\delta = \sqrt{2\ \nu_m/\sigma} = 4.0$ cm; while for wind waves with $\sigma = 0.628$ rad, $\delta = 1.9$ cm.

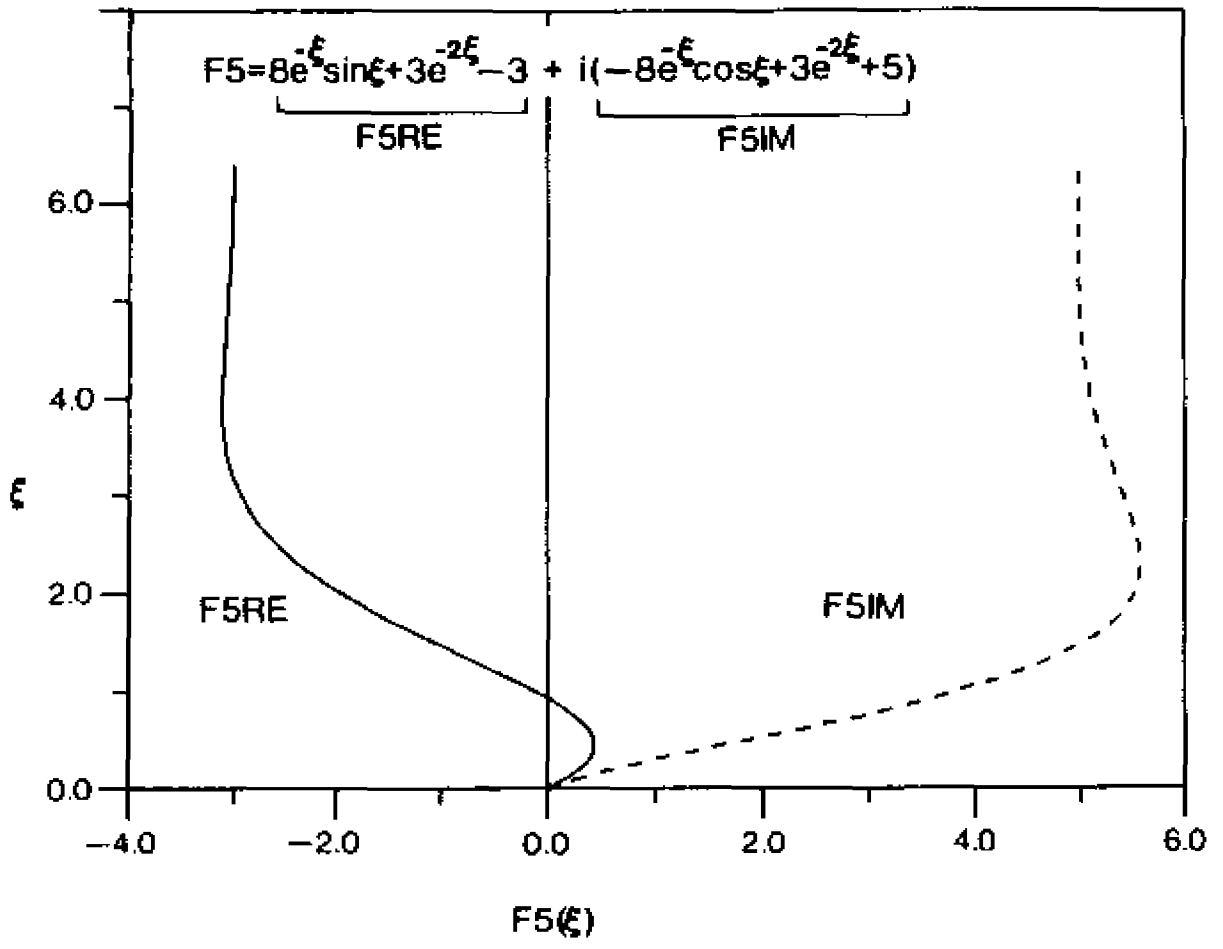

Figure 3.1: Vertical structure of the momentum transfer function F_5 given in Equation (3.19). F5RE represents the real part of the function and F5IM is of the imaginary part. The vertical scale is of a nondimensional length $\xi = z/\delta$ where the Stokes' layer thickness $\delta = (2\nu_m/\sigma)^{1/2}$.

If we define the total boundary layer as the layer from the surface to the point where $u = 0.99\ U_o$, we expect the free stream flow occurs at about $\xi = 5$ (Fig. 3.1). This corresponds to the total boundary layer of the steady flow induced by a wave with period of 50 sec to be about 20 cm; by a wave with period of 10 sec to be 9 cm.

3.3 Wave Field in the Nearshore

The behavior of waves on sloping beaches has received extensive theoretical work, laboratory and field experiments. Most investigations have been confined to the linearized approach which is invalid near the shoreline. Based on the linear theory, the progressive waves climbing a sloping beach are shoaling, breaking and eventually dissipating. The processes of wave shoaling on a nonuniform bottom are well documented while the characteristic shapes of water surface fluctuation in the surf zone are largely depending on the laboratory experiments (e.g., Dally et al., 1985).

Carrier and Greenspan (1958) presented an analysis based on the non-linear shallow water theory and obtained explicit solutions for waves that climb a sloping beach without breaking. A number of long waves such as long swell, edge waves and tsunami with very small wave steepness ($\varepsilon = \frac{a}{L} << 1$) are in the range where breaking does not occur. The presence of these nonbreaking long waves on the natural beach has been confirmed by numerous field observations as described in Chapter 2.

3.3.1 The Long Wave Field

We consider a coordinate system x, z such that $z = -h_o(x)$ denotes the bottom and $z = \eta(x,t)$ the water surface. Hence the total depth $h(x,t)$ is

$$h(x,t) = h_o(x) + \eta(x,t). \tag{3.20}$$

The origin of $x = 0$ is set at the mean shoreline with the positive direction toward offshore. Also we consider a sloping beach with the beach slope β to the horizontal so that $h_o(x) = x \tan \beta$, where β is assumed to be small so that the linearized shallow theory can be applied.

The problem has been solved by Carrier and Greenspan (1958) and Whitham (1979). We recall that the governing equations for the flow of shallow water over a nonuniform bottom using the mass and momentum conservations are

$$h_t + U h_x + h U_x = 0 \tag{3.21a}$$

$$U_t + U U_x + g \eta_x = 0 \tag{3.21b}$$

$$h = h_o + \eta \tag{3.21c}$$

where the subscripts t and x represent the derivatives with respect to the time and horizontal coordinate x respectively, and U is the water particle velocity in the interior of water column.

We assume $\frac{\eta}{h_o} = O(\varepsilon)$, $\frac{U}{\sqrt{gh_o}} = O(\varepsilon)$ and $UU_x = O(\varepsilon^2)$, where $\varepsilon \ll 1$. Introducing the velocity potential $\phi(x,z,t)$ such that $U = \frac{\partial \phi}{\partial x}$ and $\eta = -\frac{1}{g}\frac{\partial \phi}{\partial t}$ leads to a linear first-order approximation as

$$\phi_{tt} = g\beta x \phi_{xx} + g\beta\phi_x \tag{3.22}$$

Let $\phi = N(x)\, e^{-i\sigma t}$, then we obtain a complete solution as

$$\phi(x,t) = \left\{ A J_0\left(\sqrt{\frac{4\sigma^2 x}{g\beta}}\right) - iBY_0\left(\sqrt{\frac{4\sigma^2 x}{g\beta}}\right)\right\} e^{-i\sigma t} \quad , \qquad (3.23)$$

where J_0 and Y_0 are the zero-order Bessel functions of the first kind and of the second kind respectively.

When B = 0, we have the case of perfect reflection to yield a <u>standing</u> wave solution with

$$\phi_{std} = \frac{ag}{\sigma} J_0(\chi)\, e^{-i\sigma t} \qquad (3.24)$$

$$\text{where } \chi = \sqrt{\frac{4\sigma^2 x}{g\beta}} \quad . \qquad (3.25)$$

For A = B, there is no reflection, we have purely <u>incoming</u> wave with

$$\phi_{in} = \frac{1}{2}\ \frac{ag}{\sigma}\left\{ J_0(\chi) - i\, Y_0(\chi)\right\} e^{-i\sigma t} \qquad (3.26)$$

For A = -B, a purely <u>outgoing</u> wave solution is obtained as

$$\phi_{out} = \frac{1}{2}\ \frac{ag}{\sigma}\left\{ J_0(\chi) + i\, Y_0(\chi)\right\} e^{-i\sigma t} \qquad (3.27)$$

The amplitude of each solution has been obtained so that the amplitude of standing wave at the shoreline is to be $\eta = a$ at $x = 0$. The standing wave is resulted by the superposition of two progressive waves propagating in the opposite direction.

The free surface displacements and the shore-normal velocities are;

i) Standing waves

$$\eta_{std} = a\, J_0(\chi)\, \sin\sigma t \tag{3.28a}$$

$$U_{std} = -\, a\sqrt{\frac{g}{\beta x}}\, J_1(\chi)\, e^{-i\sigma t} \tag{3.28b}$$

ii) Incoming waves

$$\eta_{in} = \frac{1}{2}\, a\, \{\, J_0(\chi)\, \sin\sigma t + Y_0(\chi)\, \cos\sigma t\} \tag{3.29a}$$

$$U_{in} = \frac{1}{2}\, a\sqrt{\frac{g}{\beta x}}\, \{\, -J_1(\chi) + i\, Y_1(\chi)\, \}\, e^{-i\sigma t} \tag{3.29b}$$

iii) Outgoing waves

$$\eta_{out} = \frac{1}{2}\, a\, \{\, J_0(\chi)\, \sin\sigma t - Y_0(\chi)\, \cos\sigma t\} \tag{3.30a}$$

$$U_{out} = \frac{1}{2}\, a\sqrt{\frac{g}{\beta x}}\, \{\, -J_1(\chi) - i\, Y_1(\chi)\}\, e^{-i\sigma t} \tag{3.30b}$$

,where $J_1(\chi)$ and $Y_1(\chi)$ are the first-order Bessel functions of the first and second kinds respectively.

Figure 3.2 represents these Bessel functions along the nondimensional distance χ . It is noticeable that the function Y's are singular at the shoreline. For progressive waves without breaking, the use of the solution to present the wave structure near the shoreline is limited. However we are fortunate since the surface fluctuation at surf-beat frequencies in the surf zone is dominated by the standing waves which are represented by a bounded and regular solution of Equation (3.28a and 3.28b).

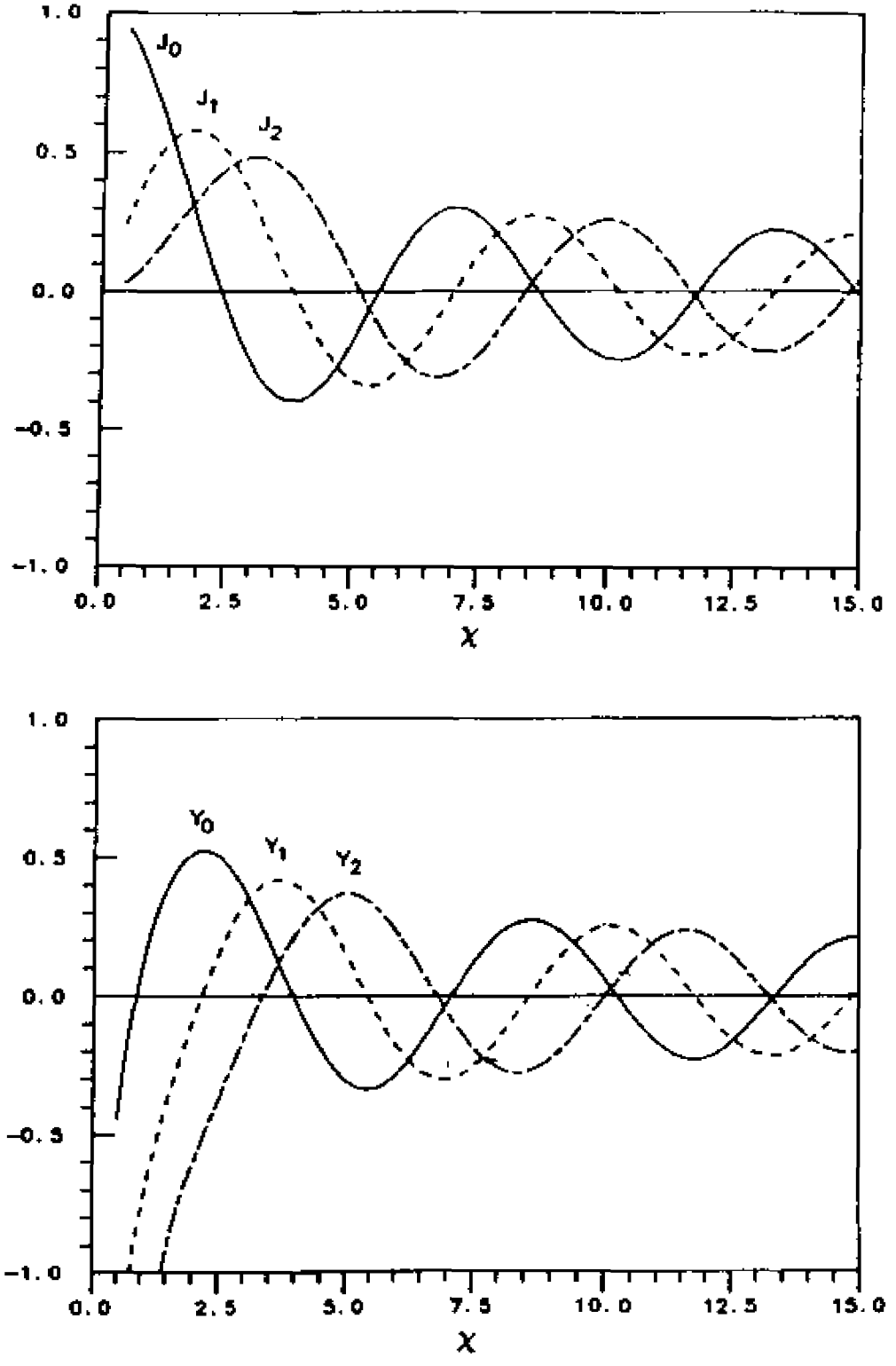

Figure 3.2: Offshore behavior of Bessel functions along a nondimensional offshore distance χ. The upper plot is Bessel functions of the first kind and the lower one is for the second kind. The second kinds have a singularity near the shoreline ($\chi = 0$).

3.3.2 Wind Wave Field

The solutionn of the small-amplitude wave theory have been widely used for application to numerous problems of coastal engineering and physical oceanographic interest. It is evident from observation that the wind waves propagating into shallow water undergo dramatic transformation in height, wave number and consequently wave energy. Modification of wind waves up to the breaking point has been rather well determined; However the wave height in the surf zone has been assumed to be saturated by local water depth or decreased exponentially from the breaking point (Dally et al., 1985).

In this section, a commonly accepted wave transformation is adopted to describe wind wave transformation in the nearshore. The algorithm developed by Ebersole et al. (1986) appears to provide a reasonable prediction of wave transformation across plane and barred beaches. The transformation algorithm outside the surf zone uses the equations of water waves accounting for the refraction and diffraction processes derived by Berkhoff (1976). Inside the surf zone, energy dissipation rate proposed by Dally et al. (1984) is incorporated into the conservation of wave energy equation. The incipient breaking wave height developed by Weggel (1972), which is a function of deepwater wave period and bottom slope has been selected for use in the algorithm. The algorithm by Ebersole et al. (1986) has been verified using several field and laboratory data on plane, stepped and barred beaches. The results reveal that the algorithm predicts wave transformation quite good even the case of multiple breaking and reformation (Figure 3.3).

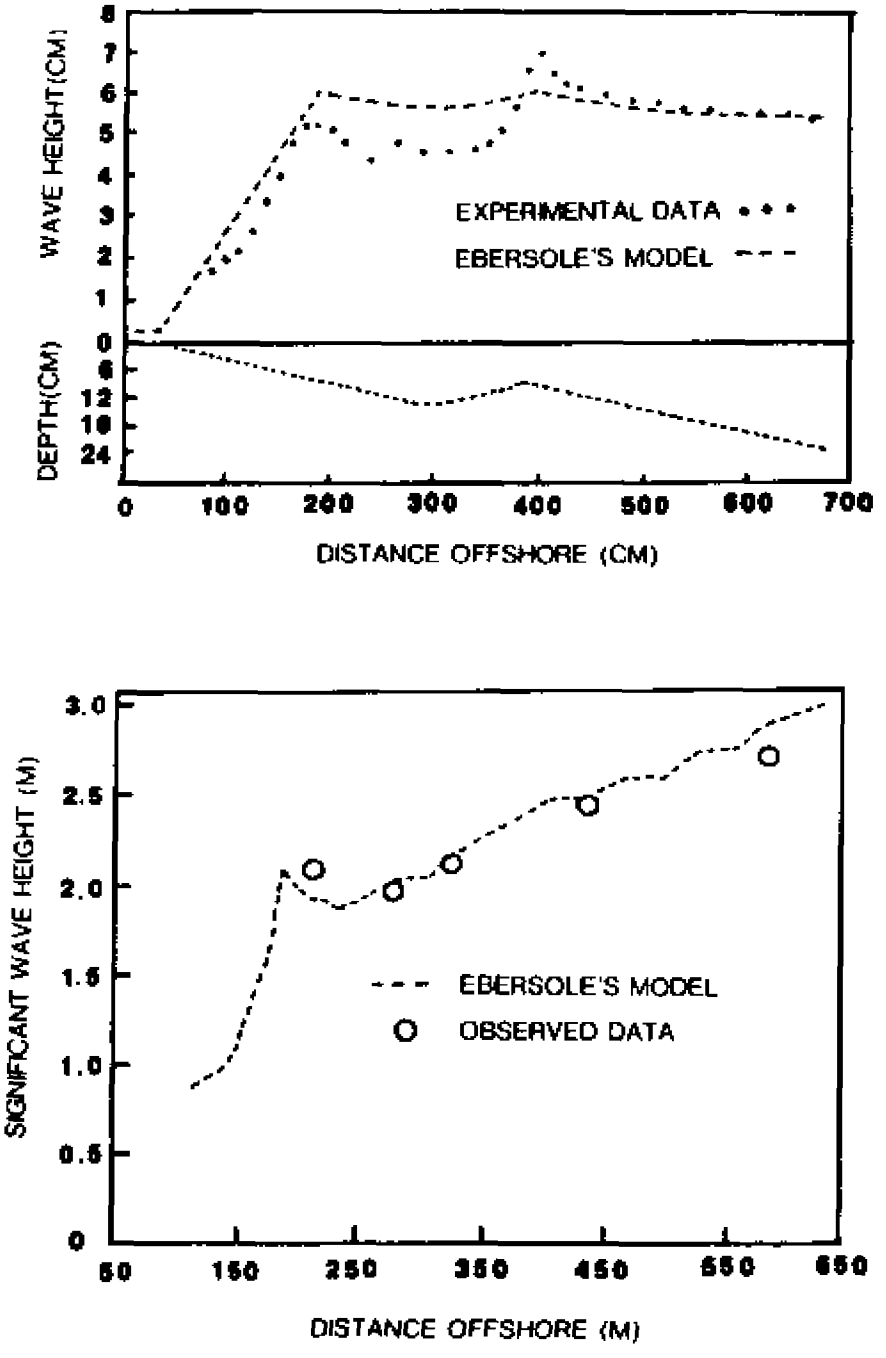

Figure 3.3: Comparison between experimental data / observed data and Ebersole's model results for wind wave transformation in the nearshore. The experimental data is Izumiya's Laboratory Experiment and the observed data is collected at Field Research Facilities of CERC at Duck, North Carolina. The Ebersole's algorithm is adopted in this study to estimate the wave transformation, which predicts wave transformation in and outside the surf zone as well as incipient breaking quite reasonably.

In the present study, the algorithm of Ebersole et al. (1986) has been implemented on plane and barred beaches to obtain the wind wave parameters across the shore-normal direction. The wave parameters which are a function of the offshore distance are used to estimate the spatial distribution of mass transport velocities which is combined with those induced by long period waves at surf-beat frequencies.

3.4 Mass Transport Distribution in the Bottom Boundary Layer

3.4.1 Long Waves

By equation (3.7), let $U(x,t) = \text{REAL}\,[Uo(x)\, e^{-i\sigma t}]$. Then we get the mass transport velocity in the bottom boundary layer according to equation (3.18).

i) Standing waves

$$\bar{U} = \frac{a^2\sigma^3}{g\beta^3\chi^3}\left[(-8\,e^{-\xi}\sin\xi - 3e^{-2\xi} + 3)\left(\frac{2\,J_1^2(\chi)}{\chi} + J_1(J_2 - J_0)\right)\right] \tag{3.31}$$

ii) Incoming waves

$$\bar{U} = \frac{a^2\sigma^3}{4g\beta^3\chi^3}\left[(-8e^{-\xi}\sin\xi - 3e^{-2\xi}+3)\left(\frac{2(J_1^2+Y_1^2)}{\chi} + J_1(J_2-J_0)+Y_1(Y_2-Y_0)\right)\right.$$

$$\left. + (-8e^{-\xi}\cos\xi + 3e^{-2\xi} +5)\,\left(\,J_1(Y_2-Y_0) - Y_1(J_2 - J_0)\right)\right] \tag{3.32}$$

iii) Outgoing waves

$$\bar{U} = \frac{a^2 \sigma^3}{4g\beta^3 \chi^3} \left[(-8e^{-\xi}\sin\xi - 3e^{-2\xi} + 3)\left\{\frac{2(J_1^2+Y_1^2)}{\chi} + J_1(J_2-J_0)+Y_1(Y_2-Y_0)\right\}\right.$$

$$\left. + (8e^{-\xi}\cos\xi - 3e^{-2\xi} - 5)\ (J_1(Y_2-Y_0) - Y_1(J_2 - J_0))\right] \qquad (3.33)$$

The mass transport velocities at the outer edge of the bottom boundary layer are obtained by substituting $\xi = z/\delta \longrightarrow \infty$ into the equations (3.31) - (3.33). Figure 3.4 shows the nondimensional mass transport velocities at the outer edge of the boundary in the form of $\bar{U} / (a^2 \sigma^3 / 4g \beta^3 \chi^3)$ along χ . The mass transport velocities of the standing wave at the outer edge of the boundary layer show the alternation of offshore and onshore directions depending on the position of the nodes and antinodes (see the J_0 solution in Figure 3.2). The boundary flows of the incoming and outgoing waves have the same direction as the direction of the wave propagation. This fact is consistent with the earlier investigations for the horizontal bottom (Longuet-Higgins, 1953, Carter et al., 1973). The results of the present study are distinct from the earlier ones by allowing the wave amplitude to vary toward the shoreline, accounting for the effect of the amplitude gradient along the wave propagation as suggested by Bijker et al. (1974).

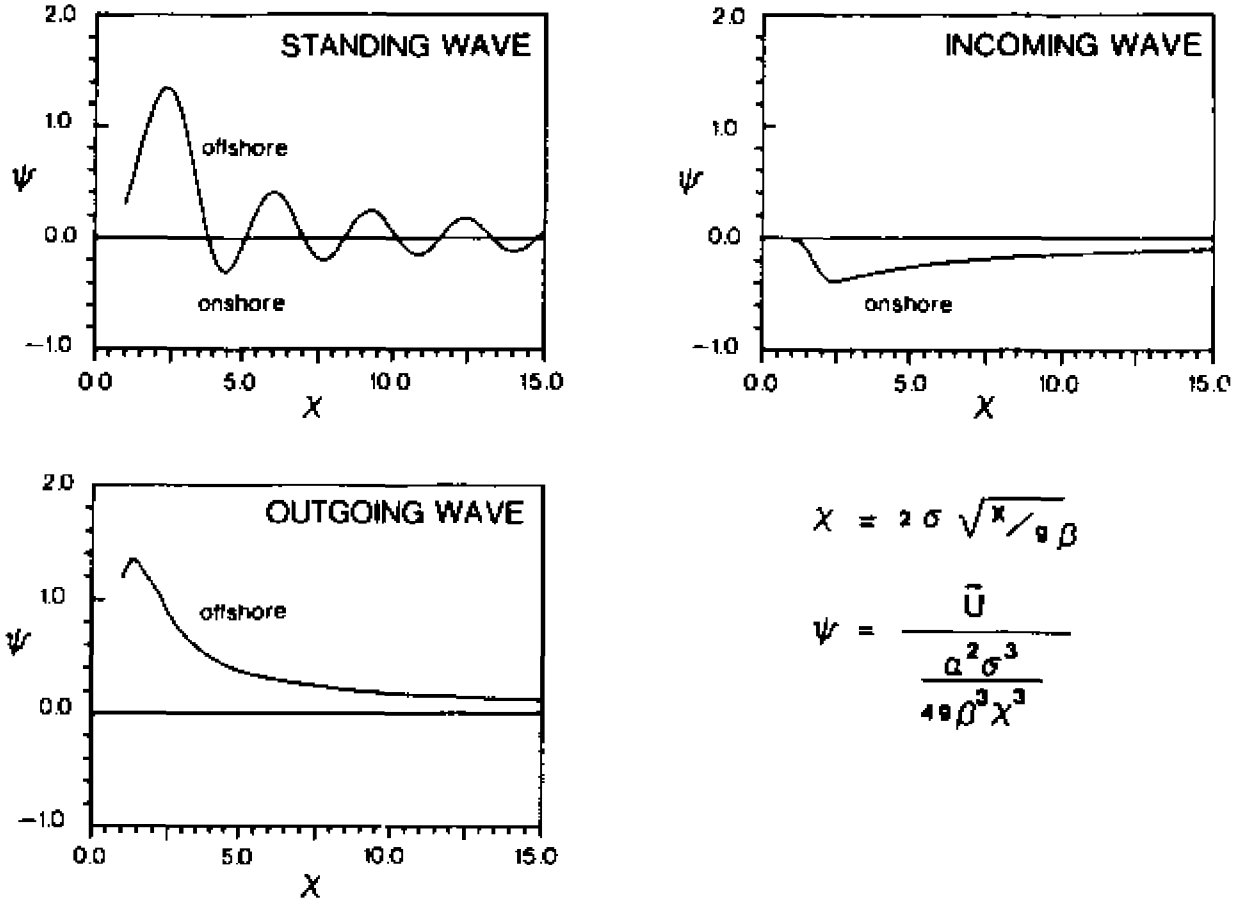

$$\chi = 2\sigma\sqrt{x/g\beta}$$

$$\psi = \frac{\tilde{U}}{\frac{\alpha^2\sigma^3}{4g\beta^3\chi^3}}$$

Figure 3.4: Nondimensional mass transport velocity (ψ) of each long wave at the outer edge of the bottom boundary layer along a nondimensional offshore distance χ. For standing waves, ψ changes its direction at every half wavelength while for progressive waves ψ has the same direction with wave propagation (the shoreline at $\chi = 0$).

Figure 3.5 shows the vertical structure of the nondimensional mass transport velocity inside the bottom boundary layer induced by a standing wave. This structure is characterized by the convection-cell type of convergence and divergence at antinodes and nodes, which is consistent with the conceptual diagram in Figure 2.4.b. However the dimensional value of $\hat{U}$ near the shoreline has a large value because of the small value of X . The direction of the boundary flow in the lower most layer is opposite to that in the upper part and the magnitude in the upper layer is much bigger than that in the lower part. Among two different processes of sediment transport by bed-load and suspension, many observations showed that the suspended transport is much significant in the surf zone due to the effects of long waves.

It has been observed on natural beaches that long waves in the nearshore zone consist of incoming waves, standing waves or outgoing waves as described in Chapter 2. A standing wave could be considered as a phase-locked superposition of incoming and outgoing waves. The incoming waves could take an energy source from the set-down in the incident wave groups (Longuet-Higgins and Stewart, 1962) and the outgoing waves be generated by the pure reflection or by the time-varying breaking points (Symonds et al., 1982). The standing wave structures along the shore-normal line are either leaky modes or edge waves of high mode.

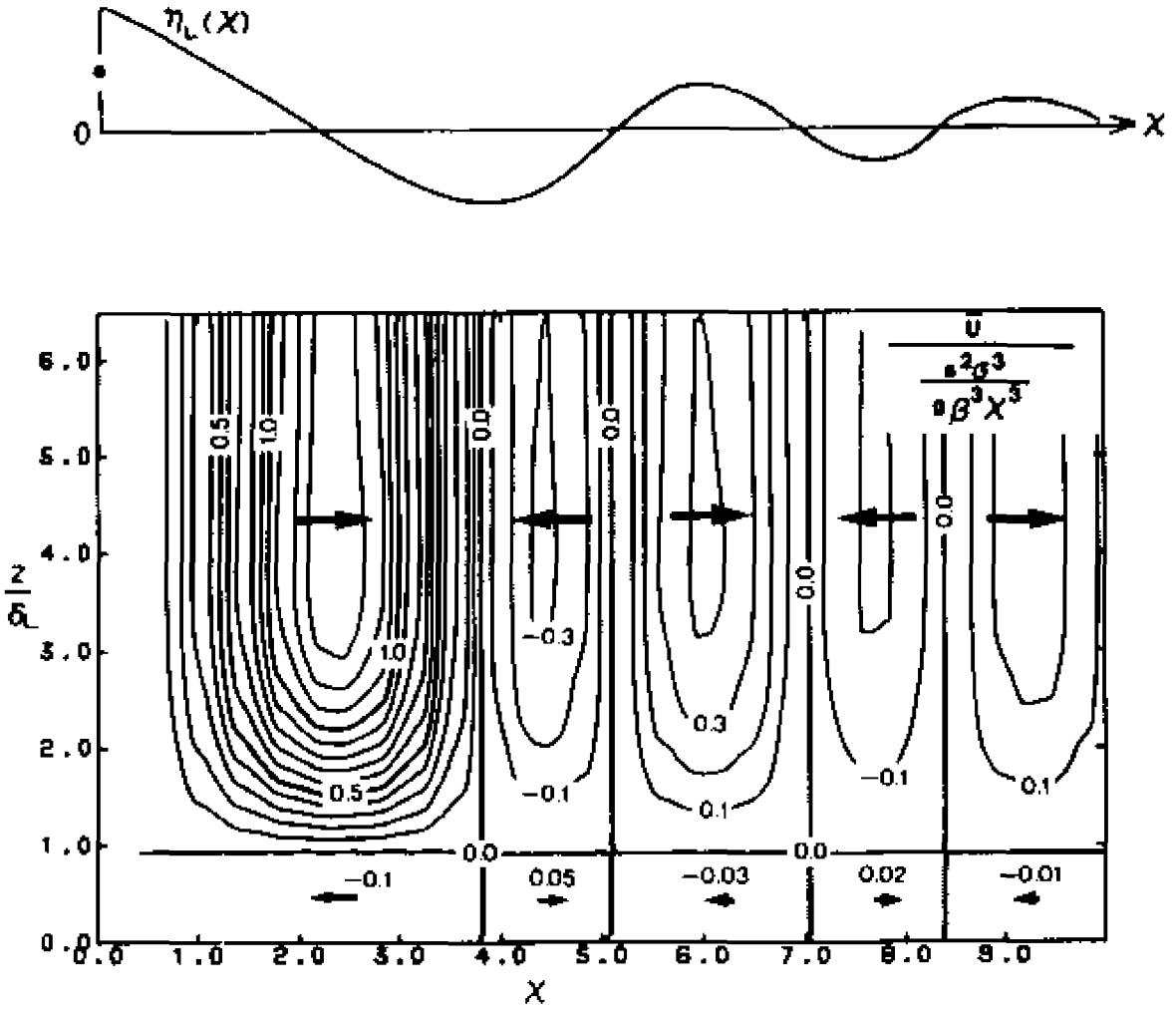

Figure 3.5: The vertical contour plot of the mass transport velocity in the bottom layer induced by a standing wave with the elevation $\eta_L(X)$ shown on top. This structure is characterized by the convection-cell type of convergence and divergence at nodes and antinodes. It is noticeable that the net direction of the bottom flow in the lower most layer is opposite to that in the upper layer, suggesting some different sediment transport processes in the bottom boundary layer.

Let us consider a wave field consisting of two waves, the incoming wave η_{in} propagating in the negative x direction and the outgoing wave η_{out} propagating in the positive x direction from the shoreline. The incoming wave is assumed to be reflected back at the shoreline to form a pure standing wave or a partial standing wave with phase difference. Then the total long-wave field can be superposed with Equations (3.29) and (3.30) through introduction of the reflection coefficient R and is given as;

$$\Phi = \Phi_{in} + \Phi_{out}$$

$$= \frac{a g}{2\sigma} [(J_0 - iY_0) + R(J_0 + iY_0) e^{-i\theta}] e^{-i\sigma t} \qquad (3.34)$$

where θ is the phase difference between the incoming and outgoing waves. With R = 1 and $\theta = 0$, we get the pure standing wave solution as of Equation (3.28), and with R = 0 the pure incoming wave of Equation (3.29) is obtained. The consequent surface fluctuation and the amplitude function of free stream velocity Uo(x) are given as

$$\eta = \eta_{in} + \eta_{out}$$

$$= \frac{a i}{2} [(J_0 - iY_0) + R(J_0 + iY_0) e^{-i\theta}] e^{-i\sigma t} \qquad (3.35)$$

$$Uo(x) = \frac{a}{2} \left(\frac{g}{\beta x} \right)^{1/2} [(-J_1 + iY_1) - R(J_1 + iY_1) e^{-i\theta}] \qquad (3.36)$$

where all the Bessel functions are function of the nondimensional offshore distance $\chi = (4\sigma^2 x / g\beta)^{1/2}$ as before. After some algebra, we get the mass-transport velocity distribution in the bottom boundary layer as

$$\tilde{U} = \text{REAL}\ \Big[\frac{-a^2\sigma^3}{4g\beta^3\chi^3} F_5(\xi)\ \Big[\ \frac{2(J_1^2+Y_1^2)}{\chi} + J_1(J_2-J_0) + Y_1(Y_2-Y_0)$$

$$+ i\ \{\ J_1(Y_2-Y_0) - Y_1(J_2-J_0)\}$$

$$+ R^2\ \Big[\ \frac{2(J_1^2+Y_1^2)}{\chi} + J_1(J_2-J_0) + Y_1(Y_2-Y_0)$$

$$- i\ \{\ J_1(Y_2-Y_0) - Y_1(J_2-J_0)\}\Big]$$

$$+ R\, e^{i\theta}\Big[\ \frac{2(J_1^2-Y_1^2)}{\chi} + J_1(J_2-J_0) - Y_1(Y_2-Y_0)$$

$$- i\ \{\ 2J_1Y_1 + J_1(Y_2-Y_0) + Y_1(J_2-J_0)\}\Big]$$

$$+ R\, e^{-i\theta}\Big[\frac{2(J_1^2 - Y_1^2)}{\chi} + J_1(J_2-J_0) - Y_1(Y_2-Y_0)$$

$$+ i\ \{\ 2J_1Y_1 + J_1(Y_2 - Y_0) + Y_1(J_2-J_0)\}\Big]\Big]$$

$$- (\ \tilde{U}\ )_{in} + R^2\ (\ \tilde{U}\ )_{out}$$

$$+ \text{REAL}\ \Big[\ \frac{-2a^2\sigma^3}{4g\beta^3\chi^3} F_5(\xi)\ R\ \Big[\ \cos\theta\ \{\frac{2(J_1^2-Y_1^2)}{\chi} + J_1(J_2-J_0) - Y_1(Y_2-Y_0)\}$$

$$+ \sin\theta\ (\ 2J_1Y_1 + J_1(Y_2-Y_0) + Y_1(J_2-J_0)\}\Big]\Big] \qquad (3.37)$$

The phase difference between the incoming and outgoing waves has been suggested to be $\theta = 0$ by the study of swash done by Guza et al. (1984), presenting that the vertical swash amplitude is twice the amplitude of long wave at surf-beat frequencies at the shoreline. When $R = 1$ and $\theta = 0$, we obtain the pure standing wave solution of Equation (3.31).

3.4.2 Wind Waves

The parameters of wind waves in the nearshore have been obtained on plane beaches by using the transformation algorithm developed by Ebersole et al. (1986). Based on the wave parameters estimated at positions across the shore-normal direction, the mass transport velocities are calculated with Equations (3.18) and (3.19). Equation (3.18) can be rewritten in H(x) and h(x) by using the dispersion relation,

$$\bar{U} = \frac{k \sigma a^2}{4 \sinh^2 kh} \left(8 e^{-\xi} \cos \xi - 3 e^{-2\xi} - 5\right)$$

$$= \frac{(gh(x))^{1/2} H(x)^2}{16 h(x)^2} \left(8 e^{-\xi} \cos \xi - 3 e^{-2\xi} - 5\right) \qquad (3.38)$$

, where a is the amplitude of water fluctuation of a progressive wave.

The orbital velocity of shallow water waves can be written as $u(x,t) = \frac{a\sigma}{\sinh kh} \sin(kx - \sigma t)$ to the first approximation. The maximum velocity is $u_{max} \simeq \frac{a\sigma}{kh}$. Comparing the maximum orbital velocity u_{max} with the mass transport velocity $\bar{U}$ at the outer edge of the boundary layer yields $\left|\frac{\bar{U}}{u_{max}}\right| \simeq \frac{5}{4}\frac{a}{h}$, which is valid for $ak \ll 1$. At the breaker point where $a \simeq 0.4\ h$, the $\bar{U}$ is about 50 % of the maximum orbital velocity, which is a subject of a systematic comparison between wave theories as for the breaking wave kinematics. It is assumed that drift velocity for incident waves is not influenced by wave breaking. Since the horizontal velocity gradient along wave propagation provides the magnitude of the mass transport velocity (Equation 3.19), the present study uses the Equation (3.38) to determine the mass transport velocity due to the wind waves.

3.4.3 The Boundary Layer Induced by the Combined Waves

Consider a steady train of waves progressing in still water which is contacting with sea bed. In the immediate neighborhood of the bottom, where the velocity is very much different from the velocity at infinite, the flow is determined practically by the action of kinematic or eddy viscosities depending upon the flow conditions. The thickness of the boundary layer may be defined arbitrarily as the distance from the bed where the velocity differs by 1 % from the velocity of the outer potential flow.

The turbulent flow counterpart of Equation (3.1) on the boundary layer approximation is

$$\frac{\partial u}{\partial t} + u \frac{\partial u}{\partial x} + w \frac{\partial u}{\partial z} = - \frac{1}{\rho} \frac{\partial p}{\partial x} + \nu \frac{\partial^2 u}{\partial z^2} - \frac{\partial}{\partial z} (\overline{u' w'}) \qquad (3.39)$$

where (') denotes the fluctuating components of velocity from the mean value.

The instantaneous shear stress is obtained by

$$\frac{\tau}{\rho} = \nu \frac{\partial u}{\partial z} - \overline{u' w'} = (\nu + \nu_t) \frac{\partial u}{\partial z} = \nu_m \frac{\partial u}{\partial z} \qquad (3.40)$$

where ν is the kinematic viscosity , ν_t is the eddy viscosity which is generally a function of both distance above the boundary and time, and ν_m is the 'effective' eddy viscosity which is the sum of ν and ν_t. However since the mass transport velocity is originated its driving force from the kinematic viscosity very near the wall, for the present formulation the eddy viscosity is assumed time invariant.

Appropriate conditions are specified as

$$u = 0, \ \nu_t = 0 \quad \text{at } z = z_o$$

$$u = U_1 \ , \ \nu \ll \nu_t \ , \ \frac{\partial \nu_t}{\partial z} = 0 \quad \text{at } z \longrightarrow \infty \qquad (3.41)$$

where z_o is the bed roughness length defined by $z_o = k_b/30$, k_b is the equivalent Nikuradse roughness which corresponds to the level of the top of the roughness scale.

The maximum wall stress τ_o is defined as

$$\frac{\tau_o}{\rho} = \nu_m \left. \frac{\partial u}{\partial z} \right|_{z=z_o} \tag{3.42}$$

and the flow in the 'wall-region' is specified by the friction velocity which is defined as

$$u_* = (\tau_o / \rho)^{1/2} \tag{3.43}$$

The viscous effects are mainly confined to the very thin boundary layer (so called ' the viscous sublayer' in the turbulent flow). However the presence of viscosity produces the steady component of velocity induced by the waves (Equation 3. 12). These time-independent terms are of particular interest because the steady flow transports sediment and pollutants from one place to another.

We propose the model wave field as a superposition of wind waves and long-period waves in the nearshore. The time-dependent components are assumed to be zero when averaged over the period, hence no direct interaction with the time-independent quantities is expected. The wave motion provides the scales of the temporal and spatial variations of the mass transport velocities. In the present approach, the mass transport velocities and related physical quantities have different wave length and period. The first approximation to the combined mass transport velocity may be obtained by summation of the contribution from each individual component separately (Collins, 1964; Sleath, 1984) assuming no nonlinear interaction with the oscillatory wave boundary layer that is much thinner than the layer considered here, which is shown in Figure 3.6.

The total velocity field (u) may be written by

$$u = \hat{U}_w + \hat{U}_L + u_w(t) + u_L(t) \tag{3.44}$$

,where u_w and u_L are the oscillatory wave velocities, and $\hat{U}_w$ and $\hat{U}_L$ are the mass transport velocities of wind waves and long waves respectively. Taking the time average over wave periods and the assumption of zero-mean value for the oscillatory flows give

$$< u > = \tilde{u}_E + \tilde{u}_S = <\hat{U}_w + \hat{U}_L >_E + <\hat{U}_w + \hat{U}_L >_S \tag{3.45}$$

, where the subscripts E and S denote the Eulerian component and the Stokes drift respectively.

The shear stress ($< \tilde{\tau} >$) due to the drift-current gradient within the boundary layer is related to the Eulerian velocity shear ($\frac{\partial (<u>_E)}{\partial z}$) by

$$\frac{< \tau >}{\rho} = \nu_m \left. \frac{\partial \tilde{u}_E}{\partial z} \right|_{z = z_o} \tag{3.46}$$

, where the bottom of the bed z_o is redefined for the case of hydraulically rough bed such that $z_o = k_s /30$, k_s being the hydraulic roughness. The Eulerian streaming ($\tilde{u}_E$) just outside the bottom boundary layer is 1.5 times the Stokes drift ($\tilde{u}_S$) for the inviscid results as seen in Equations (2.17) and (2.19).

WIND WAVE+LONG WAVES

$$u = \bar{U}_w + \bar{U}_L + u_w(t) + u_L(t)$$

$$\langle u \rangle = \bar{u}_E + \bar{u}_S$$

$$= \langle \bar{U}_w + \bar{U}_L \rangle_E + \langle \bar{U}_w + \bar{U}_L \rangle_S$$

$$\langle \bar{\tau} \rangle = \nu \frac{\partial \bar{u}_E}{\partial z}$$

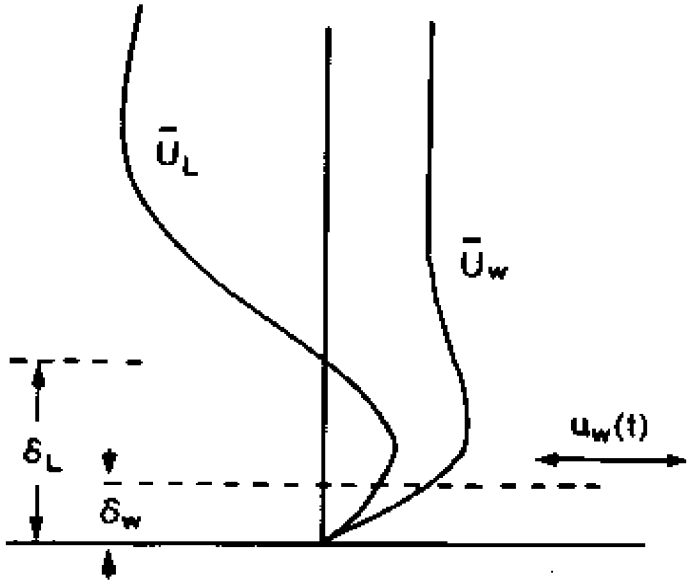

$$\delta_w = \sqrt{2\nu/\sigma_w} \simeq O(mm)\text{-}O(cm) = f(z_o, k_w)$$

$$\delta_L = \sqrt{2\nu/\sigma_L} \simeq O\left(\sqrt{\frac{\sigma_w}{\sigma_L}} \cdot \delta_w\right)$$

Figure 3.6: Schematic diagram of the bottom boundary layer produced by steady streaming of two waves at different frequencies. The subscripts w and L denote the components of wind waves and long waves, and E and S are for the Eulerian and Stokes drifts respectively. The contribution by the oscillatory components is assumed to be zero when averaged over wave periods. As the wave frequency increases, the Stokes' layer decreases.

Time averaged mean profile of the shear stress ($\langle \bar{\tau} \rangle$) in the bottom boundary layer is related to the Eulerian velocity shear ($\frac{\partial \bar{u}_E}{\partial z}$).

It is assumed that the drift velocity for incident waves is not influenced by wave breaking. The breaking and strong turbulent processes would suspend the bed materials into the water column away from the bed. The presence of the movable bed and flow reversal make the definition of the real bottom of zero velocity difficult. Instead we prefer to use the displacement thickness δ_* to determine the boundary layer characteristics. Schlichting (1979) defines the displacement thickness δ_* for steady flow such as the Eulerian streaming within the bottom boundary layer in this study as

$$\delta_* = \int_0^{\infty} \left(1 - \frac{u_E}{(u_E)_o}\right) dz \qquad (3.47)$$

, where u_E is the Eulerian streaming velocity within the bottom boundary layer and $(u_E)_o$ is value at the outer edge of the boundary layer. The displacement thickness indicates the distance by which the external streamlines are shifted owing to the formation of the boundary layer. In the layer lower than the δ_*, the velocity-defect from free stream velocity and consequently the shear stress are quite large. Hence δ_* is considered as a measure of hydraulic roughness for the sediment transport, most likely in the form of high concentration of suspended material. The bed roughness due to individual grains does not affect the mass transport velocity (Sleath, 1984). It is sensible to use the displacement thickness with the lower limit $z_o = \delta_* / 30$ for determination of the wall shear stress τ_o. The friction velocity is estimated by Equation (3.43).

The length scale of Stokes boundary layer is given as

$$\delta = (2 \nu_m / \sigma)^{1/2} \qquad (3.48)$$

The length scale of δ depends on the viscosity and wave frequency. Hence the wave field imposed with different frequencies gives different Stokes length. Any quantities which are a function of the frequency in the combined field can be shown to be compatible with each other, i.e.,

$$\delta_w = (2 \nu_m / \sigma_w)^{1/2}$$

$$\delta_L = (2 \nu_m / \sigma_L)^{1/2}$$

$$\frac{\delta_L}{\delta_w} = (\sigma_w / \sigma_L)^{1/2} = (T_L / T_w)^{1/2} \qquad (3.49)$$

The total boundary layer thickness ℓ is approximately (Figure 3.6)

$$\ell \simeq 5 \zeta = 5 (z/\delta) \qquad (3.50)$$

where δ is a function of the wave frequency.

3.4.4 Method of Analysis

Perhaps the most strong indicator for the sediment transport is the distribution of the steady flow induced by the wave action and of the shear stress in the bottom boundary layer. The problem of particular interest in this chapter is how the mass transport velocities distribute across the bottom boundary induced by the combined waves with different frequencies. The wave motion is responsible for creating the steady components of flow. However the presence of the steady current with different boundary layer thickness due to the frequency difference, and the physical parameters such as the vertical scale height and the magnitude are solely induced by the waves. At this points, the present problem is distinct from the conventional treatment of the interaction of a surface wave and a current.

All the mass transport components are assumed uncorrelated, so that the linear system is considered. The amplitudes and frequencies of the forcing waves are specified, hence the free stream velocities just outside the boundary layer are determined. The topography is of plane slopes with smooth bottom, which is extended to account for nonplanar beach in next chapter.

In this chapter, the mass transport velocities in the bottom boundary layer are determined under different wave conditions on two different beach slopes. With different incident wave conditions, we need to know the relationship between the parameters of the wind waves and the infragravity waves which are defined as the long-period waves. An extensive analysis on this problem has been done by Guza and Thornton (1985). Run-up which is the maximum vertical excursion of water is composed of a super elevation of mean water level (set-up) and of fluctuation about the set-up level (swash). Run-up energy spectra at wind wave frequencies (f) show a saturation with an f^{-3} (Guza and Thornton, 1982) or f^{-4} (Huntley et al., 1977) dependence, while at surf beat periods run-up energy increases approximately linearly with increasing incident wave energy (Guza and Thornton, 1982). Increasing the incident wave height increases the steady set-up (Bowen et al., 1968), but not the swash oscillation at wind wave frequencies. Hence it is generally accepted that steady set-up constitutes the greater part of the total run-up height (Battjes, 1974). It is clearly shown that the low frequency run-up energy is associated with linear standing waves having on/offshore sea surface elevation profiles given by long wave theory (Suhayda, 1974; Guza et al., 1984; and many more).

Hence it is sensible to consider the vertical run-up excursion (R^V) as twice the amplitude of standing wave on the vertical coordinate. The vertical run-up excursion R^V at surf-beat frequencies, twice the swash amplitude ($R^V = 2\ a^S$), is related to Ho as shown in Figure 3.7 . The relation can be expressed by the best-fit line as

$$R_s^V \simeq Ho_s \tag{3.51}$$

where the subscript s denotes the significant value. Hence once we set the incident wave parameters in deep water as input on a sloping beach, the amplitude of long-period wave projected on vertical coordinate at the shoreline has been estimated by (Guza et al., 1984; Guza and Thornton, 1985)

$$a = \frac{1}{2} Ho_s \quad . \tag{3.52}$$

Vertical and horizontal scales are referenced by the scales for long waves by the expression of Equation (3.47). However the reference frequency of long wave is set in an arbitrary way in order to investigate the dynamic effect of the frequency ratio of two waves to the boundary flows.

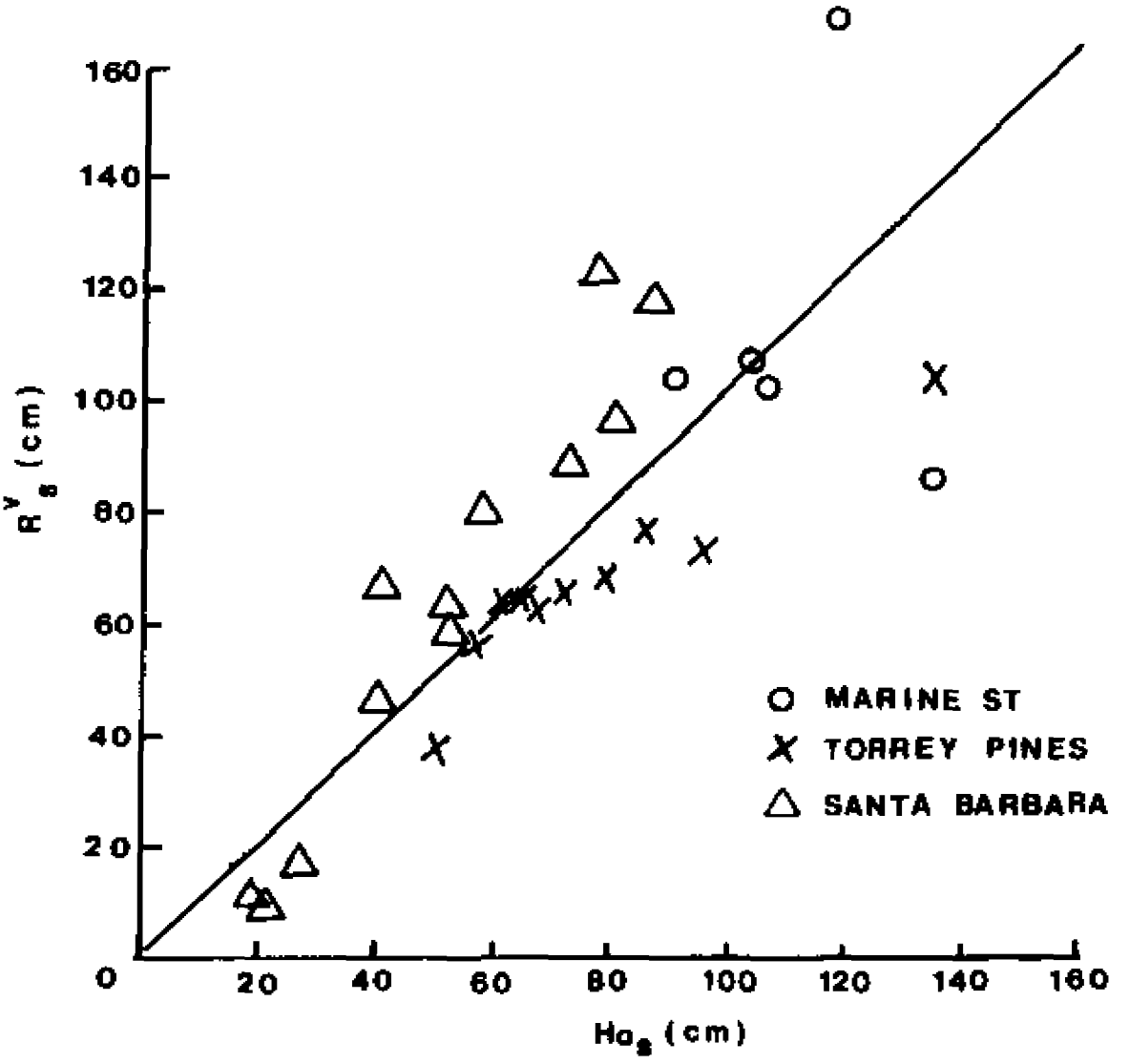

Figure 3.7: Significant vertical swash excursion R_s^v versus significant incident wind wave height Ho_s. Solid line is the best fit straight line constrained to pass through the origin, R_s^v (cm) = 1.00 Ho_s (From Guza and Thornton, 1985). Data sets were obtained from three different California beaches (Marine Street and Torrey Pines in San Diego, and Leadbetter Beach in Santa Barbara).

3.5 Results

The results of the model are presented for two cases of beach slopes. The steep slope case is for the plane beach with $\beta = 0.05$ and the mild case is for $\beta = 0.02$. In fact these two typical slopes could represent the natural beach slopes except very near the steep foreshore. The incident wave conditions which are used as inputs are grouped in a calm condition with $H_o = 0.3$ m, an intermediate condition with $H_o = 1$ m and a storm condition with $H_o = 2$ m. For each of these case studies, the distribution of the mass transport velocity in the bottom boundary layer is estimated and interpreted in connection with the essential role to control the amount and direction of the sediment transport in the nearshore.

Figure 3.8 shows the vertical structure of the mass transport velocity in the bottom boundary layer induced by the long waves and superposed wind waves on the beach of $\beta = 0.02$. The input wave conditions are $T = 10$ s and $H_o = 1$ m. The conditions of the long waves are $T = 50$ s and $a = 0.5$ m. The breaking occurs at $x = 128$ m with breaking height $H_b = 2$ m.

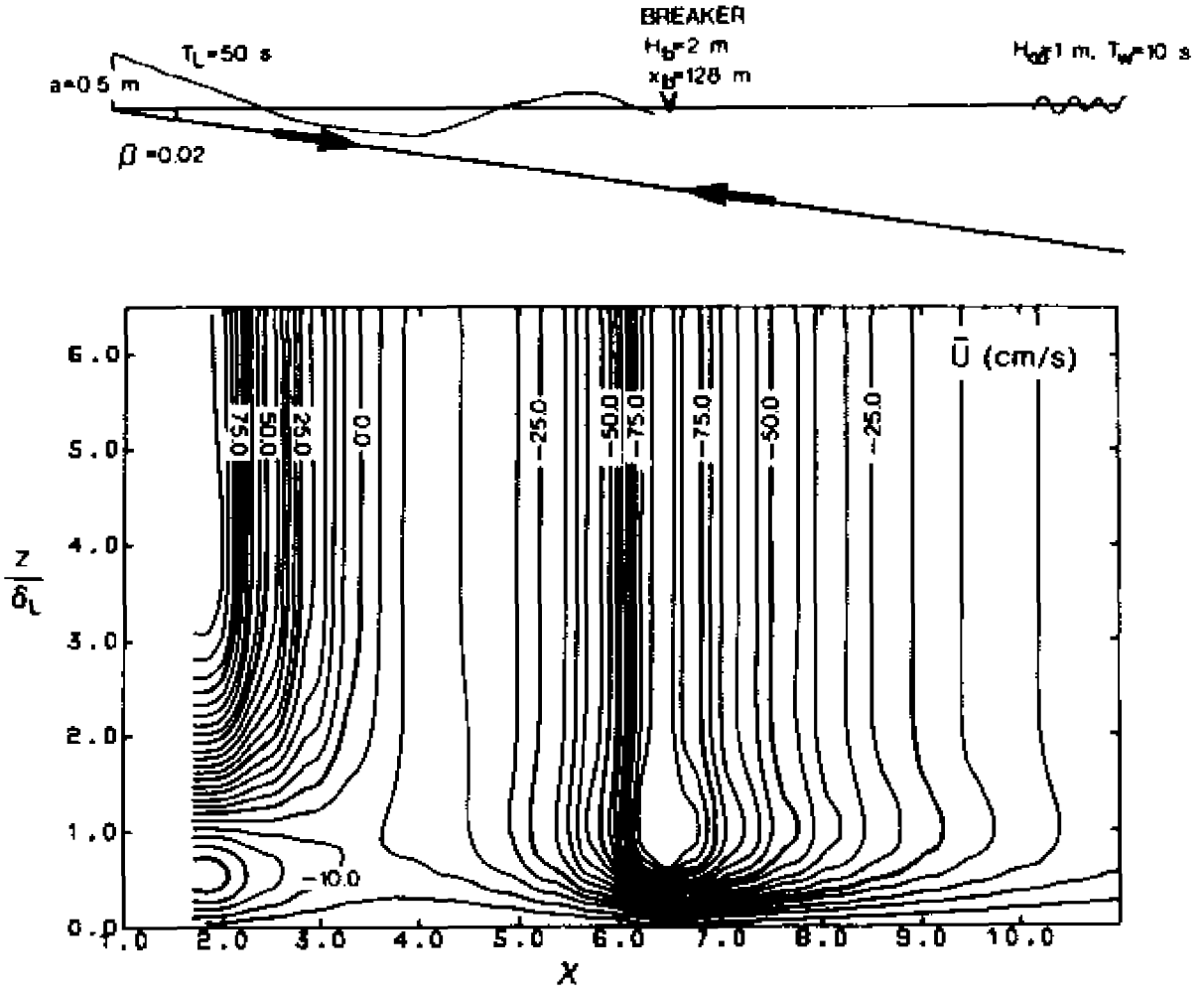

Figure 3.8: Vertical distribution of mass transport velocities in the bottom boundary layer induced by a superposition of wind wave (Ho = 1 m and T_w = 10 s) and long wave (a = 0.5 m and T_L = 50 s) on a plane beach of β = 0.02. Contour interval is 5 cm/s and negative values are the shoreward flows. The vertical axis is in the unit of Stokes' layer δ and the horizontal scale is the nondimensional offshore distance χ . Under the wave field considered, a convergence of steady streaming around χ = 3.4 (x = 36 m) is clearly visible, suggesting a process of initial bar formation.

The x-axis is represented by non-dimensional offshore distance $\chi = 2\sigma(x/g\beta)^{1/2}$. The vertical axis is nondimensionalized by the Stokes layer of the long wave. The contours show that the mass transport velocities flow onshore outside the breaker and offshore well inside the surf zone. One striking feature is that in the lower-most layer the boundary flow has the same direction as the incident waves, while above $z/\delta = 1$, a reversed flow is predicted. This lower layer of order 1-2 cm could be the bed load layer from which sediment is brought into suspension by wave action. Bed load and suspended load differ in the speed, direction and concentration (Deguchi and Sawaragi, 1984). Under these bi-directional systems, one mode of load could surpass the other if we consider the net rate of sediment transport. Apparently seaward mass transport prevails in the surf zone shoreward of $\chi \simeq 3.4$ (x = 36 m). As long wave period increases, the offshore distance of this convergence increases. The zone of convergence is a potential location of accumulation of sand to form a bar. The mode of cross-shore sediment transport can be inferred from the direction of shear stresses. The examination of the vertical structure of the $\tilde{U}$ across the offshore positions reveals that strong vertical gradients of the boundary flow in the lower-most layer develop underneath the breaking waves while close to the shoreline the strong gradients develop above the boundary layer induced by wind waves. Outside the surf zone the bed load in the onshore direction would be the dominant mode, while inside the surf zone suspended load probably moves offshore. This has been widely observed (e.g., Deguchi and Sawaragi, 1984; Richmond and Sallenger, 1984).

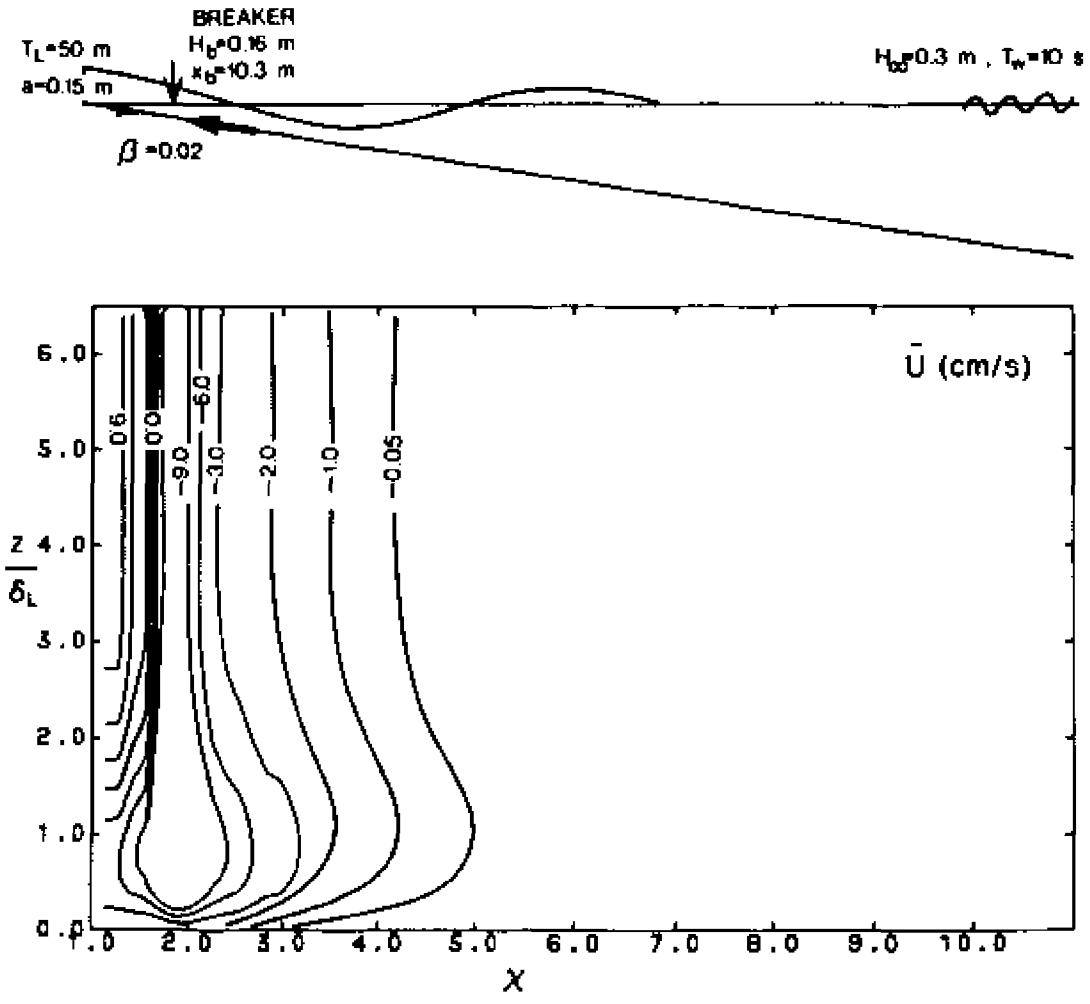

Figure 3.9: Same as in Figure 3.8 but wave conditions (Ho = 0.3 m, T_w = 10 s, a = 0.15 m and T_L = 50 s). Under calm condition, mass transport velocity directs shoreward up to the swash dominant region, suppressing the seagoing bottom flows.

Figure 3.9 shows the results of the same run as in Figure 3.8 except that H_o = 0.3 m. For very calm conditions the effect of the long waves has been suppressed such that shoreward boundary flows dominate across the water column up to the point very close to the shoreline.

Steepening the beach to β = 0.05 while holding other conditions constant yields the results shown in Figure 3.10. Even under the moderate wave condition, the reversed flows are confined to the inner ten meters where backwash dominates. This is consistent with observations that barred topography is rarely developed on steep beach profiles.

3.6 Discussion

There is a big difference between the previous studies and the present study in examining the wave-bed interaction. The most obvious is the combination of wind waves and long waves in the nearshore wave field, of which the mass transport velocities in the boundary layer are determined. Most of the previous studies assumed either a monochromatic wind wave (Lau and Travis, 1973) or an infragravity wave (Holman and Bowen, 1982) in determining the mass transport velocities on a nearshore topography. When the present model is separated into these two different modes of waves, the general agreement with other models is to be expected (e.g., Figures 3.4 and 3.5).

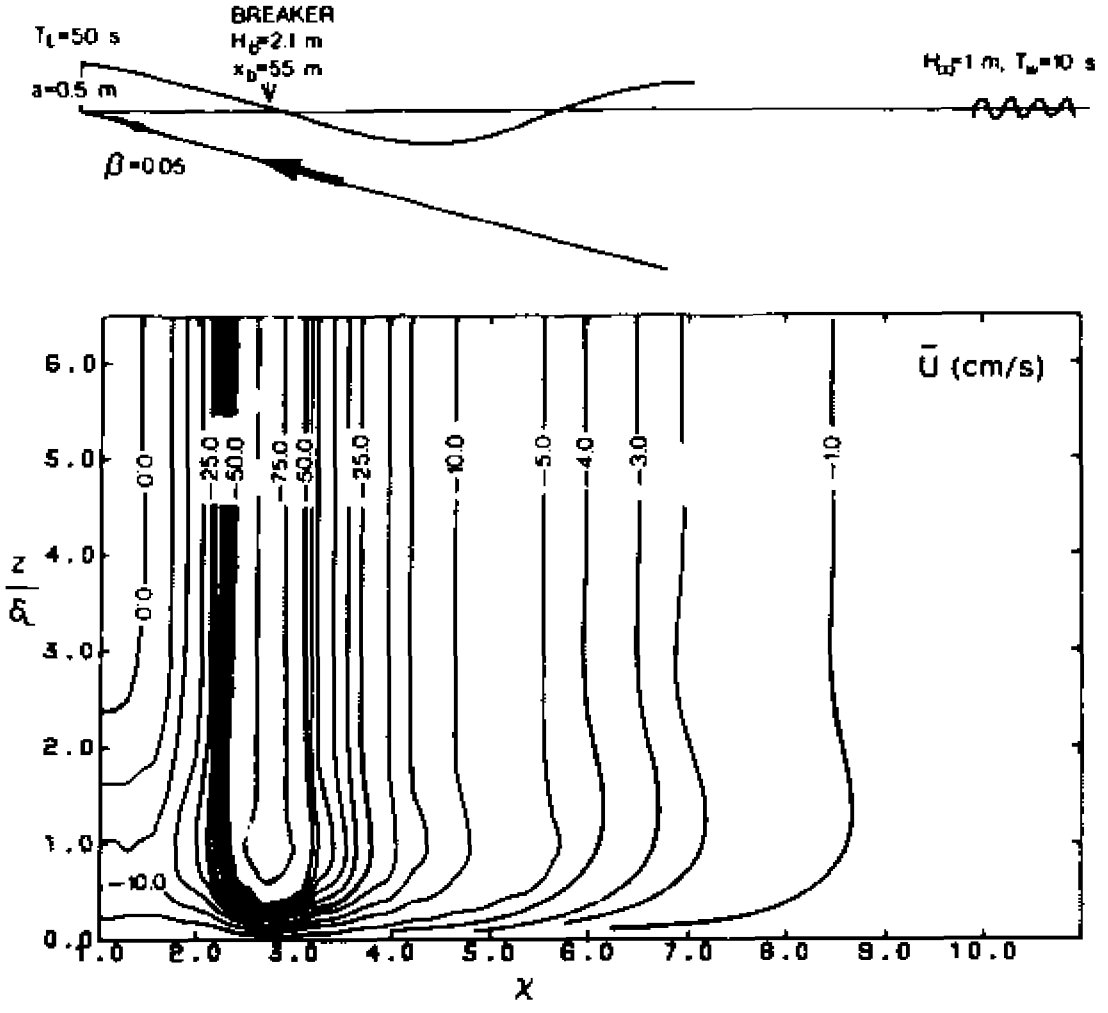

Figure 3.10: Same as in Figure 3.8 except the beach slope (β = 0.05). As the beach slope gets steeper, bar formation is not likely favored by strong shoreward bottom flows.

The long wave amplitude at the shoreline is based on the relation between the run-up and the significant wave height in deep water, which is confirmed in extensive studies (Guza and Thornton, 1985). The run-up measurement can be considered as the sum of a super-elevation of the mean water level (set-up) and fluctuations about the mean (swash). Hence the effect of undertow (flowing seaward along the foreshore) driven by the setup toward the shoreline might be included in the low frequency fluctuation when its amplitude is estimated from the run-up height. However the run-up relation to the wave height in deep water seems to hold for the surf similarity parameters (known as Irriban number) $\xi o = \beta/(Ho/Lo)^{1/2}$ greater than 1.0. During severe storms with Ho > 3 m, the Irriban number is usually in the range of 0.5 - 1.0, for which the total run-up height is reduced from the relation as given in Figure 3.7. Application of the present assumptions to severe storms of Ho higher than 3 m would overestimate the components of long waves.

The boundary layer properties are assumed to be linear between the contributions of waves at different frequencies. The boundary layer of the oscillatory wind waves are in the order of one Stokes layer (Equation 3.46) while that of the combined streaming velocity has the order of 5 Stokes layer. If there is a significant interaction between these two layers, the present approach would need some modification. However the present study focussed its interest in the steady state, the contribution of oscillatory motion with mean zero value would not provide a significant alteration to the boundary layer parameters considered, except to the modification of wind waves through energy dissipation which has been already accounted for.

Based on the assumptions described above, the numerical investigation has been applied on plane beaches. The pricipal results are;

1) The boundary layer flows are characterized by bidirectional flows with the directions shoreward outside the surf zone and seaward well inside the surf zone. Strikingly, the position of convergence of two flows is determined by the relative strength, rather than by the nodal position of infragravity wave itself. This problem has long been uncertain among those who examined the nodal position of long wave and observed energy spectra which sometimes are wide-banded instead of a single predominant frequency. The results of the present approach imply that the long wave energy does not require to be of a single frequency but it requires a relatively high energy level sufficient to counterbalance the shoreward bottom flows induced by a single or multiple frequencies.

2) The distibution of mass transport in the bottom is sensitive to the beach slope such that the mild-slope beach is favored for development of the converging flow; i.e., bar formation. This fact is good agreement with the field observation of the beach profiles in nature.

3) Moderately high energetic wave climate shows a strong possibility for bar formation rather than very calm wave conditions.

CHAPTER 4

INFLUENCE OF NEARSHORE WAVES ON LONGSHORE BAR MIGRATION

4.1 Introduction

A common feature of the nearshore topography is the presence of longshore bars. Essentially the bar crests and troughs are oriented parallel to the shoreline. The number of bars, their spacing and the geometric features have been observed by numerous investigators. Multiple bars are observed along the Great Lakes Coasts (Saylor and Hands, 1970) and along the coasts of inland bays (Lau and Travis, 1973) while one or two well-defined bars on beaches with slopes steeper than those in inland bays are observed along the coasts exposed to the highly energetic open ocean (Sallenger et al., 1985). According to the observations, the spacing between crests in the offshore direction increases in an exponential fashion. The slope landward of the bar crest is steeper than the slope seaward of the bar crest, suggesting that bar configuration overriding on an approximately plane beach is not symmetric about its crest axis. The stability and permanency of the bars have been noted by numerous investigators in relation to varying tidal levels (King and Williams, 1949), wave height and steepness (Keulegan, 1948), breaker position (Shepard, 1950) and standing waves at incident wave frequencies resulted from significant reflection on the order of 40% which requires a beach slope of about $\beta = 0.31$ (Carter et al., 1973). The usual relationships of the variability of longshore bars to these causing factors do not explain the behavior of longshore bars in nature as observed by Sallenger et al. (1985).

In the present study, it is hypothesized that the mass transport velocity in the bottom boundary layer induced by wave field combined with long waves and wind waves would control the bar formation (as seen in Chapter 3) and the migration processes. In this chapter, a barred topography is modeled based on general observation of the bar topography in nature. On the model topography, the bottom flow structures are obtained using the basic approaches as described in Chapter 3 under varying wave conditions. The boundary layer parameters characterizing the flow field and the magnitude with direction of the sediment transport have been estimated.

Finally the principal results of the numerical experiment are interpreted in connection with the bar migration before, during and after the storm period.

4.2 Methods and Criteria for the Numerical Experiment

4.2.1 A bar-topography model

Although the general properties of longshore bars on natural beaches have been described widely in the literature, quantitative aspects of bar geometry are lacking. The lack of precise geometry may come from the difficulty in measuring the continuously changing geomorphology which is a function of grain size, ever-changing waves and currents, tide level and abundance of source materials, etc.. However for the purpose of the numerical experiment, it is desirable to set up a model topography based on simple but sensible assumptions. Most beach profiles show an ever-varying equilibrium profile in either exponential slope very near the foreshore or planar slope outside the typical surf zone, or in cycle during beach process. Characterizing a beach in terms

of never-achieving equilibrium profile seems to be a very subjective matter depending on the study interest whether confined in the surf zone or extended farther offshore.

The present study is concerned with the response of barred topography to the wave field combined with long waves and transforming incident gravity waves. Due to the availability of the analytic solution for long waves on a plane beach as shown in Section 3.3.1, it is a sensible assumption that the overall slope ($\bar{\beta}$) of a barred topography will be of a plane beach slope (β). To produce a barred topography, a perturbation of depth is added to a plane beach profile. Considering the asymmetric shape of bar with respect to the vertical axis of bar crest and the ratio of bar-crest-depth to bar-trough-depth to be about 1.5 - 1.8 (Komar, 1976: for review of previous observations; Sallenger et al., 1985: for recent observation), the perturbation of depth from a plane beach of slope β is modeled by sinc functions as follows;

$$\delta h(x) = b_i \frac{\sin 4\pi P}{4\pi P}, \quad x < L_i$$

$$= -b_i, \quad x = L_i$$

$$= -b_i \frac{\sin (\pi/2) P}{(\pi/2) P}, \quad x > L_i \qquad (4.1)$$

where $P = \frac{x - L_{i-1}}{L_i - L_{i-1}} - 1$, $(i = 1, 2, 3, \ldots n)$, x is the distance offshore, b_i denotes the crest height of the ith bar and L_i denotes the offshore distance of the ith bar from the shoreline with $L_0 = 0$ at the mean shoreline.

Equation (4.1) allows the cases of multiple bars on any plane beach by adjusting the b_1's and L_1's. For the sake of simplicity of numerical experiment on bar migration, the model topography is adapted to a predominant single bar with bar height b_1= 1 m at L_1 = 100 m on a plane beach of $\tilde{\beta}$ = 0.02. These scales and parameters are quite reasonable for barred topography along the coasts exposed to open ocean. Figure 4.1a shows a form of depth perturbation (δh) as given in Equation (4.1) normalized by bar height (b_1) along the distance offshore (x) normalized by the distance offshore of the bar (L_1). The slope landward of the bar crest is set to be 8 times steeper than the slope seaward of the bar crest, which could be variable with environmental condition and place. Figure 4.1b is the model bar-topography with bar height of 1 m at distance offshore x = 100 m on a plane beach $\tilde{\beta}$ = 0.02. The ratio of bar-crest-depth to bar-trough-depth in this case is about 1.6 which is also consistent with the range observed in nature.

The present study applies on an arbitrary bar-topography with an overall planar slope due to the lack of analytic and numerical solutions of long waves on an arbitrary topography without any characteristic average slope. Hence application on the topography such as multi-sloped profiles is limited or some deviations from the main results obtained in this study are expected.

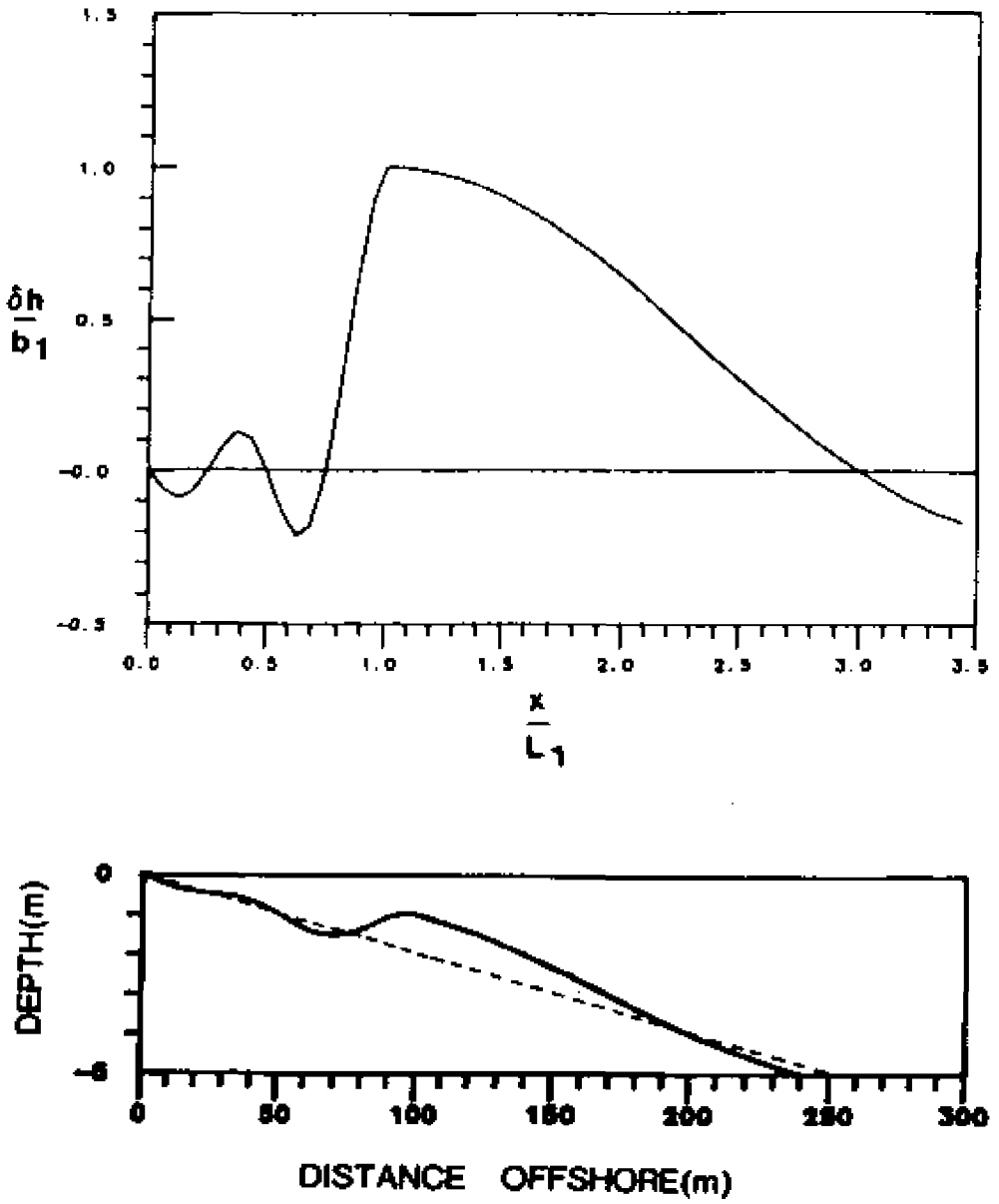

Figure 4.1: Sample profiles for a plane beach and a barred topography. (upper) The profiles of depth perturbation from a plane beach simulated with Equation (4.1). The offshore distance x is normalized by the offshore distance (L_1) of bar crest, and the height above the plane beach is normalized by the bar-crest height (b_1). (lower) A plane beach profile (dotted) with $\beta = 0.02$ and a barred profile with bar crest at x = 100 m and bar-crest height 1 m in water depth of 2 m.

4.2.2 Wave and Bottom Flow Field

In Chapter 3, the distribution of mass transport velocity across the shore-normal line was obtained on plane beaches. As shown in Chapter 3, the mild-slope beach is favored to produce the barred topography. In the present analysis, the overall beach slope of the model topography is chosen as $\tilde{\beta} = 0.02$ as described in previous section.

Due to the presence of bar, the wind wave will transform in a quite different manner from that on a plane beach. The wind wave information along the offshore direction has been obtained by using the algorithm developed by Ebersole et al. (1986) as before. A sample of wind wave transformation on a plane beach of $\beta = 0.02$ and a model bar-topography with slope $\tilde{\beta} = 0.02$ is given in Figure 4.2. The chosen wave heights in deep water represent the cases of calm (Ho = 0.3 m), intermediate (Ho = 1 m) and storm (Ho = 2 m) conditions. It is notable that there are remarkable differences in breaking point and in wave height in the surf zone between the barred and plane beaches. On the barred topography, the waves inside the first breaker line reform in the trough and break again close to the shoreline. Even for the waves with wave height higher than 2 m under severe storms, the change in wave height inside the bar falls in the same range as shown in the lower plot of Figure 4.2 due to increase in the breaking depth, consequently more dissipation while propagating up to the bar. The position of the bar plays a critical role on the wind wave breaking. Hence an accurate measurement of the bar topography along with wave conditions at each event on a natural beach is desirable at the application stage. The variation in wave height and local depth are used to estimate the mass transport induced by wind waves along the shore-normal line according to Equation (3.38).

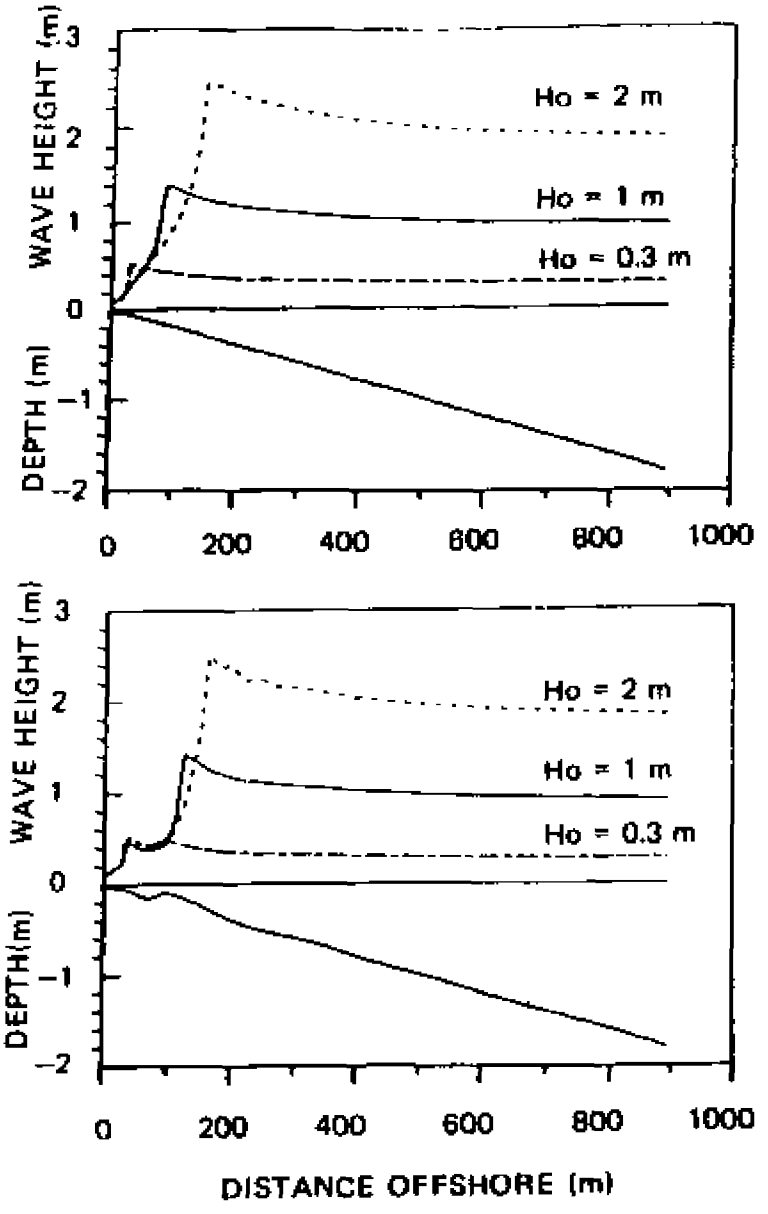

Figure 4.2: Wind wave transformations predicted by Ebersole's algorithm for three different wave conditions on the plane and barred beaches as shown in Figure 4.1. Reformations of wind wave in bar trough are noticeable. The wind wave information at positions are used to predict a part of mass tranport velocities in total wave field superposed with long waves.

The energy of the long wave is assumed to be proportional to the wind wave energy as inferred from Figure 3.7 and as described in field observations (Guza et al., 1984; Kim and Huntley, 1985). As a first approximation, the structure of long waves on a plane beach of slope $\beta = \hat{\beta}$ is assumed to be unaffected by the presence of bar as long as the typical wave length is much longer than the horizontal length scale of bar shape deviating from a plane beach profile and $kh \ll 1$. The input amplitude of the long wave at the shoreline is chosen by the deep water wave height according to Figure 3.7. In Figure 3.7, the vertical amplitude of run-up, twice the amplitude of long standing wave, is scattered as wind wave height increases above $Ho_s = 1$ m. This fact may imply that the run-up will not grow with Ho by $R_s^v = Ho_s$ under severe storms of Ho = 3 m or more. Until field data under these conditions is available, it is sensible to confine the wave height up to Ho = 2 m to estimate the interaction between the barred topography and wave field. The periods of long waves are chosen at 50 s, 75 s and 100 s, which are in the typical range of surf-beat period in nature. The period of wind wave is fixed at 10 s for the numerical experiment. When the field data accounting for the present scope becomes available, it may be possible to use the observed data as input conditions for the model to predict the behavior of bar on a real topography. The mass transport velocities induced by long standing waves and wind waves are assumed to be in a linear system as in Chapter 3. The nondimensional scales in horizontal and vertical coordinates have been converted to those of long wave frequencies according to Section 3.4.3.

4.3 Results

4.3.1 The distribution of the mass transport velocity

The ultimate objective of the present study is a better understanding of the bar migration under varying wave conditions; Hence we consider three cases of wind waves of Ho = 0.3 m, Ho = 1 m and Ho = 2 m as well as three long wave periods of 50 s, 75 s and 100 s on a given bar topography.

We first consider the case of long waves of periods of 50 s under deep water wave heights of 1 m and 0.3 m. Figure 4.3 shows the contour plot of the mass transport field in a vertical boundary plane crossing the offshore direction. In comparison with the case of plane beach (Fig. 3.8), the mass transport velocities around the bar crest (χ = 5.67) on the bar topography are generally reduced due to the breaking point farther offshore (Fig. 4.2). Underneath the breaker point (χ = 6.3), large velocity gradient below $\xi = z/\delta = 1$ is developed in a small vertical length scale, implying high turbulent bottom flow associated with high dissipation rate around this region. The flows in the lower-most layer ($\xi < 1$) up to the shoreline are characterized as weak onshore flows. However the oscillatory boundary layer thickness (δ_{os}) induced by wave orbital velocity takes the form of $\delta_{os} = r \frac{\pi}{2} (2 \nu_m / \sigma)^{1/2}$ $\simeq 0.7 \delta$ with r = 0.45 (Christoffersen and Jonsson, 1985). Here physical reasoning such that the boundary layer of mass transport velocity lower than $\xi = 1$ would be merged to the wave boundary layer, would be sensible and appropriate. Hence the lower-most layer below $\xi = 1$ is considered as a region in which the oscillatory boundary flows act to entrain the sediment into suspension.

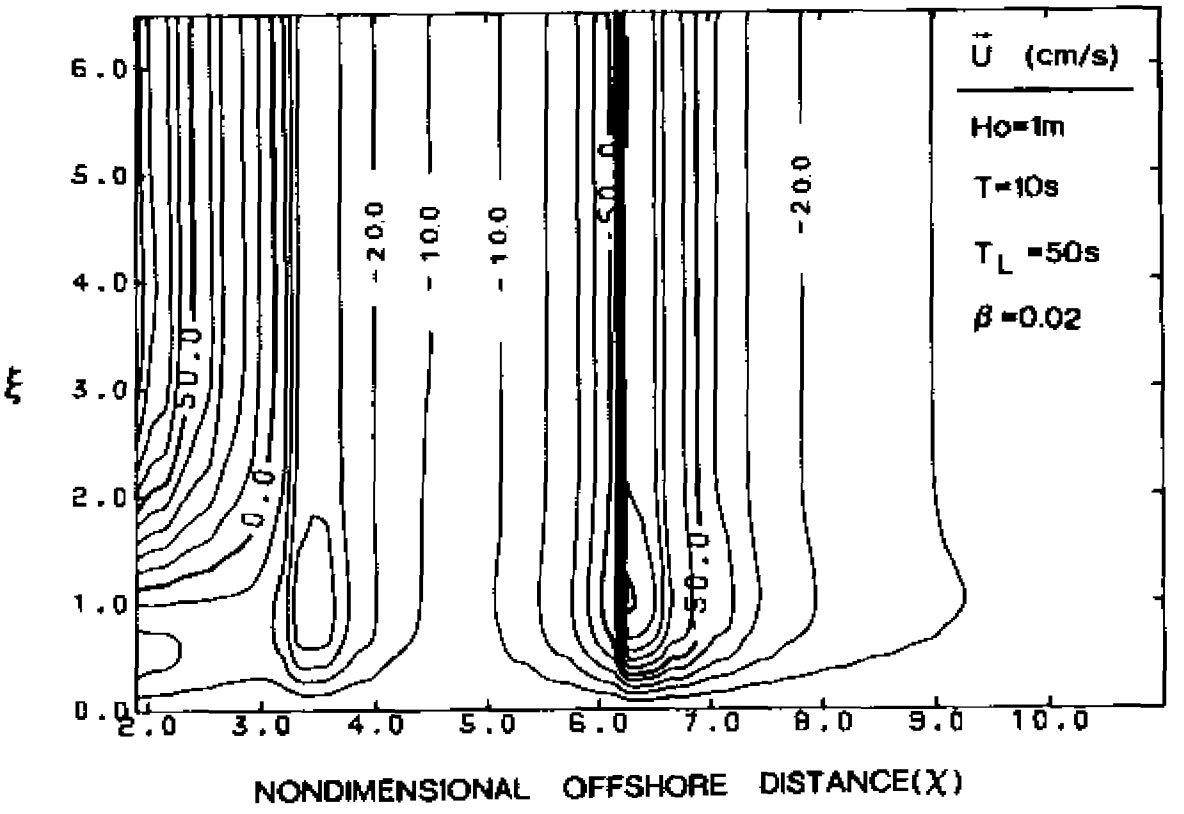

Figure 4.3: Vertical profiles of the mass transport velocities of a wave field (Ho = 1 m, T = 10 s, a = 0.5 m and T_L = 50 s) along χ on a barred topography ($\bar{\beta}$ = 0.02). The bar is located at χ = 5.7 (x = 100 m) while the convergence of the bottom flow is predicted at about χ = 3.1 (x = 30 m), suggesting a possible instability o persisting bar system. It is noticeable that in the lower most layer which is in the same range with the oscillatory wave boundary layer, shoreward streaming even in the surf zone is predicted.

Intriguingly the bottom flow field above ξ = 1 shows a compensation of bidirectional flows with zero velocity, indicating a convergence of two flows; shoreward outer of χ = 3.1 and seaward inner of χ = 3.1 (x = 30 m).

It is worth to note that the offshore distance of this compensation does not necessarily coincide with the node or antinode of long waves as shown in Figure 3.2. Rather the position is determined by the counterbalance of mass transport velocities induced by wind wave and long wave. Many investigators have proposed the positions of accumulation of bed materials to be at node or antinode as described in Chapter 2. Recent analysis of field experiment (Sallenger and Holman, 1987) shows the discrepancy between the existing theory on node-antinode stuff and the field observation in nature. The first node of velocity in this case is at χ = 3.8 while Figure 4.3 shows the zero value near χ = 3.1. Including the streaming by wind waves, the present study provides a closer step toward detailed examination of the boundary streaming flows which are believed to be essential to determine the bar migration process. The present study does not account for the boundary separation over the bar crest. It is clearly shown that the shoreward boundary flow dominates over the bar crest (χ = 5.67, x = 100 m) up to χ = 3.1 (x = 30 m) while reversed boundary flow directing offshore is determined inner of χ = 3.1.

A similar plot in Figure 4.4 for the case of the same with Figure 4.3 except Ho = 0.3 m shows dominant onshore flow with evidence of weak reversed flow near the shoreline. The bar is located at χ = 5.67 (x = 100 m) and the wind wave breaks at χ = 3.7 (x = 42 m).

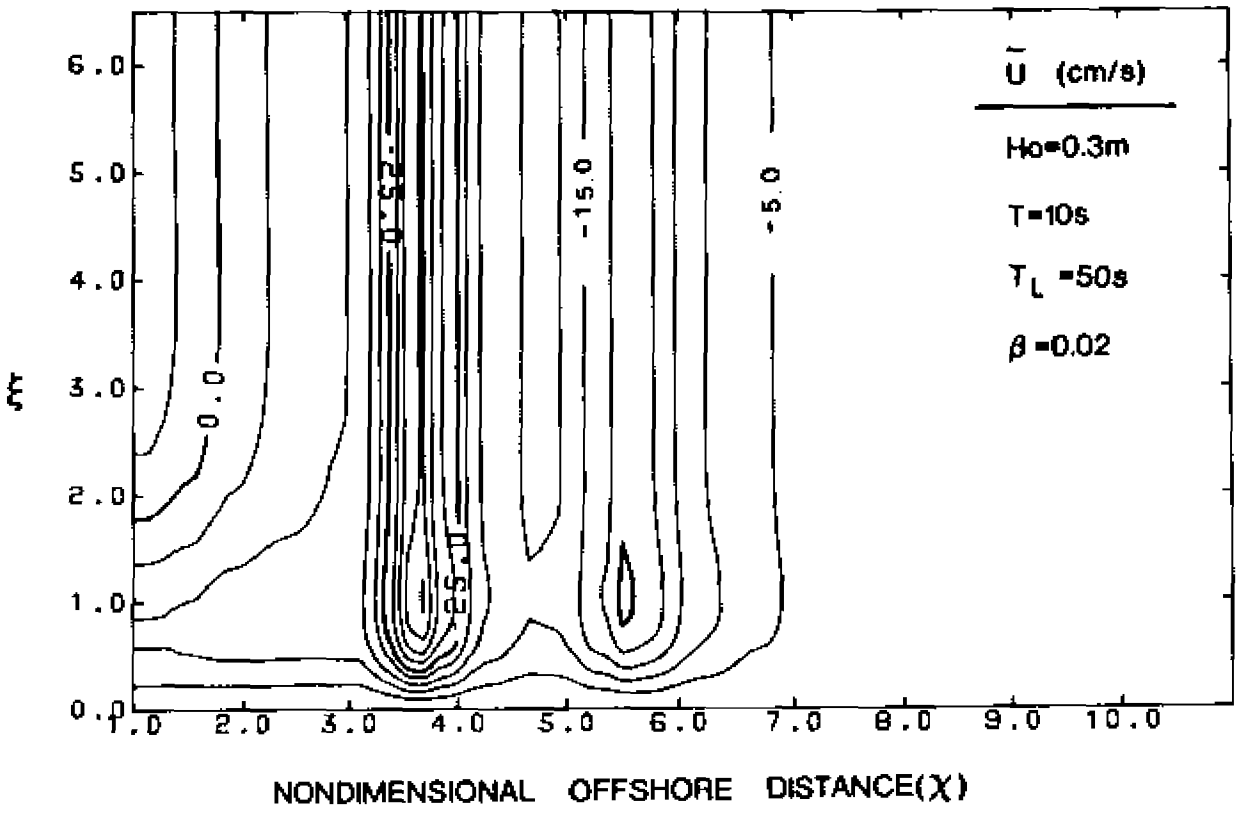

Figure 4.4: Same as in Figure 4.3 but Ho = 0.3 m and a = 0.15 m. Decreasing the incident wave height results in weakening the seaward bottom flow.

The onshore boundary flow prevails over the region up to χ = 1.8 (x = 10 m). Shoreward of χ = 1.8 a weak seaward flow is developed, suggesting that under calm conditions the seaward mass transport in the boundary layer is not a significant mode of transporting the substances in the water. With Ho = 0.3 m fixed, changing the long wave periods to 75 s and 100 s does not yield any different distribution of the mass transport velocity from Figure 4.4. This fact suggests that the mass transport field is not much sensitive to the long wave periods when the incident wave height is very low much less than 1.0 m.

It is interesting to examine the dynamic effect of long wave period to the boundary flow field under moderate and severe wave condition. The reason is that as the wind wave height increases the long wave energy increases (e.g., Guza and Thornton, 1985). We consider the flow field with Ho = 1 m and long wave period of 75 s (Figure 4.5). This long wave period is of a possible resonant period with the bar located at x = 100 m (χ = 3.8 for the given condition; $\chi = 2\sigma (x/g\ \beta)^{1/2}$ and β = 0.02). Referencing Figure 3.2a, the first node of velocity (J_1 solution) is noticed at χ = 3.8. If the long wave of period of 75 s is solely a dominant mode on the given topography we would expect the node at around χ = 3.8 according to Figure 3.5 and many proposals made based on the node of velocity at the bar crest. Figure 4.5 shows the velocity node at χ = 2.0 (x = 28 m) instead of χ = 3.8 at which the bar crest locates. Strikingly the reversing flow induced by the long wave confines inner of x = 28 m. The effect of wind wave breaking seaward of the bar penetrates shoreward of the bar trough.

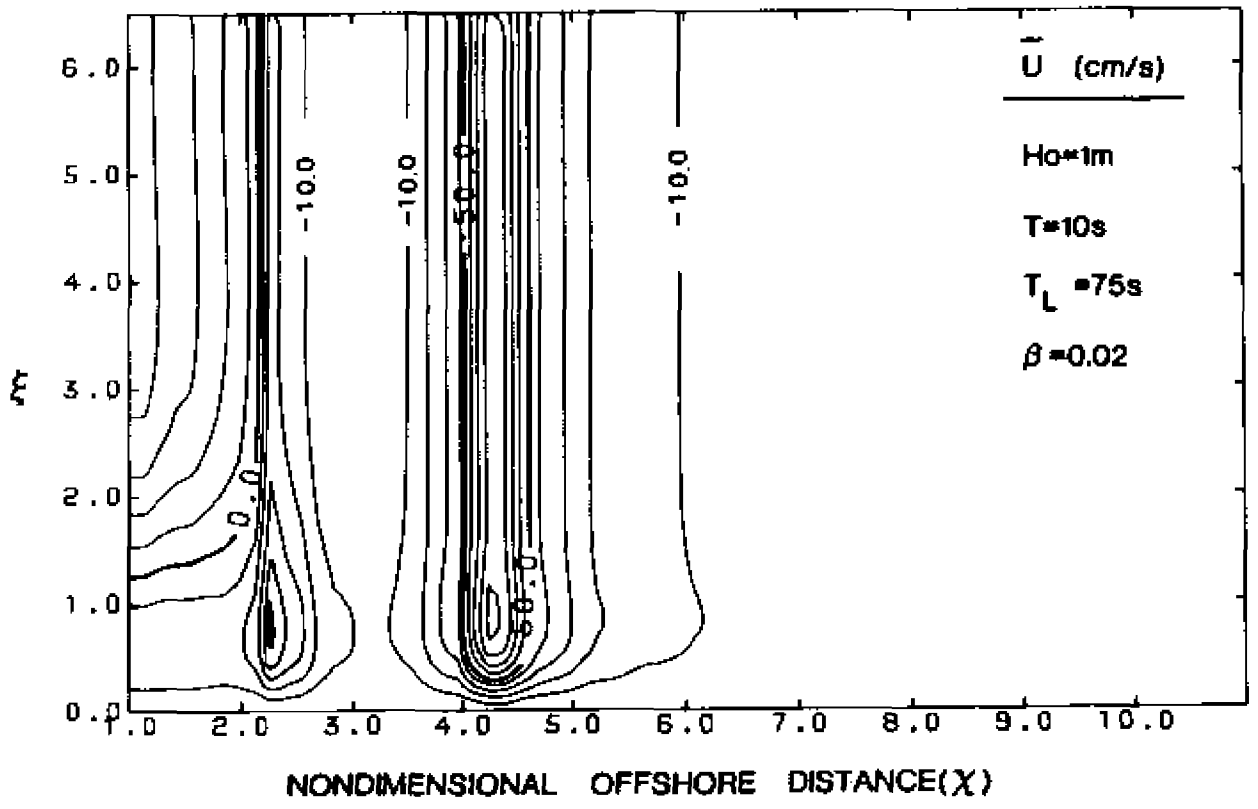

Figure 4.5: Same as in Figure 4.3 but T_L = 75 s. Increasing the long wave period by holding the other wave parameters does not yield any change in the velocity nodal position (x = 30 m) of low waves (Ho $\leq$ 1 m). The long wave period 75 s is coincident with the half wave resonant period of the bar at x = 100 m (χ = 3.8). One striking feature is that the velocity node is predicted at about χ = 2.0 (x = 30 m) instead of χ = 3.8 (x = 100 m).

Figure 4.6 is for the same conditions as Figure 4.5 except Ho = 2 m representing a storm. The wind wave breaks well outside the bar crest, which drives strong onshore boundary flow. It is noticeable that the zero velocity boundary proceeds out to χ = 3.5 (x = 80 m). In comparison with Figure 4.5 for Ho = 1 m, we could expect a quite different dynamic process in the boundary layer under varying wave conditions. This case as shown in Figure 4.6 is close to the half-wave resonant condition in which the antinode of the elevation (or node of velocity) is expected to develop at χ = 3.8 near the bar crest (χ = 3.8). The estimated node of velocity is determined to occur at χ = 3.5 instead of χ = 3.8 due to the effect of the wind wave. In regard to the findings, the offshore positions of the mass transport velocity nodes are determined by relative strength of streaming velocities induced by wind wave and long wave rather than solely determined by the frequency of long wave and its nodal position.

Similar investigation for the case of long wave period of 100 s under varying wind wave conditions has been done. For the long wave period of 100 s, the bar location at x = 100 m is equivalent to χ = 2.8 and the antinode of the elevation (node of the velocity) is at χ = 3.8 (x = 180 m). Figure 4.7 represents the distribution of the mass transport velocity induced by the long wave of period of 100 s under Ho = 2 m. The wind wave breaks at $\chi \simeq 3.7$, generating strong onshore bottom flow in this region.

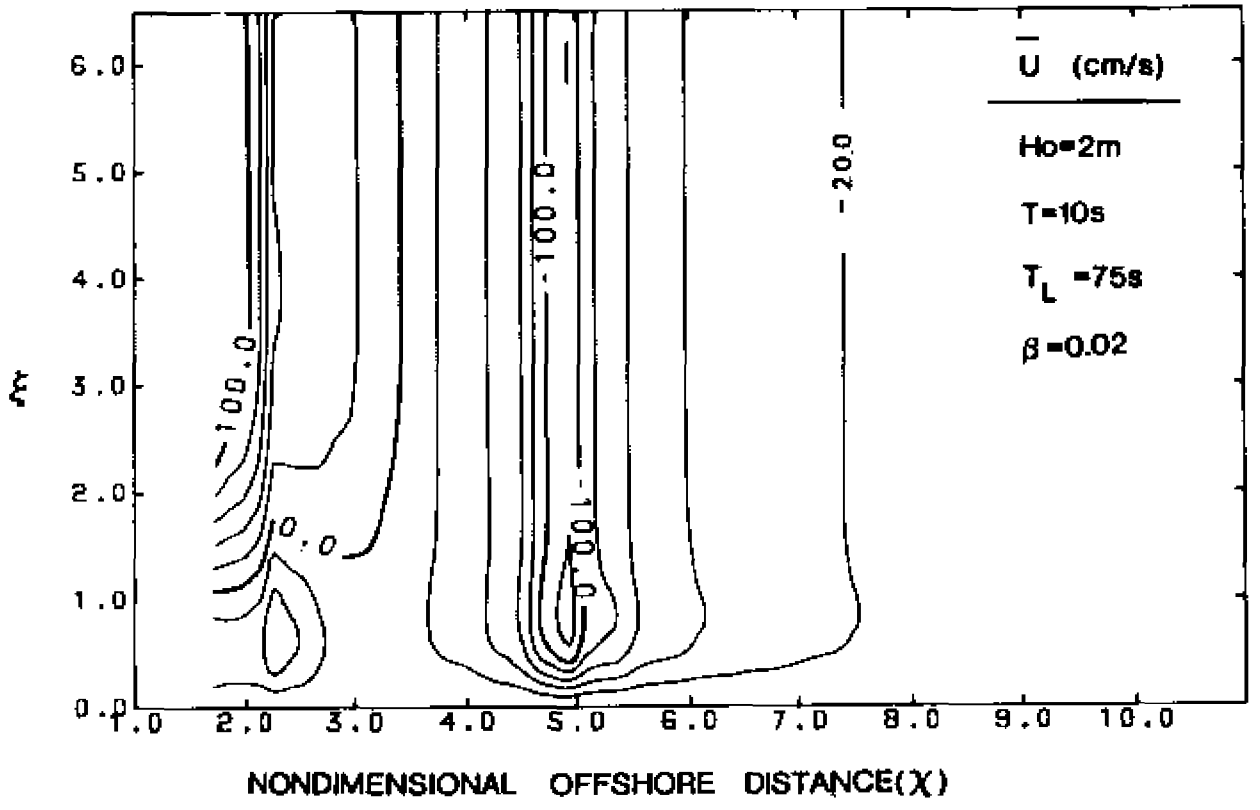

Figure 4.6: Same as in Figure 4.3 but Ho = 2.0 m and a = 1 m. Increasing wave height to a stormy condition pulls the velocity node seaward to χ = 3.5 (x = 80 m).

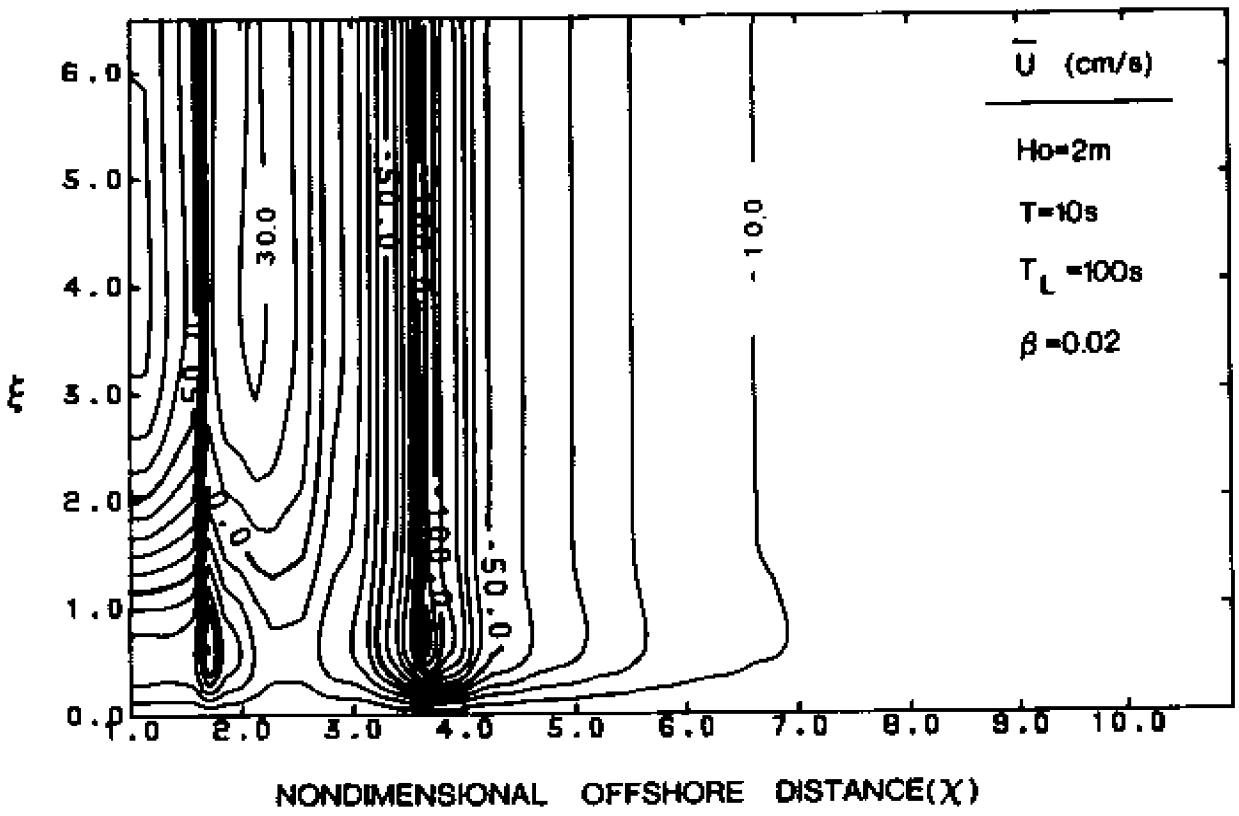

Figure 4.7: Same as in Figure 4.6 but T_L = 100 s. Under stormy conditions, long waves of longer period contributes the velocity nodes to move seaward to χ = 2.8 (x = 100 m) which is approximately on the bar crest.

In contrast to the velocity nodal position at χ = 3.8 proposed by the long wave structure alone, Figure 4.7 shows the velocity node at $\chi \simeq$ 2.8 (x = 100 m) which is approximately on the bar crest. Under the case considered in Figure 4.7, a convergence of two flows is shown at the bar crest, implying that any small amount of long wave energy exceeding the mass transport balance would make the velocity node proceed seaward the bar crest. This fact will be dealt more in detail in terms of the frictional velocity in later parts. Due to the rebreaking of wind wave after reformation within the bar trough (Figure 4.2), the shoreward velocity in the lower boundary layer has the intensified cell near χ = 1.8, consequently the mass transport driven by long wave above the oscillatory wave boundary layer (usually lower than ξ = 1.0) has been raised upward.

Under the same conditions except with moderate deep water height of Ho = 1 m, the distribution of mass transport has been dramatically changed (Figure 4.8). Above the bar crest (χ = 2.8) strong shoreward flow develops, and within the trough (around χ = 2.5) the vertical velocity structure is featureless with weak current. The node of seaward flow is retreated back to χ = 1.5 above $\xi \simeq$ 1.7, indicating that offshore transport may not be significant under the moderate conditions.

In summary, the distribution of mass transport velocity in the bottom boundary layer is controlled by relative magnitude of the streaming velocities induced by the wind wave and the long wave. For a given topography, there are two modes of distribution depending on the wind wave conditions; calm and moderate conditions, and stormy condition. Under calm and moderate conditions with wind wave height

about 1 m or less, the net mass transport velocity across the boundary layer is typically shoreward with less sensitivity to the long wave period. Under stormy conditions with Ho higher than 2 m, the net velocity field is bidirectional; shoreward outside the surf zone and seaward close to the shoreline. The position of compensation between two flows is determined by the relative magnitudes of two flows rather than the nodal position of velocity of the long wave alone. The dynamic effect of the long wave period is such that with fixed amplitude the seaward flow transverses farther offshore as the long wave period increases. Hence favorably potential conditions to move the bar offshore are the high long wave energy which is driven by the stormy condition and the long wave period longer than the half-wave resonant (antinodes of the elevation at the shoreline and the bar crest) with the antecedent bar position.

On natural beach it is often observed that the infragravity wave energy consists of wide-banded frequencies instead of a predominant frequency as considered in this section. In principle, there is no limitation in use of the present approach even for the wide-banded frequencies. Assuming the linear system between discrete frequencies, the contribution of each frequency to total long wave amplitude can be estimated on the base of the spectral energy information. The resultant velocity structure in the boundary layer can be set up by summation. In order to convert the nondimensional scale to dimensional scale, a particular frequency of reference should be fixed based on the energy spectrum. The effect of multi-frequency at surf beat is investigated and presented in Chapter 6 which is a part of application to the field observations.

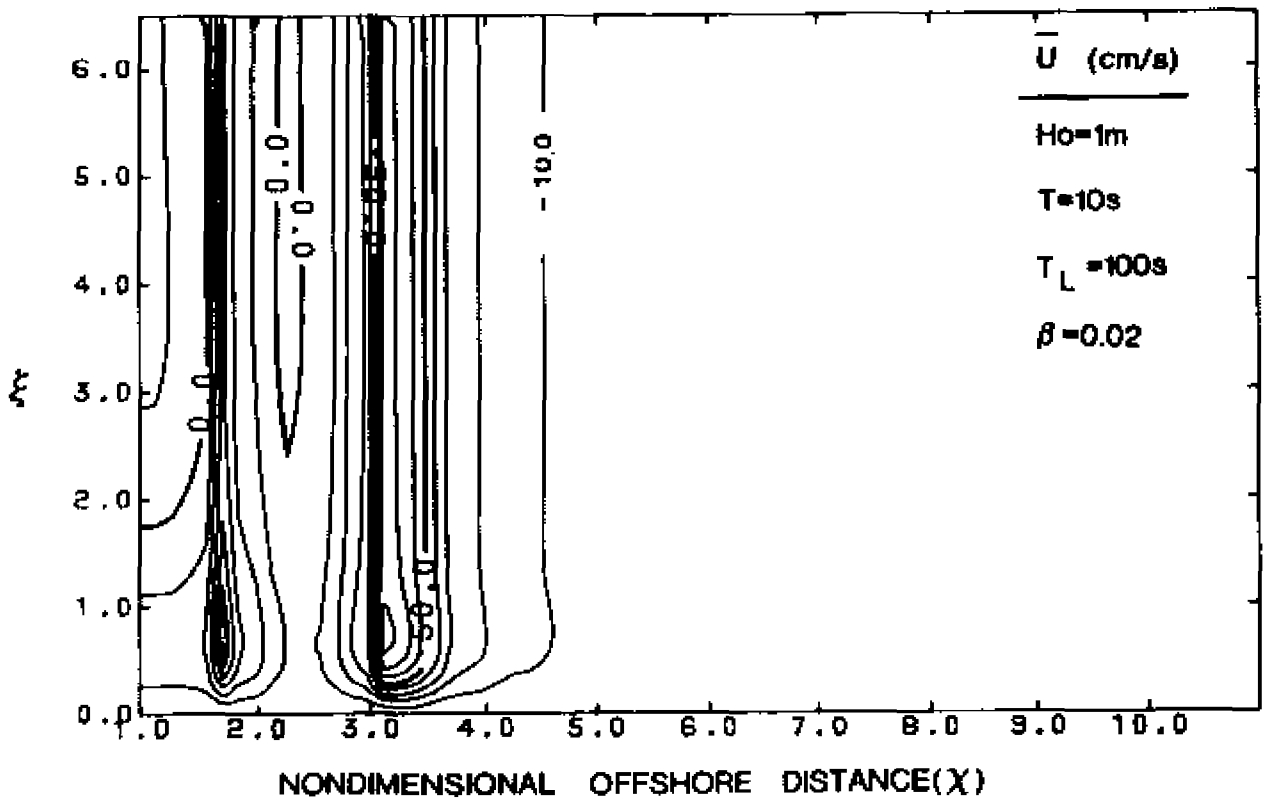

Figure 4.8: Same as in Figure 4.7 but Ho = 1.0 m. Under fair wave condition, the presence of long waves of period longer than that of the half-wave resonance does not help keep the velocity node above the bar crest (χ = 2.8).

4.3.2 The variation of friction velocities with varying wave conditions

In order to examine the vertical velocity structure and consequent shear stress field, detailed cross-sections of the mass transport velocities along the offshore distance are presented in Figures 4.9 and 4.10 for selected cases. Figure 4.9 is for the case of Ho = 2 m and long wave period of 100 s equivalent to Figure 4.7. Figure 4.10 is for Ho = 2 m and long wave period of 50 s. The maximum mass transport velocities are either due to the breaking waves, which are approximately 50 % of the maximum orbital velocities as discussed in Section (3.4.2), or due to the seaward flow induced by the maximum amplitude of long waves at the shoreline. The upper figures show the vertical structures of the velocity indicating relative strength of shoreward (negative; leftward from the vertical axis at each point) and seaward (positive; rightward) flows at selected nondimensional offshore positions. The bar position at x = 100 m is indicated by a shade triangle in the lower figure. The lower figures show the cross-sectional shear stresses (sign and direction in the same manner with the velocity) across the bottom boundary layer along the distance offshore. The shear stresses have been estimated according to Equation (3.40) with the 'effective' eddy viscosity of 1 cm^2/s (Carter et al., 1973).

The boundary of the free shear layer grows outward from the bottom as the convergent zone is approached. Also the shear stresses show the bidirectional structure inside the bar (bar is at χ = 2.8 for T_L = 100 s, and χ = 5.7 for T_L = 50 s).

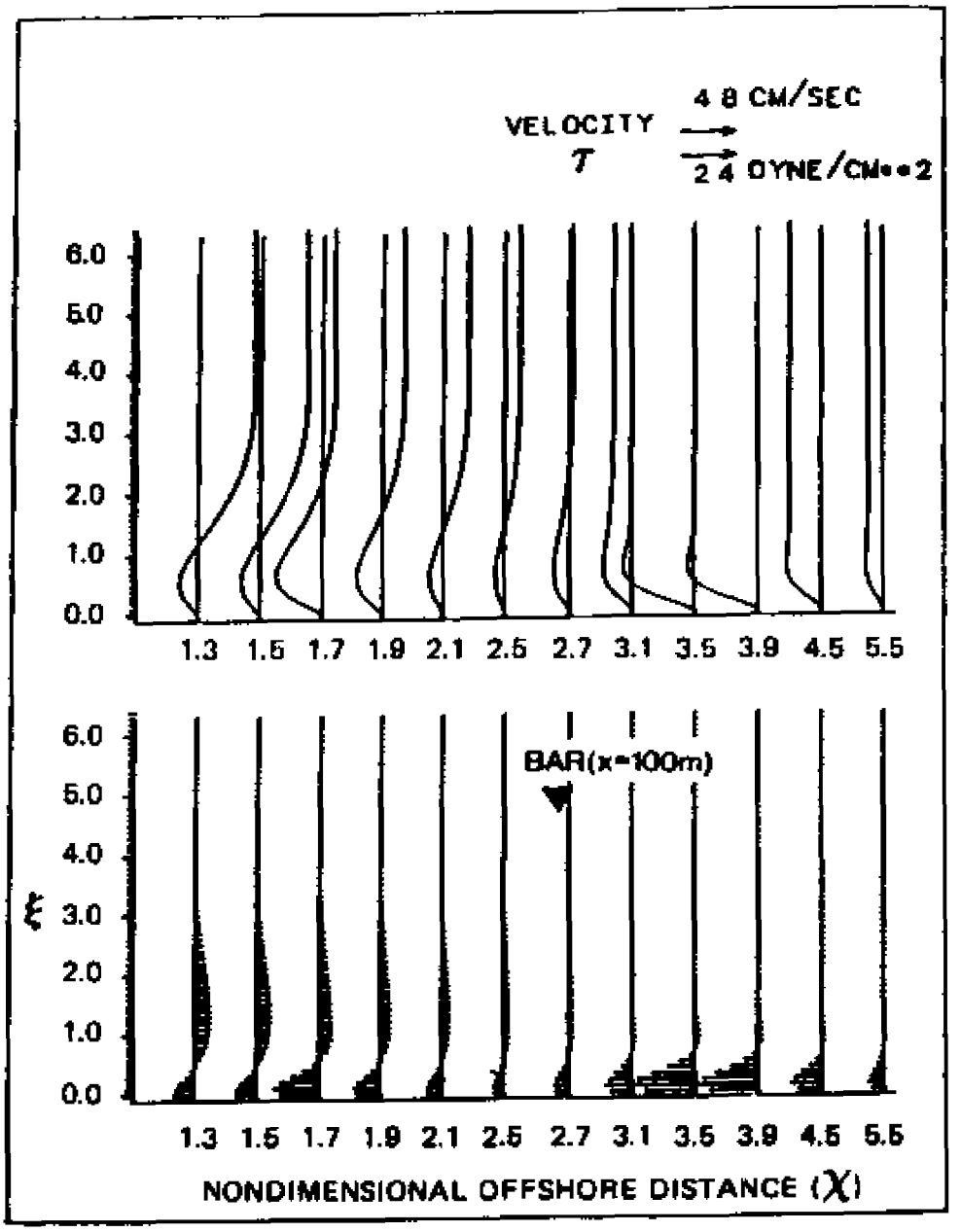

Figure 4.9: Vertical structure of mass transport velocity and shear stress of the wave field as given in Figure 4.7. In the bar trough, a free shear layer is developed with seaward flows on top of shoreward flows in a very thin layer.

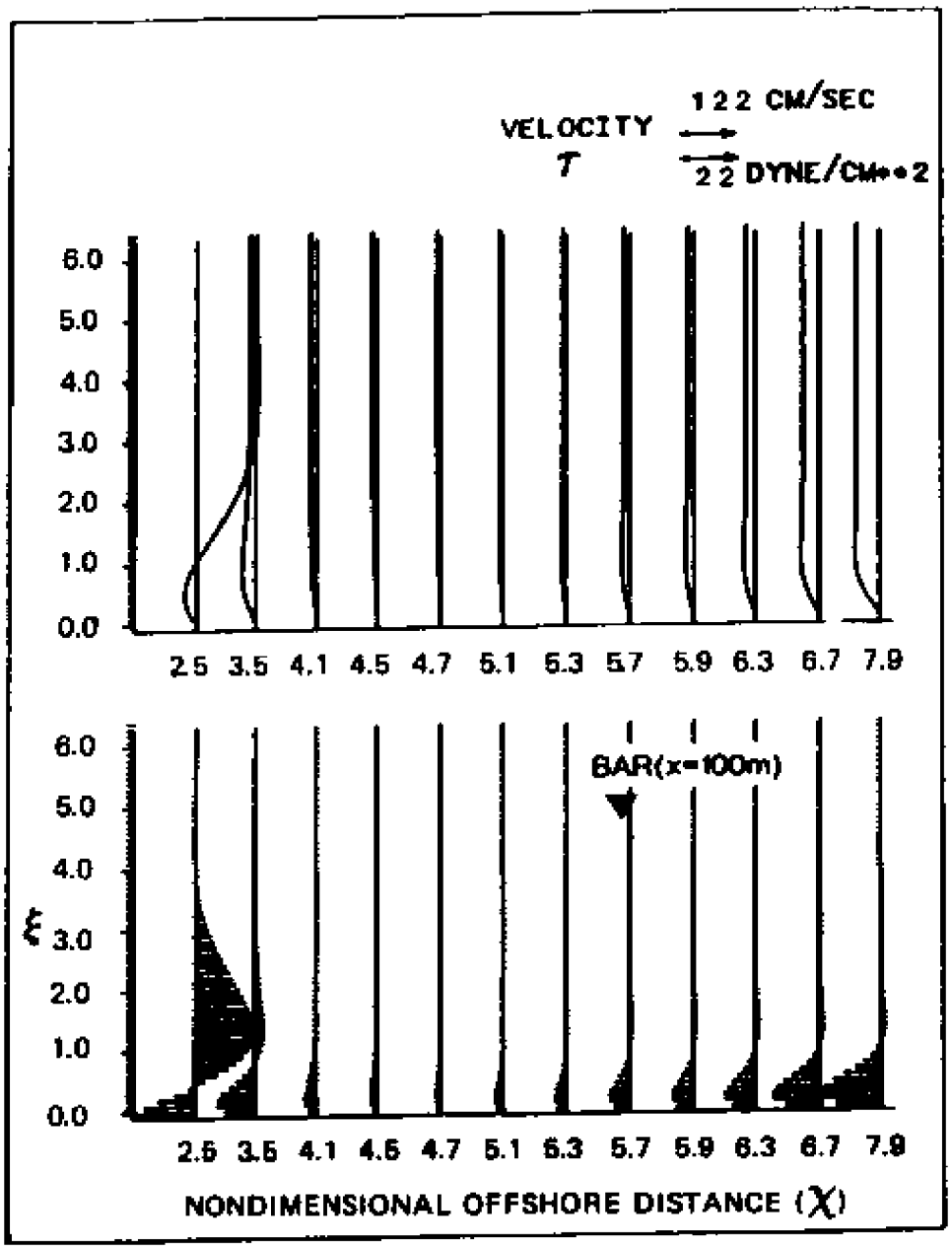

Figure 4.10: Same as in Figure 4.9 but the long wave period T_L = 50 s. Presence of long wave at shorter period retreats the free shear layer shoreward.

The shoreward stresses at the bottom might be coincide with the oscillatory wave boundary layer of order of a few millimeter, hence its mode would be characterized as the bed-load layer (Bailard, 1981). Strongly offshore-directed stresses are found above the immediate vicinity of the bottom for both periods; offshore stress extends to the bar crest for T_L = 100 s and to the bar trough for T_L = 50 s.

Considering the most predominant mode of sediment transport in suspended load (Bailard, 1981), this boundary layer above approximately $\xi \simeq 0.7$ (wave oscillatory boundary layer) is effective to transport the materials which are brought up from the bed-load layer by the turbulent action and supported by the fluid via turbulent diffusion. For the runs with H_o = 0 3 m, the $\bar{U}$ and the stresses are in the onshore direction up to the immediate proximity of the shoreline.

The maximum value of the stress was found to be about 24 dyne/cm^2 . The critical shear stress for sand with uniform grain size 1.0 mm is about 10 dyne/cm^2 and about 2 dyne/cm^2 for the grain of 0.3 mm (Sleath, 1984). For a bed of mixed sizes and densities, the finer-size fractions requires higher stresses than uniform beds (Komar, 1987). At each local point, once the sediment is in motion by wave action, these steady current superimposed on the oscillatory flow will cause a net transport of sediment in the direction of the steady flow.

Figure 4.11 summarizes the variation of friction velocities for several cases. Figure 4.11a is for T_L = 100 s, Figure 4.11b is for T_L = 75 s and Figure 4.11c is for T_L = 50 s. This result shows clear evidence of the mechanism of bar migration under different waves. Under calm condition (H_o = 0.3 m), the friction velocities are shoreward all the way up to the shoreline regardless the long wave period. Under moderate conditions (Ho = 1 m), the friction velocities outside the bar are shoreward. Immediate inner of the bar, friction velocities tend to stagnate except for T_L = 50 s in which the friction velocity flows shoreward, suggesting that long waves with longer period enhance the seaward flows in the surf zone. Under storm conditions (H_o= 2 m), offshore-directed u_* inside the bar for T_L = 100 s could be sufficient to move the bar offshore as observed on natural beaches (Figure 4.11a) while Figure 4.12b shows the case of stable condition with the balance between shoreward and seaward flows around the bar. When the long wave period is much shorter than that of approximate resonant period (in this case, 75 s), shoreward velocity was obtained over the bar, implying possible shoreward migration of the bar. This figure explains, qualitatively, the observations of bar migration tendencies under different wave conditions as observed by Sallenger et al. (1985). For the initial bar developed by antecedent waves, long wave period also determines the behavior of the bar depending on the location of the initial bar.

Figure 4.11: Predicted cross-shore distribution of frictional velocities (u*) under different wave conditions on the given barred topography.
(a) Long wave period T_L = 100 s, incident wave heights of 2 m (solid line), 1 m (dotted) and 0.3 m (dashed). A close inspection of u* reveals that under stormy waves of Ho = 2 m and higher the bar crest experiences seaward frictional velocity, while under fair waves the bar crest is exposed to the shoreward frictional velocity.
(b) Same as in (a) but T_L = 75 s. A 2 m-wave will be enough for the given bar system to persist at that position while the waves of 0.3 m or 1.0 m in height will move the bar onshore.
(c) Same as in (a) but T_L = 50 s. The presence of a long wave with relatively short period will move the bar onshore regardless of wave height.

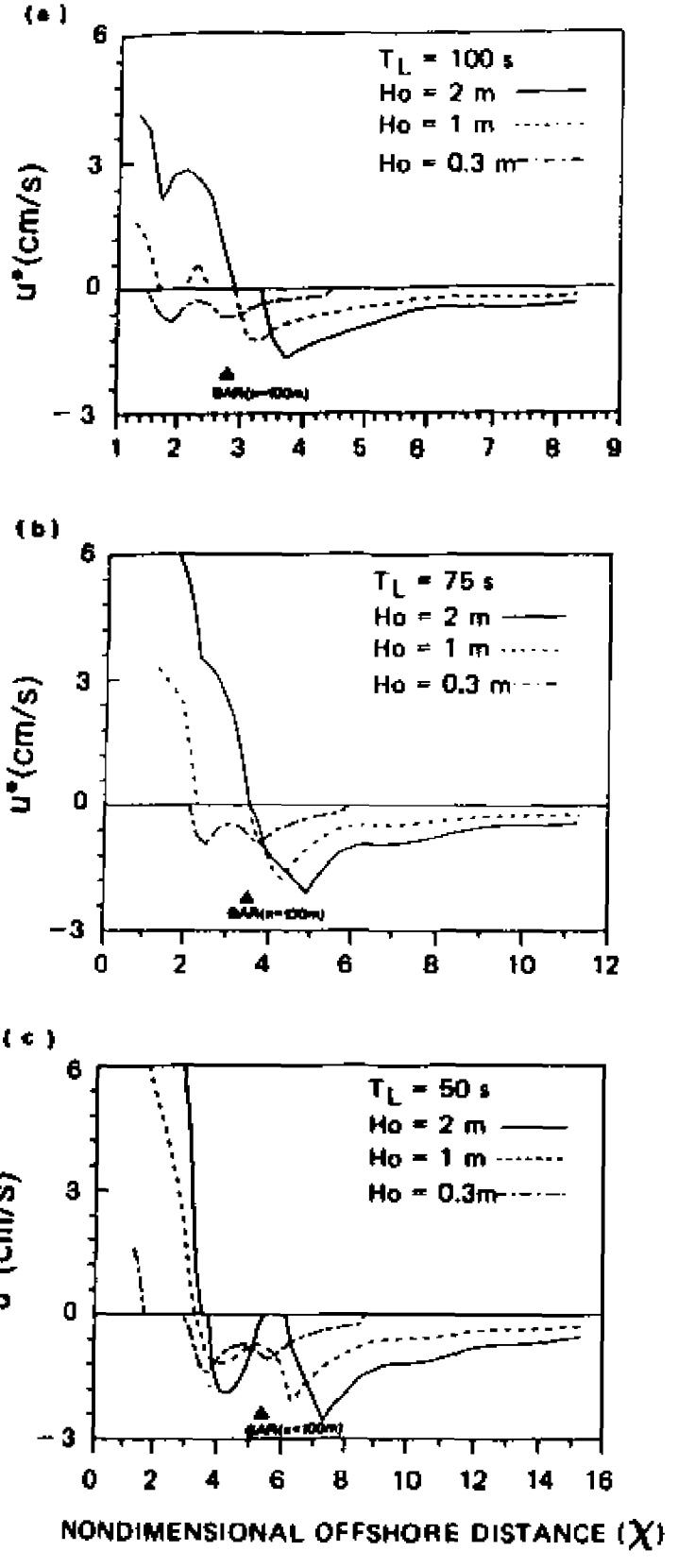
(a)
T_L = 100 s
Ho = 2 m
Ho = 1 m
Ho = 0.3 m
u*(cm/s)
6
3
0
−3
1 2 3 4 5 6 7 8 9
(b)
T_L = 75 s
Ho = 2 m
Ho = 1 m
Ho = 0.3 m
u*(cm/s)
6
3
0
−3
0 2 4 6 8 10 12
(c)
T_L = 50 s
Ho = 2 m
Ho = 1 m
Ho = 0.3m
u*(cm/s)
6
3
0
−3
0 2 4 6 8 10 12 14 16
NONDIMENSIONAL OFFSHORE DISTANCE (χ)

4.5 Discussion

In the context of the present numerical model, there are two ways in which the bar on a given overall beach slope may respond to migrate offshore or onshore. The first is the energy level of low-frequency waves, consequently incident wave conditions. The second one is the period of long wave on a given bar topography. For both cases considered above, the beach slope plays a critical role to determine the long wave structure, hence the distribution of mass transport velocity in the bottom boundary layer as seen in Chapter 3. Generally weak flows have been predicted on steeper beach resulting in less active contribution of mass transport velocity to rework the profile in wave-dominant environment.

In the first case, under fair wave condition with wave height about 1 m or less, the net mass transport velocity across the boundary layer is typically shoreward with less sensitivity to long wave period. This fact suggests that a barred topography would achieve an equilibrium profile without any extreme migration offshore under fair wave condition regardless long wave period. The case of stormy condition imposes the importance of long wave period to determine whether the bar migrates shoreward or seaward depending upon the antecedent bar position. Under stormy condition with wave height 2 m or higher, the bottom flow field is bidirectional: Seaward inside the velocity node and outside the node. Strikingly, the position of the node of the mass transport velocity is determined by relative magnitude of opposite-directed flows rather than the velocity nodes of infragravity waves alone. Normally the velocity

node due to the combined flow of wind waves and long waves has been predicted shoreward of the velocity node estimated by infragravity wave structure alone. The discrepancy between the theoretical nodal position based on long wave structure and the velocity node predicted using the dominant frequency observed in nature has been reported in field studies (Sallenger and Holman, 1987), which would be a consequent effect of combined wave field. The dynamic effect of long wave period has been observed such that seaward flow develops over the bar when long wave period is longer than the half-wave resonant period of the bar system.

Due to the bidirectional nature of the flow in a very thin boundary layer, a diagnostic parameter to determine the behavior of bar has been developed using the bed friction velocity. Any time-dependent motions such as the oscillatory boundary layer or turbulent diffusion are assumed to bring the sediment into suspension up to the boundary layer, considered in this study, which is 5 - 6 times thicker than the oscillatory wave boundary layer.

Since the present scope is confined to a quasi-steady flow induced by the waves, the effective eddy viscosity (ν_m) which transfers the momentum vertically, is assumed to be constant resulting from the contributions of kinematic viscosity decreasing with height from the bottom, and of eddy viscosity increasing with height linearly or exponentially. In turbulent flow, the effective eddy viscosity (ν_m) is on the order of 1 cm^2/s (Carter et al., 1973), yielding the boundary layer thickness $5\,\delta = 5\sqrt{2\,\nu_m/\sigma} \simeq O(10 - 20\ cm)$ for infragravity waves with σ = 0.125 rad. The total boundary layer of the steady flow is

much thicker than the oscillatory wave boundary (O(1 cm)) or individual bed roughness (O(0.1 cm)). Hence the hydraulic roughness due to the nature of bidirectional flow is assumed to be larger than the bed roughness due to the individual grain, ripple or movable bed.

Based on these assumptions, the bed friction velocity (u*) is estimated through the friction coefficient according to Kajiura (1968). The direction and magnitude of u* are assumed to play the key role in the interaction between the flow and the seabed, hence in the sediment transport. The node of the bed friction velocity in the bottom boundary layer of the steady flow due to the combined wave field provides the possible location of bar crest under varying wave condition. However a quantitative relation between the transport rate and the friction velocity, consequently the temporal bottom change is left for another task to be solved, which is guaranteed for future work.

CHAPTER 5

INFLUENCE OF BAR AND BOTTOM STRESS ON LONG WAVES

5.1 Introduction

The numerical calculation of incident wave transformation on a plane beach and a barred topography shows a remarkable difference as described in Chapter 3 and Chapter 4. The wind wave breaking is visibly sensitive to the bottom change, particularly for the case of barred topography. The long waves in the form of standing wave in the nearshore would be resulted from the reflection at the beach, of which the original energy source would be driven by the incident wind waves.

Many of the early investigations of the long wave profile used the analytic solutions on a plane beach (Eckart, 1951; Ursell, 1952; Carrier and Greenspan, 1958; and Whitham, 1979). In field investigation, Suhayda (1974) demonstrated the presence of long waves in the form of the Bessel function solution. Many other investigators utilized the plane beach solution to relate the nearshore geomorphology and the bar positions (for review, Bowen and Huntley, 1984). However recent investigations by Ball (1967), Holman and Bowen (1979) and Kirby et al. (1981) have demonstrated that long wave profiles can be significantly altered from the plane-beach predictions by the effect of nonuniform topography. Furthermore it is anticipated that the long waves would be affected by the bottom friction and the horizontal velocity gradient in the nearshore. Previous investigations in modification of long waves due to the barred topography confine their attention on the edge wave characteristics for a stable bar system.

In the present study, using the finite difference scheme and the shallow water equation on an arbitrary topography (Carrier and Greenspan, 1958), a further case of the modification of long wave characteristics of leaky mode by a barred topography has been investigated. Also special attentions are given to the effects of the spatially-varying bottom friction and horizontal velocity gradient which have been resulted uniquely in the nearshore wave field combined with incident wind waves and infragravity waves as shown in Chapter 3 and Chapter 4.

5.2 Methods

For long waves in shallow water propagating toward the shoreline subject to modification due to the water depth, the equation of motion (Equation 3.22) on a nonuniform bottom can be written

$$\phi_{tt} = g \frac{\partial}{\partial x} \left(h \frac{\partial}{\partial x} \phi \right) \tag{5.1}$$

where $\phi(x,t) = \eta(x)\, e^{-i\sigma t}$, (5.2)

ϕ is the velocity potential, $\eta(x)$ is the structure of surface elevation and h(x) is the local water depth given in Equation (3.20).

Substitution of (5.2) into (5.1) yields

$$\eta''(x) + \frac{h'}{h} \eta'(x) + \frac{\sigma^2}{g h} \eta(x) = 0 \tag{5.3}$$

where the (') denotes the derivatives with respect to x.

For a plane beach, h' is equivalent to β and the solutions of Equation (3.23) are obtained. The present problem is assumed to be in a steady state and the structure of η (x) along the offshore distance x on an arbitrary bottom is of interest. To investigate the effects of the depth variation along x, the radian frequency σ is assumed to be fixed. Since the bottom profile h(x) is not analytic on an arbitrary topography, Equation (5.3) is solved for the case of standing wave by simple backward finite differencing. The horizontal dimension is divided into equally spaced intervals, each Δ x wide.

The surface elevation η_i at succeeding grid points is calculated by

$$\eta_i\left(\frac{1}{\Delta x^2} + \frac{1}{h_i \Delta x^2}(h_i - h_{i-1}) + \frac{\sigma^2}{g h_i}\right) = \frac{1}{\Delta x^2}(2\ \eta_{i-1} - \eta_{i-2}) + \frac{1}{h_i \Delta x^2}(h_i - h_{i-1})\ \eta_{i-1} \qquad (5.4)$$

for i = 2, 3, ...

The boundary conditions are $\eta_{(0)} = J_0(0)$ at the shoreline and $\eta_{(1)} = J_0(1\ \Delta x)$ with assumptions such that the long wave structure over an arbitrary bottom is similar to that on the plane beach of the average slope of the arbitrary bottom, at least near the shoreline. The appropriate width of Δ x has been chosen in such a way that the estimation of η on a plane beach based on Equation (5.4) and the analytic solution on a plane beach given by Equation (3.23) are to be identical. For long waves with period longer than 30 s on the plane beach of β = 0.02, the Δ x at 5 m gives the identical structure with the difference less than 1 % in wave amplitude.

Having fixed Δx width, Equation (5 4) is solved on an arbitrary topography represented by discrete depth at each point. The long wave amplitudes estimated on the given bar topography (Figure 4.1b) and analytic solution on the plane beach of the same average slope with the barred profile have been compared.

5.3 Results

The ultimate objective in this chapter will be an estimation of the degree of long wave modification due to the presence of bar and due to the uneven distribution of bottom stress The present approach is somewhat limited by the nature of long wave and the geometry of bottom topography upon which it is based. However the procedure provides a diagnostic way of examining the relative effect on long wave modification. We consider three different long wave periods (T_L = 100, 75 and 50 s) on the given topography under varying incident wave conditions (T = 10 s; Ho = 2, 1 and 0.3 m). The long wave periods considered fall in the range of surf beat periods commonly observed in nature. The bar is located at x = 100 m on the beach of average slope of $\tilde{\beta}$ = 0.02. The nondimensional offshore distances of bar are χ = 2.8 for T_L = 100 s, χ = 3.8 for T_L = 75 s and χ = 5.7 for T_L = 50 s. The first antinode of the profile for long waves coincides approximately at χ = 3.8 (Figure 3.2).

We first consider the long wave field of T_L = 100 s. Figure 5.1 shows the surface profiles (η) with values normalized by the shoreline amplitude, $\eta(0)$, along the dimensionless offshore distance $\chi = 2\sigma(x/g\beta)^{1/2}$, for (a) Ho = 0.3 m and (b) Ho = 1.0 m. The plane beach and barred beach profiles between Figures 5.1a and 5.1b are identical on the normalized scale of $\eta/\eta(0)$. Comparison of plane beach profile and barred beach profile in Figure 5.1 reveals a clear tendency for the antinode of the barred case to be amplified by up to 50 % from the plane beach profile.

The position of antinode of the barred case is shifted inshore towards the bar crest at χ = 2.8, indicating trapping of antinode over the bar crest which is in line with the study by Kirby et al. (1981) for edge wave trapping over barred topography. Due to shifting of antinodes towards the bar, the wave length of long wave has been shortened by about 80 m relative to that of plane beach. According to the disperaion relation, tendency of shorten wave length will result in increasing the frequency. This fact might have a very important implication to the transient process of bar-wave interaction; When the strength of bottom stress and sediment supply are not sufficient to move the bar (i.e., in a self-maintaining condition), the long wave field consisted of the period longer than the natural period of the bar system would adjust the frequency by increasing to the resonant frequency as long as the incident waves are steady: Otherwise the bar will be forced to move by those processes as described in Chapter 4.

Figure 5.1: Cross-shore behavior of the surface elevation of a long wave at period of 100 s. The amplitudes (η) are normalized by the amplitude η (0) at the shoreline. The bar is located at χ = 2.8 (x = 100 m). Dashed line is the solution on a plane beach, dotted line is the surface profile accounting for the presence of the bar. (top) Ho = 0.3 m, (bottom) Ho = 2 m. The presence of the given bar amplifies the surface fluctuation at antinodes by about 50 % more. The position of the antinodes on plane beaches has shifted toward the bar crest, indicating tendency of antinode trapping over the bar crest.

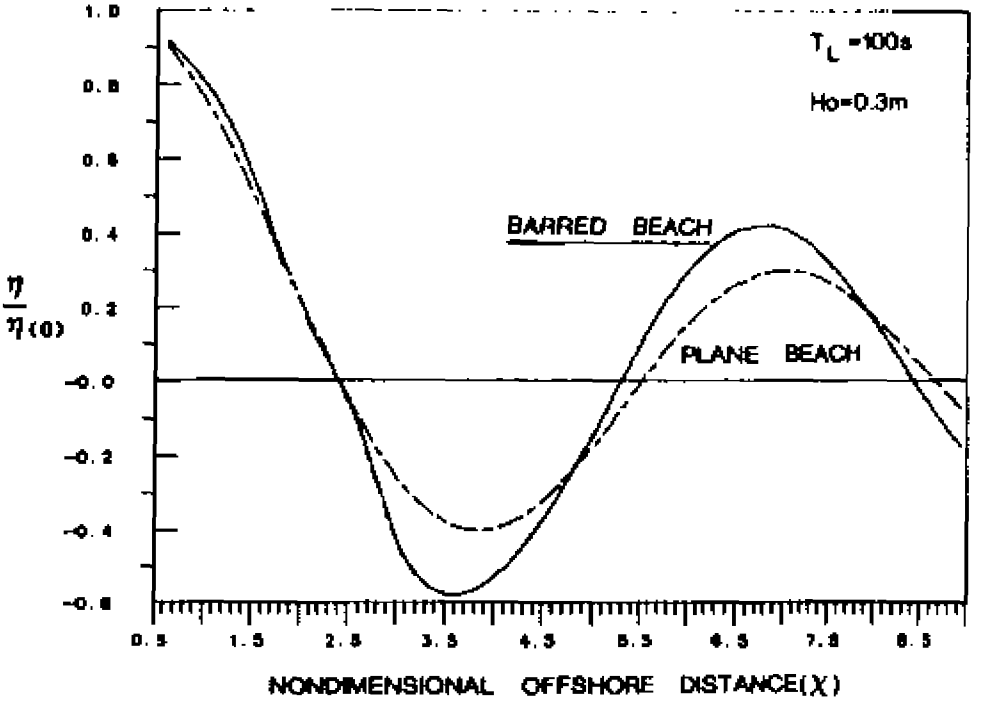
T_L =100s
Ho=0.3m
BARRED BEACH
PLANE BEACH
$\frac{\eta}{\eta(0)}$
1.0
0.8
0.6
0.4
0.2
-0.0
-0.2
-0.4
-0.6
0.5
1.5
2.5
3.5
4.5
5.5
6.5
7.5
8.5
NONDIMENSIONAL OFFSHORE DISTANCE(X)

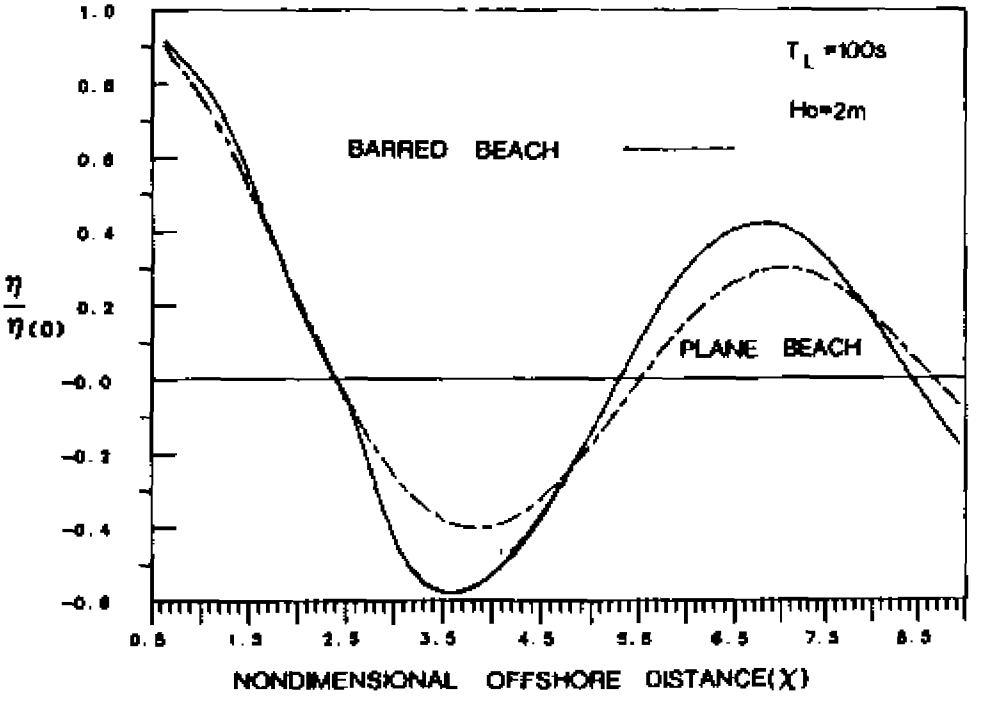
T_L =100s
Ho=2m
BARRED BEACH
PLANE BEACH
$\frac{\eta}{\eta(0)}$
1.0
0.8
0.6
0.4
0.2
-0.0
-0.2
-0.4
-0.6
0.5
1.5
2.5
3.5
4.5
5.5
6.5
7.5
8.5
NONDIMENSIONAL OFFSHORE DISTANCE(X)

Figure 5.2 shows the amplitude fluctuations on plane beach and barred beach with and without the frictional correction for long waves at period of 75 s. This period is coincident with the natural period of half-wave resonance on the given bar topography (the bar and the first antinode at x = 100 m or χ = 3.8). The amplitude over the bar crest is enhanced by about 25 % more than that of plane beach solution. It is notable that the first antinode of amplitude does not tend to shift away from the bar crest, clearly indicating the strong trapping for the wave at period matching with the natural resonant period. The case of Figure 5.2 is considered as a self-maintaining bar system as long as the long waves have the predominant period of the half-wave resonant frequency through any process such as frequency selection or self-adjustment. In other words, when the bar system is stable under steady wave forcing, a preferential frequency satisfying the resonant condition would dominate in the long wave field.

We now consider the long wave peiod of 50 s which is shorter than that of the natural period for the resonance (Figure 5.3). The bar is located at χ = 5.7 and the first antinode of plane beach solution falls on χ = 3.7. Comparison of plane beach and barred beach solutions demonstrates a clear shift of the antinodes for barred beach towards the bar crest, indicating a trapping tendency of antinodes. This case is of a transient one in a manner of either adjusting the wave period to the stable bar system or relocating the bar to match the natural frequency and the wave frequency by the process described in Chapter 4. For the case of multiple frequencies the bar will be located in the region where the bottom shear stresses are balancing, and the multi-frequency will be tuned based on the new natural frequency as long as the bar is stable.

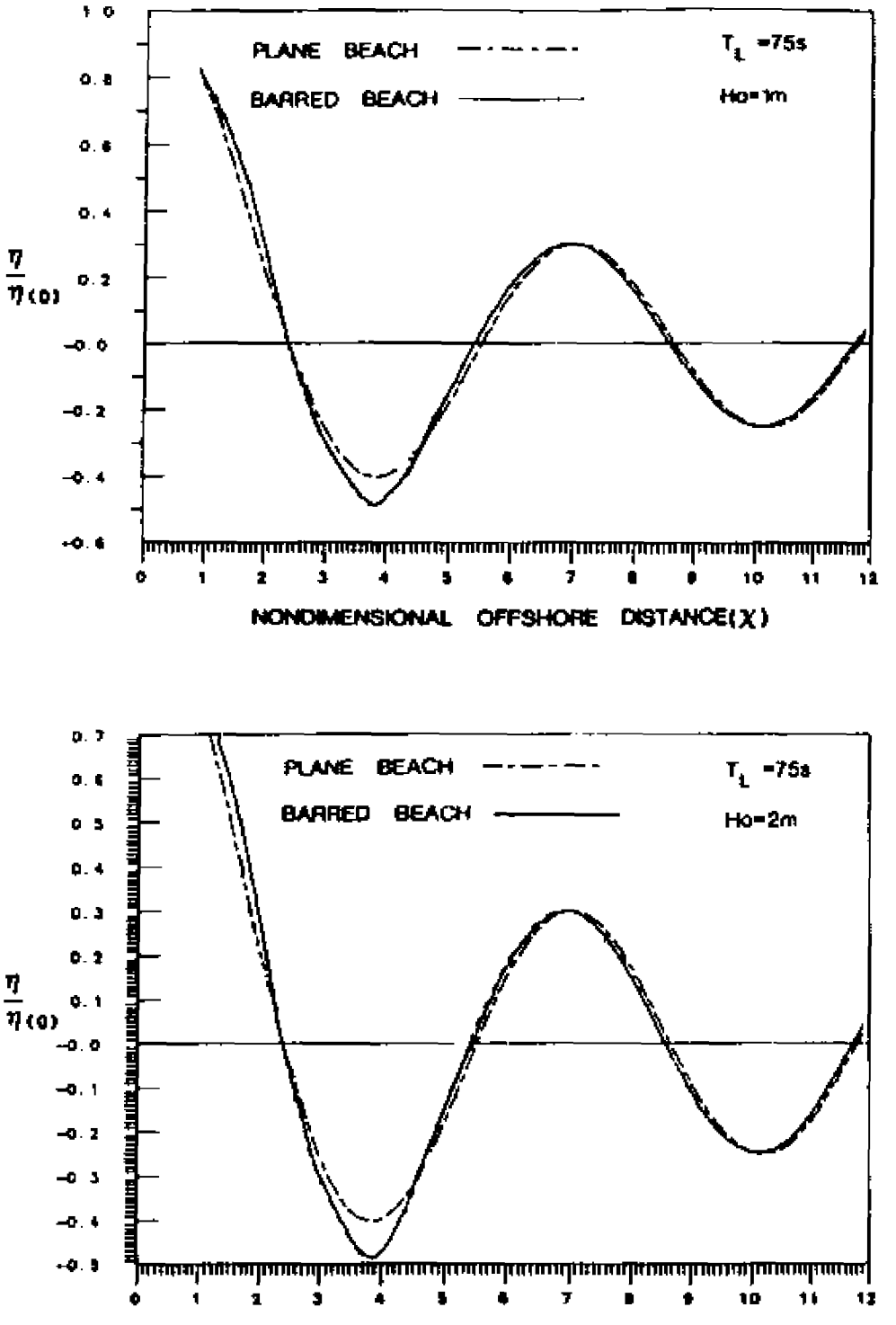

Figure 5.2: Same as in Figure 5.1 but T_L = 75 s which is the natural period for resonance. (top) Ho = 1 m, (bottom) Ho = 2 m, the bar at X = 3.8. The antinode predicted using Jo solution (dashed) is at X = 3.8 which coincides with the bar position. The antinode for the given bar topography (solid) is predicted over the bar crest, showing the tendency of antinode trapping over the bar crest.

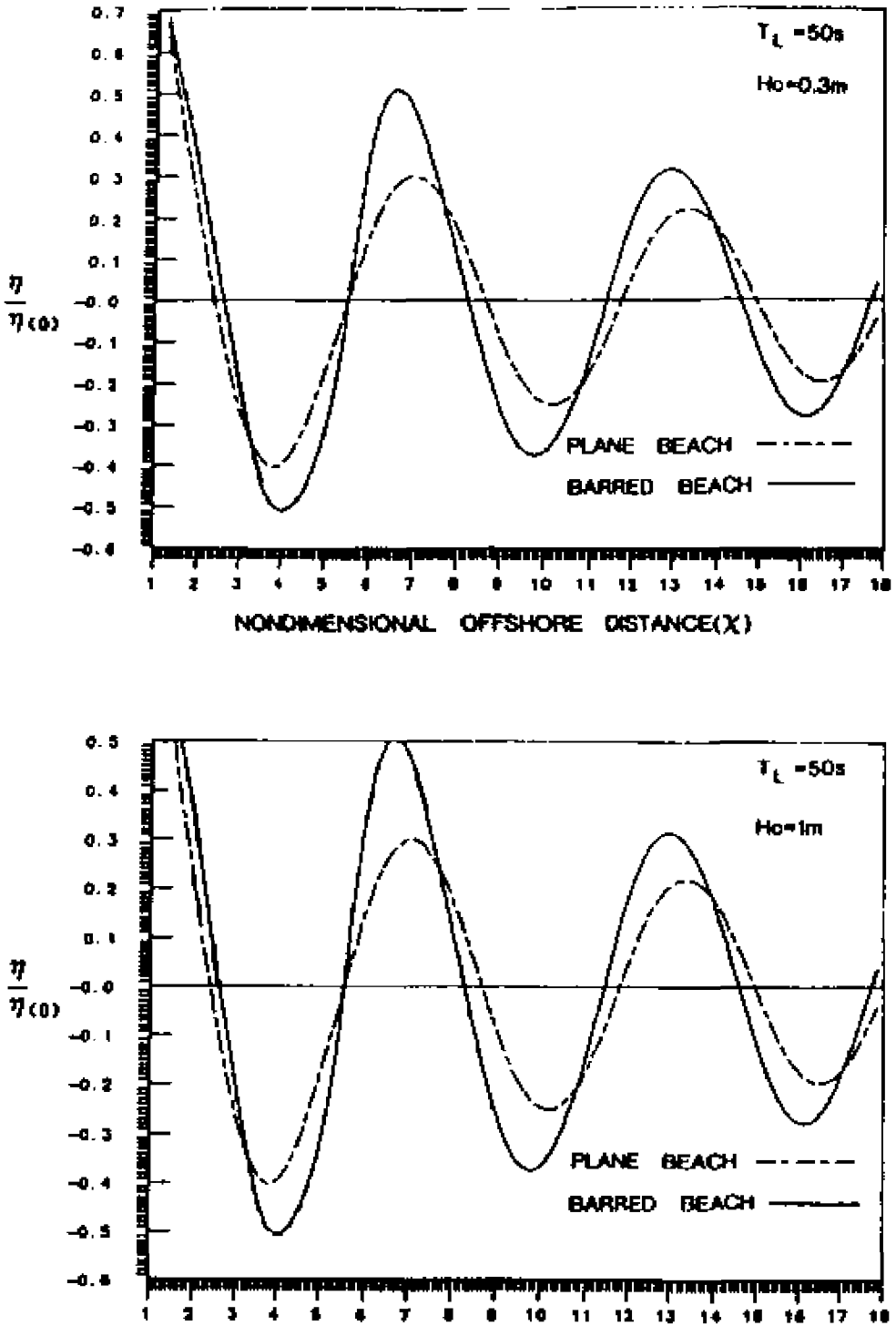

Figure 5.3: Same as in Figure 5.1 but T_L = 50 s.
(top) Ho = 0.3 m, (bottom) Ho = 1 m, the bar at χ = 5.7.
The behavior of antinode is in the same manner with that in Figure 5.1, showing shifting of the plane beach solution (dashed) toward the bar crest (χ = 5.7).

5.4 Discussion

There are a few differences between existing formulations to investigate modification of long waves on barred topography and the present formulation. The most obvious are the numerical schemes and the inclusion of frictional effects. In the study of edge wave modification by barred topography (Kirby et al., 1981) or by complex profiles (Holman and Bowen, 1979), both solved the linear shallow-water equation using the eigenvalue approach (Kirby et al., 1981) or a Runge-Kutta technique (Holman and Bowen, 1979). The boundary conditions require an appropriate beach slope at the shoreline, where the slope is represented by the foreshore slope in Holman and Bowen (1979), or a mean beach slope of the barred topography (Kirby et al., 1981). According to the analysis of Holman and Bowen (1979), approximating a real beach profile by a single linear slope will normally lead to serious errors in edge wave kinematics, implying high sensitivity of foreshore slope. Considering the difficulty in selecting the appropriate beach slope, the present study solves the linear shallow-water equation for a steady state on an arbitrary topography directly using the finite difference technique. Boundary conditions are set at the shoreline and the next grid point such that the elevation profile of long wave is invariant from the plane-beach solution at least at these two points even on an arbitrary topography. The main interest is to see the effect of bar on modification of long wave profile away from the immediate vicinity of the shoreline.

Numerical solutions for a corresponding plane beach were found and compared with the known analytic solution in order to obtain the numerical accuracy and optimum increment (Δx) of successive grid. The x has been fixed at 5 m with accuracy within 1 %.

The principal results obtained in the approach are;

(1) The long wave profile shows a clear tendency of amplification by barred topography (e.g., Figure 5.1), which is in agreement with Symonds and Bowen (1984).

(2) The antinodes of long wave tend to shift toward the bar crests, indicating trapping of the antinode over the bar as suggested by Kirby et al. (1981), Symonds and Bowen (1984) and Sallenger and Holman (1987). This trapping of antinode over the bar would provide a mechanism for preserving existing bars if wind waves are steady over time scales considered.

(3) When the long waves are of broad-band frequencies as of groups in the incident waves, the response of the beach is twofold; When the strength of bottom stress and sediment supply are not sufficient, it would prefer the resonant frequencies to maintain the existing bar; Otherwise the bar will be forced to move until the natural frequency is identical with the tuned long wave frequency.

CHAPTER 6

FIELD OBSERVATIONS

6.1 Introduction

The numerical studies of steadily streaming velocities in the bottom boundary layers as described in Chapter 3 and Chapter 4 provide a mechanism of bar formation and migration. It has been indicated that wave parameters, bottom topography and beach slope are important to determine the behavior of the submarine bars.

The purpose of this chapter is to verify the numerical studies by using the data observed on natural beaches. To do this it is necessary to measure directly the mass transport velocity in the bottom boundary layer in a Lagrangian sense to follow the streak of water particle. This approach has been done by a few investigators. Among them, Bagnold (1947) conducted an experimental study in a wave tank by using dye. His observations show a strong forward drift near the bottom, and a weaker backward drift at higher water column, which is reasonable agreement with Longuet-Higgins' (1953) theory for Stokes' waves. Others such as Zenkovitch (1946) and Murray (1967) who conducted field observations using marked sand of different sizes, show the coarsest particles moving onshore and the fine ones moving offshore, leaving the mechanics unknown. Most laboratory experiments are generally idealized to some very simple situation in which, ignoring the presence of long waves at surf beat period, scale effects may seriously alter the basic physics of the problem. Neither the wave effects, particularly the distribution of drift velocity, nor the sediment dynamics are likely to be reproduced very exactly in small-scale experiments (Bowen, 1980).

This fact strongly suggests the need of a field observation to evaluate the numerical study on bar formation and migration.

Ideal measurements in the field observation will include (1) the distribution of mass transport velocity in the bottom boundary, (2) complete determination of wave structures of wind waves and long waves in time and space, (3) associated direction and amount of sediment transport, and (4) temporal and spatial evolution of the bottom topography with equivalent resolution of hydrodynamic parameters. However, detailed observations of drift velocity in natural beaches from the bottom boundary layer point of view are uncommon, due to the difficulty in setting up such an experiment to measure the Lagrangian tracks in the bottom boundary layer which is itself very thin and varying with wave and bottom conditions. So there is little in the way of a direct observational basis for the wave - barred topography interaction problem in nature.

As long as no genuine method exists, the present study will adopt an approach based on causality - response to verify the numerical study by using field data in the limit of keeping the basic assumptions.

The model wave field consists of transforming wind wave and long waves at surf-beat period. For these forcing parameters, numerous field experiments have been conducted in the nearshore by deploying a horizontal array of instruments. The response of bottom topography to the wave field needs to be measured quantitatively with changing wave conditions. The present model requires input parameters such as deep water wave height and period, long wave amplitudes and periods, and bathymetric data with overall slope. Given these inputs, a critically important parameter to determine the behavior of barred topography is the direction and magnitude of the bed friction velocity induced by the

shear of the drift velocity in the suggested bottom boundary layer which has longer scale than the usual oscillatory wave boundary layer (Section 4.3.1).

In this Chapter, a most feasible field experiment which provides wave climate including storm events, quantitative bathymetry measurements and run-up energy spectra to estimate the periods and relative amplitudes of long wave, is sought and used to verify the numerical study.

6.2 Approach to Field Data and Methods of Verification

Among numerous field experiments measuring nearshore processes, the Duck Experiments over a few years revealed as the most comprehensive and quantitative one The Duck Experiments which are multi-agency nearshore process experiments were conducted in October, 1982 (Hereafter DUCK82), September, 1985 (DUCK85) and October, 1986 (SUPERDUCK) at the Field Research Facility (FRF) of the U.S. Army Engineer Waterways Experiment Station, Coastal Engineering Research Center (CERC), Vicksburg, Mississippi. The FRF is located near Duck, North Carolina on the northern end of North Carolina's Outer Banks fronting the Atlantic Ocean (Figure 6.1). The nearshore area at Duck is exposed to the storms which usually attack the area in October and is observed to change in the nearshore bar system along with wave climate. One of the task to these Duck Experiments was to measure the nearshore geomorphological response to storm-induced waves and currents (Mason et al., 1984). The experimental setting and the results of data analysis based on the scope of each participating group are widely reported in literature (Mason et al., 1984; Richmond and Sallenger, 1984; Sallenger and Holman, 1985, 1987 for DUCK82: Wright et al., 1986 for DUCK85: Whitford and Thornton, 1987 for SUPERDUCK).

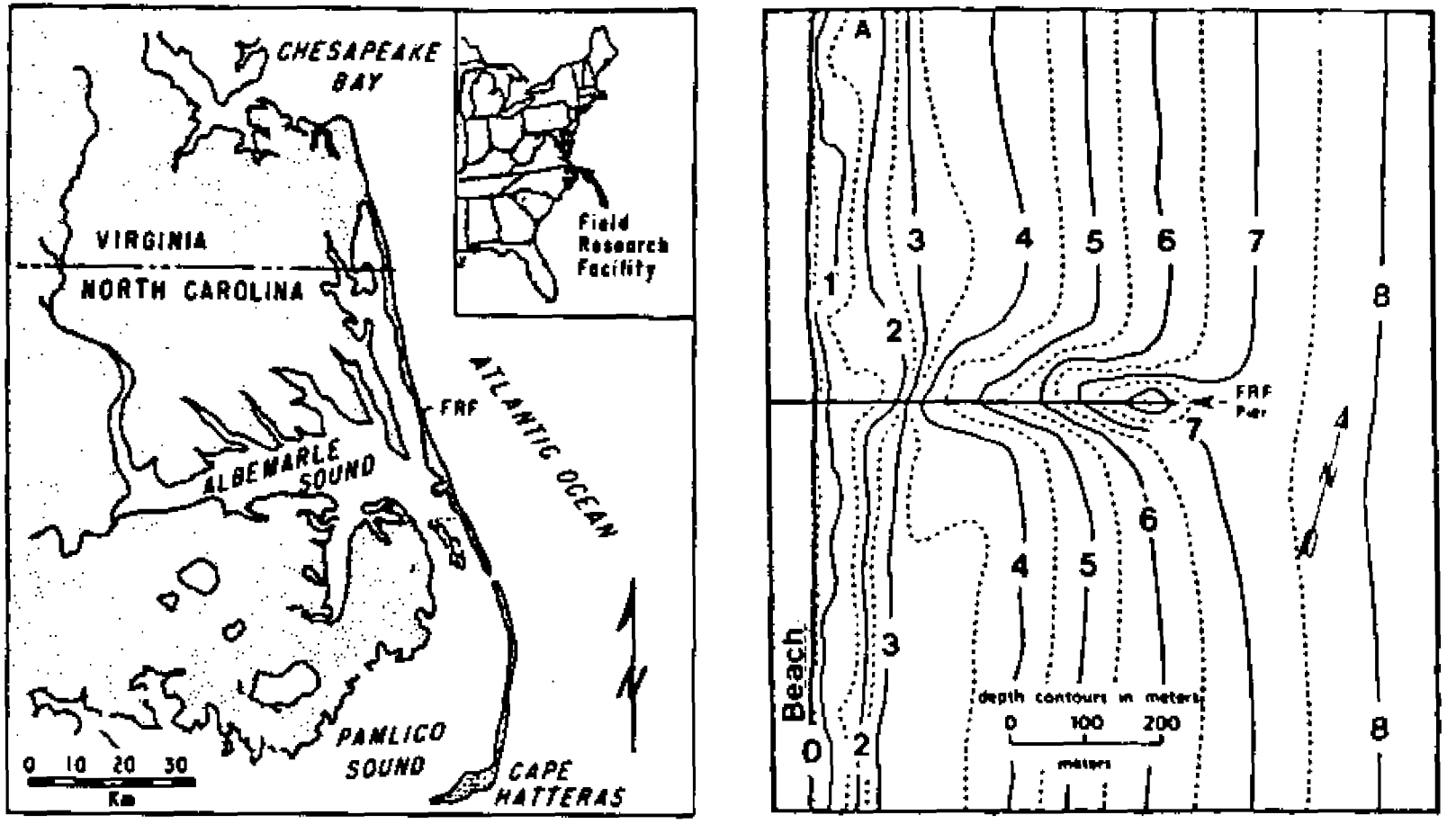

Figure 6.1: Location map (left) of the Field Research Facility (FRF) and depth profiles (right) around the FRF pier. Nearshore survey line using the USGS sled system was about 460 m north of the pier.

At present the data from the later two experiments (DUCK85 and SUPERDUCK) are being analyzed by each group of participants. The experimental setting and methods, and environmental data during DUCK82 experiment are described in many reports, including the energy spectra of infragravity waves and run-up data (e.g., Mason et al., 1984; Sallenger and Holman, 1987).

This chapter is intended to verify the numerical experiment by using the observed data in the field. The basic data required as inputs for the numerical investigation are adopted from the informations in the published papers for DUCK82 experiment, which are extracted from Miller et al. (1986), Birkemeier (1984), Sallenger and Holman (1987) and others.

6.2.1 Experiment

General Description: The Field Research Facility (FRF) is located near Duck, N.C. (Figure 6.1), consisting of a 561-m-long research pier made of a reinforced concrete structure. The FRF is located near the middle of a 100-km unbroken stretch on the northern end of barrier islands, bordered by the Atlantic Ocean to the east.

Nearshore bathymetry at the FRF is characterized by regular shore-parallel contours, a moderate slope, and a single bar with a second, smaller, nearshore bar occasionally appearing except in the immediate vicinity of the pier where a trough runs along the pier due to scouring (Miller et al., 1986). The pier axis which is normal to the average shoreline points offshore at angle of about 67.5^{o} from true north.

Sediments in the area vary greatly in size. The foreshore typically exhibits a bi-modal size distribution comprised of a coarse ($\bar{}$

1 mm) fraction interspersed with finer ($\tilde{=}$ 0.3 mm) sands, with a median size of about 0.75 mm. Offshore, sands decrease in median size from about 0.2 mm on the nearshore bar to less than 0.1 mm in 20 m of water (Mason et al., 1984).

The nearshore profiles were measured with the USGS sled system (Sallenger et al., 1985) using a Hewlett-Packard infrared total station and optical prisms on top of sled's 10-m mast. The sled was towed by a double-drum winch and triangular line arrangement along a shore-normal transect about 460 m north of the pier to avoid effects of the pier. Birkemeier (1984) overplotted 155 surveys of a profile line collected for 3 years to see the range of vertical change at the study site. Most profile activity is restricted to depths less than 7 m (about 500 m offshore) with little measurable vertical variation at deeper depths where offshore slope is represented by 0.006. Although the profiles have varied from nearly unbarred to triple barred, they typically exhibit a double bar configuration with a narrow inner bar at about 100 m offshore from the mean shoreline and a wide outer bar at about 300 m offshore. The location and horizontal movement of the bar crest is one of the best indicator of sediment volume change, since there was little or no change in bar crest depth. When there were two (inner and outer) bars, the behavior of bar movement was observed such that the outer bar moved in the same direction and speed with the inner bar depending upon the wave conditions (Mason et al., 1984).

Waves tend to approach most frequently from north of the pier in the fall and winter and south of the pier in the summer; whereas, annually they are evenly distributed between north and south. Observed at the end of the pier, the annual mean significant wave height is 0.9 m

with a standard deviation of 0.6 m; the annual mean peak spectral period is 8.5 sec with a standard deviation of 2.9 sec; and annual mean direction falls in the range of $\pm 5^{o}$ with respect to the pier axis. During the DUCK82 experiment, two waverider buoy gauges were deployed offshore at 0.6 km and 3 km from the baseline. The deep water wave condition was represented by the wave gauge moored in 20 m of water 3 km offshore. Additional wave information was collected by 4-cm-diameter electromagnetic current meters (Marsh-McBirney model 512) mounted in a vertical array at 0.5 m, 1.0 m and 1.75 m above the bottom and a pressure sensor on the sled.

The energy spectra of the data collected by the electromagnetic current meters are used to provide the magnitudes and periods of long waves. Time series of run-up were measured at locations 300 m and more away from the sled line.

Storm Events: Most of the data discussed in this chapter were obtained during a 3-day storm, October 10-12, 1982 at the FRF. Figure 6.2 shows the time history of waves and winds at the FRF during October, 1982. Northeast winds reached a maximum sustained speed 13 m/s and generated steep waves to over 2 m (measured by the offshore waverider). Prior to the storm, nearshore morphology was characterized by a well-developed berm and relatively small nearshore bar (Figure 6.3; profile on 7 October). During the storm, the bar crest migrated offshore 13 m over a six-hour period on the 10th, yielding a very rapid migration rate of 2.2 m/hr.

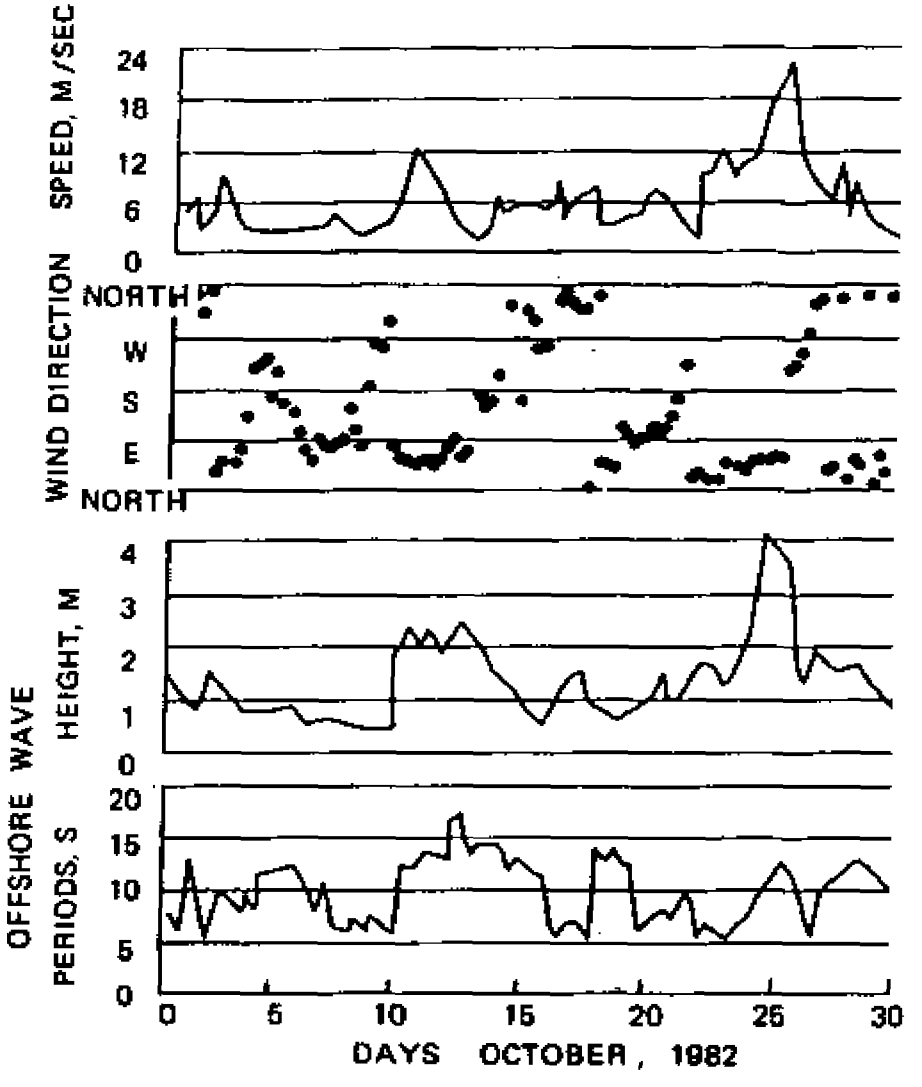

Figure 6.2: Wind and wave conditions in October, 1982 at Duck, North Carolina (after Mason et al., 1984).

By October 12, the storm had moved offshore, winds decreased to only about 7 m/s. However the storm center on the east continued to generate large waves principally of the swell type, and significant wave heights in excess of 2 m. The energy spectrum was relatively narrow with a dominant period of about 17 sec (Sallenger and Holman, 1985).

Between the 10th and 11th, the bar was stable, while between 11th and 12th, it again migrated offshore, at a rate of 1.4 m/hr (Figure 6.3). During the 3 days of the storm the bar became better developed, and the bars are essentially linear when incident waves are large as observed by Short (1979).

Between the 15th and 17th, the wave condition was recovered to a calm condition and the bar showed an apparent landward migration at the rate of 0.5 - 1.2 m/hr. By the 19th the bar had disappeared, leaving a platform similar to that of 7 October.

It is noticeable that the patterns of bar formation and offshore movement observed by Birkemeier (1984) and Mason et al. (1984), always occur well within the surf zone. Therefore, it is clear that the inner bar could not have based on 'a plunging breaker hypothesis'. This observation supports the basic hypothesis of this study on bar formation /migration such that the effects of infragravity waves having periods greater than 30 sec would attribute much of these processes as inferred by Sallenger et al. (1985).

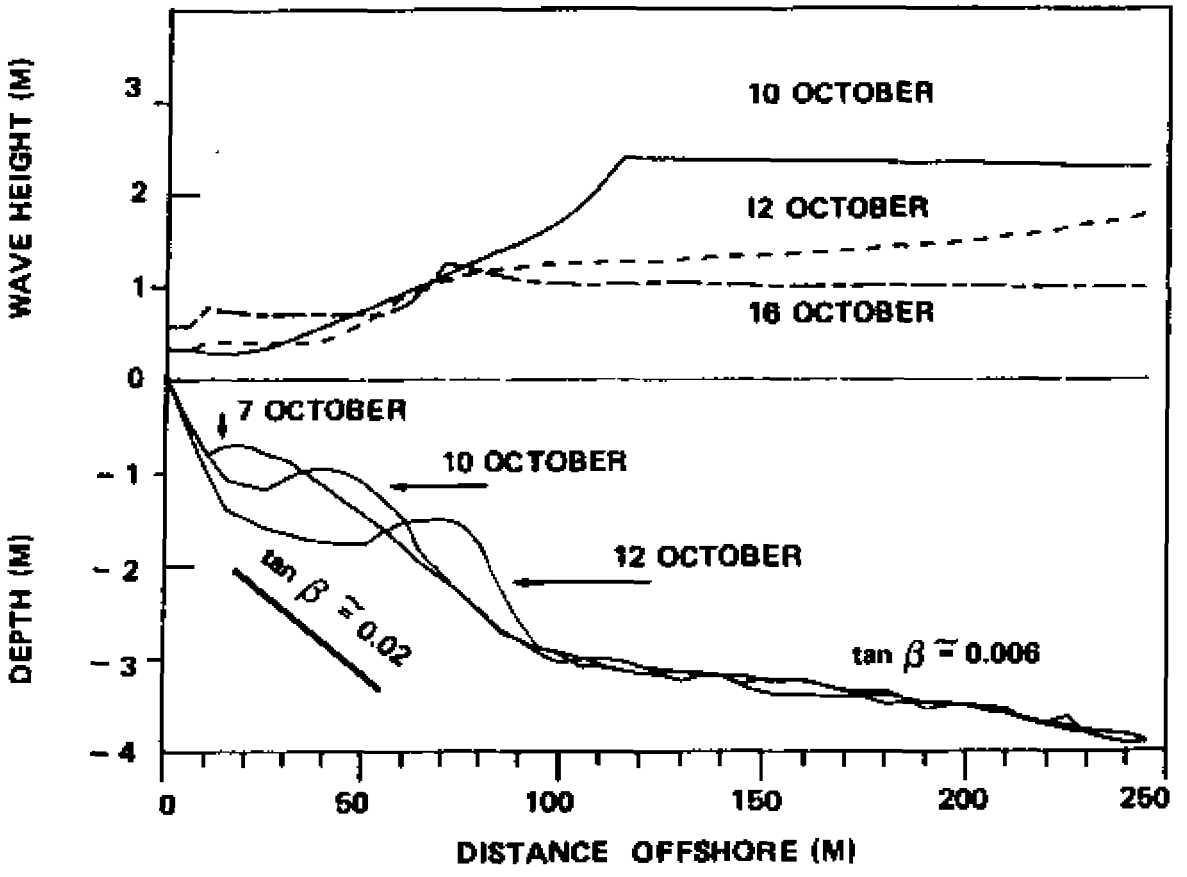

Figure 6.3: Wave heights and profiles along the sled line, 7-16 October, 1982. Significant wave height on the 12th was in excess of 2.4 m with plunging breaker at about 500-600 m offshore. The profiles show the response of the bar during the storm (10 and 12 October), migrating offshore. By 19 October, the profile was recovered to the same as on 7 October, migrating onshore.

6.2.2 Methods of Verification

Verification of the numerical study with field data collected during DUCK82 is based on events which are distinct in wave condition and geomorphologic configuration. The events are grouped into 4 different groups of wave/bathymetry pairs, representing a pre-, developing, fully developed and post- stage of the storm. Assuming the gradual changes in bathymetric profiles from platform (e.g., 7 October in Figure 6.3) to well-developed bar system (e.g., 12 October in Figure 6.3), and in wave condition (Figure 6.2), the events for verification of the numerical study are selected such that (Figure 6.4):

I) run with wave condition early on 10 October on the featureless profile on 7 October to predict the profile on 10 October, which resulted in the first half of 10 October;

II) run with wave condition on 12 October on the bar profile on 10 October to see whether the earlier bar profile is subject to offshore migration;

III) run with wave condition on 16 October on the well-developed bar profile on 12 October to examine the recovery to the featureless profile;

IV) run with wave condition on 10 October on the profile on 10 October to investigate the sustaining profile as observed during 10-11 October.

It has been clear that frequency information of long waves is directly associated with the run-up spectrum in the infragravity band (Guza and Thornton, 1985; Sallenger and Holman, 1987). The long wave information was obtained from the run-up spectra measured 300 m away from the sled line.

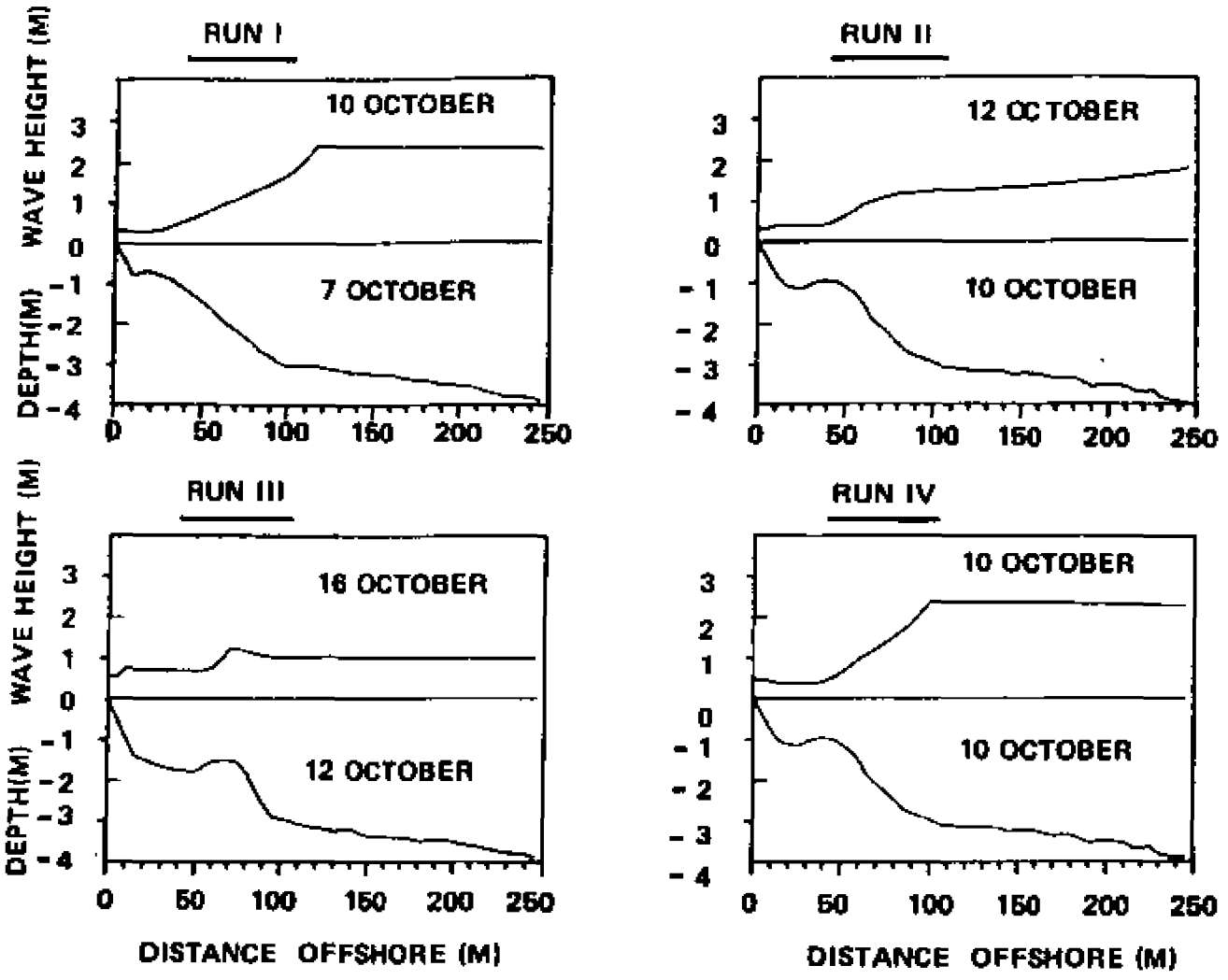

Figure 6.4: Wave heights (upper in each plot) and bathymetric profiles (lower in each plot) along the shore-normal line of 4 different events, representing a developing stage (Run I), fully developed stage (Run II), post-stage (Run III) and steady state (Run IV) of the storm.

The assumption of alongshore homogeneity in bathymetry and waves at the study site has been applied. This assumption does not violate the observational evidence, since the structure of the measured run-up spectrum compares closely to the estimated spectrum based on the current meter data at the sled line (Sallenger and Holman, 1987). From the run-up spectrum of each run, the frequencies of the most energetic peaks of the spectrum were picked up for the use of infragravity wave frequencies. The total amplitude of infragravity waves which is the half of the vertical run-up height is assumed to follow the relation as shown in Figure 3.7. The amplitude of long waves at each peak-frequency is assumed to consist of partitions based on the relative amplitude ratio estimated from the measured run-up spectrum by taking the square root of energy density at each frequency. For a given set of wave conditions, the wind wave transformation was estimated based on the algorithm developed by Ebersole et al. (1986) in and outside the surf zone as done in Chapter 4.

Table 6.1 summarizes significant wave height, peak period of incident waves, long wave frequencies with relative amplitudes. The long wave frequency on 16 October was not measured, but selected based on the typical frequency on the study site, which was given at 0.015 Hz. When the incident waves are in calm condition, changing the long wave period yields little change in the result as shown in Section 4.3.1.

Table 6.1 Input wave conditions for verification of the numerical study.

Run#	Wave Data on	Incident Waves		Long Waves		Initial Bathymetry on
		Significant Wave Height	Period	Period	Relative Amplitude	
I	10 Oct	2.25 m	6.9 s	28 s 67	1.4 1.7	7 Oct
II	12 Oct	2.40	16.8	30 46 67 105	2.65 2.45 2.45 2.82	10 Oct
III	16 Oct	0.8	11.0	67	1.0	12 Oct
IV	10 Oct 12 Oct	2.25 2.40	6.9 16.8	28 67 30 46 67 105	1.4 1.7 2.65 2.45 2.45 2.82	10 Oct 12 Oct

6.3 Comparison of Duck Data with Model Prediction

Due to the lack of field experiment which is intended specifically for the scope of this study, the basic approach for verification is due to the assumption such that the wave conditions selected for test runs exerted steadily on the preceding beach profile (Table 6.1). The approach developed in Chapters 3 and 4 has been applied with given input data of waves and topography to estimate the mass transport velocity as a function of offshore distance and the distribution of the bed friction velocity in the bottom boundary layer has been compared with the beach profile measured on the date of input wave condition.

Figure 6.4 shows the transforming wind waves on precedent profiles for test runs. A three-day storm lasted for 10-12 October, 1982. Run I represents a case of developing storm on a prestorm profile to see the process of bar formation; Run II is a case of fully developed storm on developing bar system to see the process of bar migration offshore; Run III is a case of poststorm on well-developed bar system to see the process of bar migration shoreward; Run IV is a case of persisting bar, i.e., an assumed steady-state storm on 10 October on a bar profile of 10 October, which was generated by the input storm.

To each case of run with input data in Table 6.1, the numerical study described in Chapter 3 and 4 has been applied. The resultant distribution of the friction velocity in the bottom boundary layer is presented and compared with the bottom profile measured through the field experiment.

Run I: Run I is selected to examine a case of bar formation from a featureless profile obtained prior to the storm. At the experimental site, the beach profile prior to the first day of storm on 10 October, was characterized by a small bar close to the shoreline as shown on 7 October in Figure 6.3. As the storm developed on 10 October, a prominent bar was observed about 40 m offshore from the shoreline.

Figure 6.5 is the result of the numerical study run on the initial bottom profile of 7 October with wave conditions of 10 October. The upper plot shows the distribution of the friction velocity (positive offshore) in the bottom boundary layer induced by a superposition of long waves and incident waves (Table 6.1). The lower plot shows the precedent profile on 7 October (solid line) and a profile observed on 10 October (dotted line) which is subject to the comparison with prediction based on the friction velocities in the upper plot. The distribution of the friction velocity is characterized by an oppositely directed flow system with a velocity node where offshore flow (positive u_*) meets the landward flow (negative u_*). The node of friction velocity for Run I occurs at 40 m offshore from the shoreline. Landward of the node, a relatively strong friction velocity would force the bottom material which is brought up into suspension by turbulent diffusion, to move offshore while the shoreward flow seaward of the node would bring the material to pile up near the node. The beach profile observed on 10 October is presented in lower plot (dotted line), showing a bar crest at about 40 m offshore from the shoreline.

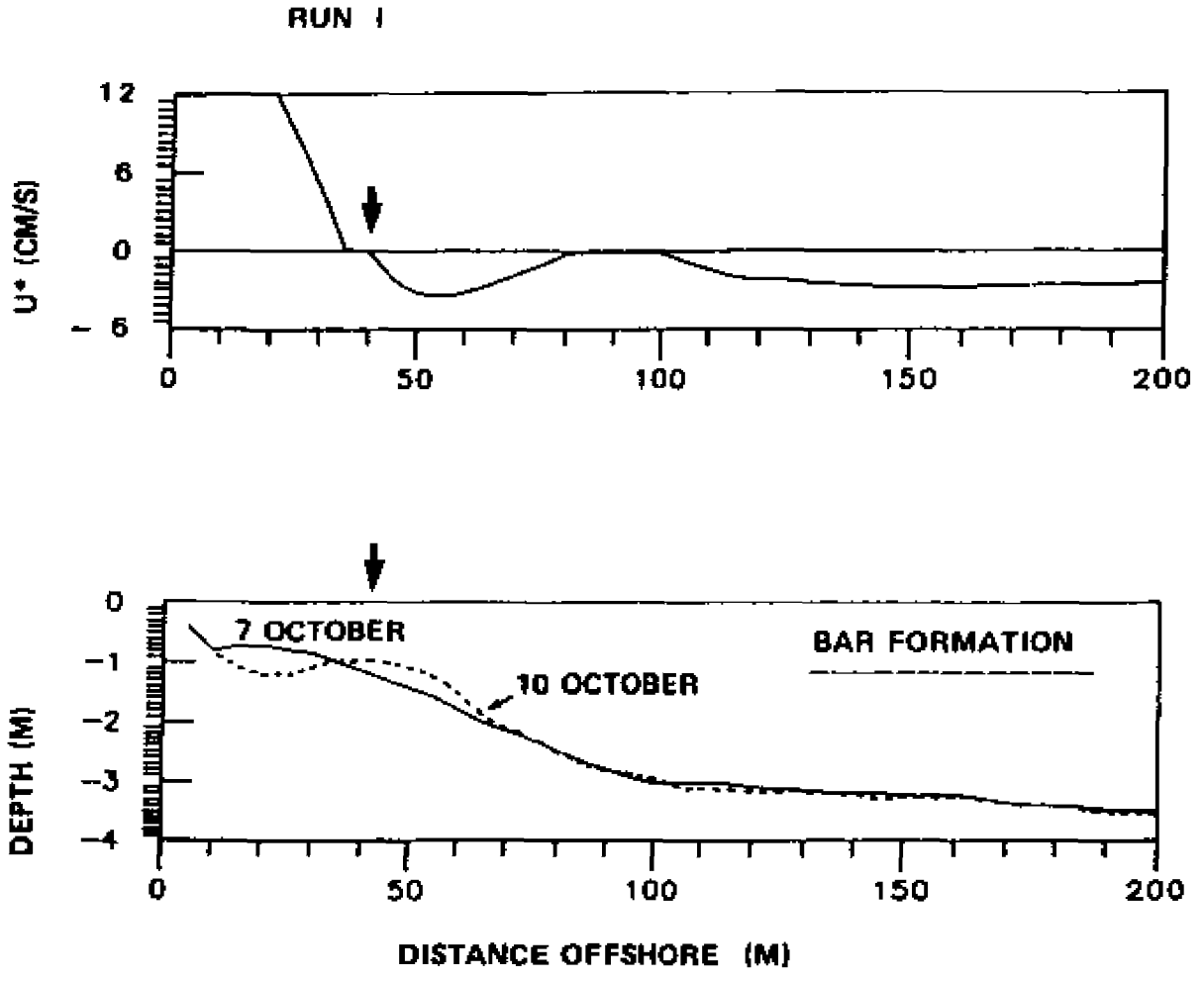

Figure 6.5: Results of running model for Run I (bar formation), comparing predicted node of the friction velocity (+u*: offshore) and observed position of bar crest. (upper) distribution of the friction velocity in the bottom boundary layer with the node around 40 m offshore; (lower) the initial profile (solid line) before the storm and storm-developed profile (dotted line) with bar crest (downward arrow) around 40 m offshore. This process during developing stage of the storm illustrates bar formation.

The bar crest is defined as a position where the gradient of bar configuration with respect to the offshore increment is zero. Clearly the profile observed on 7 October changed to yield the profile on 10 October with a prominent bar crest at about 40 m offshore.

The prediction of the process of bar formation (or migration) based on the friction velocity (upper) is in excellent agreement with the profile observed at the site.

Comparison of two profiles observed during pre- and transient storms reveals that there is little change in configuration beyond approximately 150 m offshore. This fact suggests that the bottom flows with even small magnitude across the node would have more implication to the modification of profile than uniform flows in one direction as shown out of 100 m offshore. Considering a differential control volume, the mass flux through upstream face would be equal the mass flux out of the control volume, resulting no net accretion or erosion.

Run II: Run II is selected to examine the process of bar migration offshore during the wave condition changing from an early stage to fully developed storm. Run II was implemented with wave condition on 12 October which was applied on the initial beach profile on 10 October (Table 6.1). During 10-11 October the bottom configuration showed little change (Mason et al., 1984) until the storm moved eastward on 12 October. On 12 October, the wave energies in the incident wave band and infragravity wave band have risen dramatically higher than that on 10 October (Sallenger and Holman, 1987). Incident waves broke primarily further 600-700 m offshore and secondary breaking occurred around 60 m offshore.

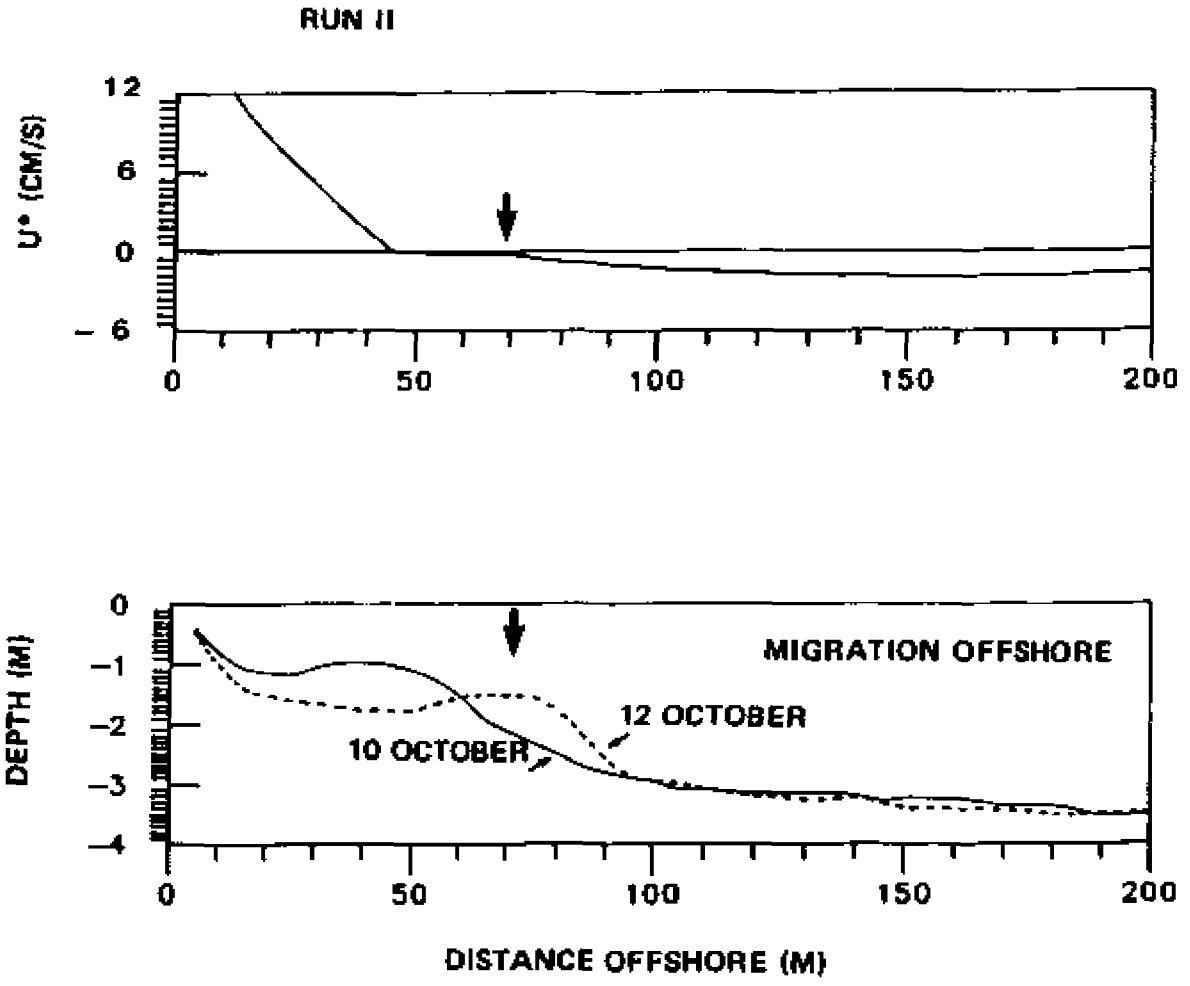

Figure 6.6: Results of running model for Run II (migration offshore), comparing predicted node of the friction velocity (-u*; offshore) and observed position of bar crest. (upper) distribution of the friction velocity in the bottom boundary layer with zero value (arrow) around 70 m offshore; (lower) the initial profile (solid) on 10 October and profile observed two days after (dotted), showing the bar crest migrating offshore by about 30 m. The bar crest positioned at about 70 m offshore, which is in agreement with predicted node of the friction velocity.

The node of the friction velocity in the bottom boundary layer was predicted around 70 m offshore with very weak flow around 50-70 m offshore (Figure 6.6). Comparison with the observed profiles (dotted line in lower plot) on 12 October reveals that the prediction of the friction velocity node is consistent with the bar configuration with the bar crest which moved from 40 m to 70 m offshore during this period.

The average migration rate is estimated at about 1.2 m/hr. However the bar migration does not occur steadily, but migrates with varying speed depending on the varying wave condition. According to the observation by Mason et al. (1984), between 10-11 October, the bar was stable, while between 11-12 October, it migrated offshore at a rate of 1.4 m/hr. Usually it has been observed that the most rapid change in configuration occurred during the transient stage from one wave condition to the other.

Run III: Run III is selected to examine the process of bar migration landward when the storm subsided. Run III was implemented with calm wave condition of 16 October on the initial bathymetry observed on 12 October (solid line in lower plot in Figure 6.7). The wind speed decreased after 12 October until 16 October with decreasing significant wave height from 2.4 m to 0.8 m.

The bottom profile was observed such that by 19 October the profile recovered to a featureless one as observed on 7 October. The velocity node (upper plot in Figure 6.7) was predicted at around 30 m offshore from the shoreline. The observed profile after the recovery on 19 October (dotted line in lower plot in Figure 6.7) shows a consistent trend of the bar creat which was in the process of landward migration on 16 October during the waning stage of the storm.

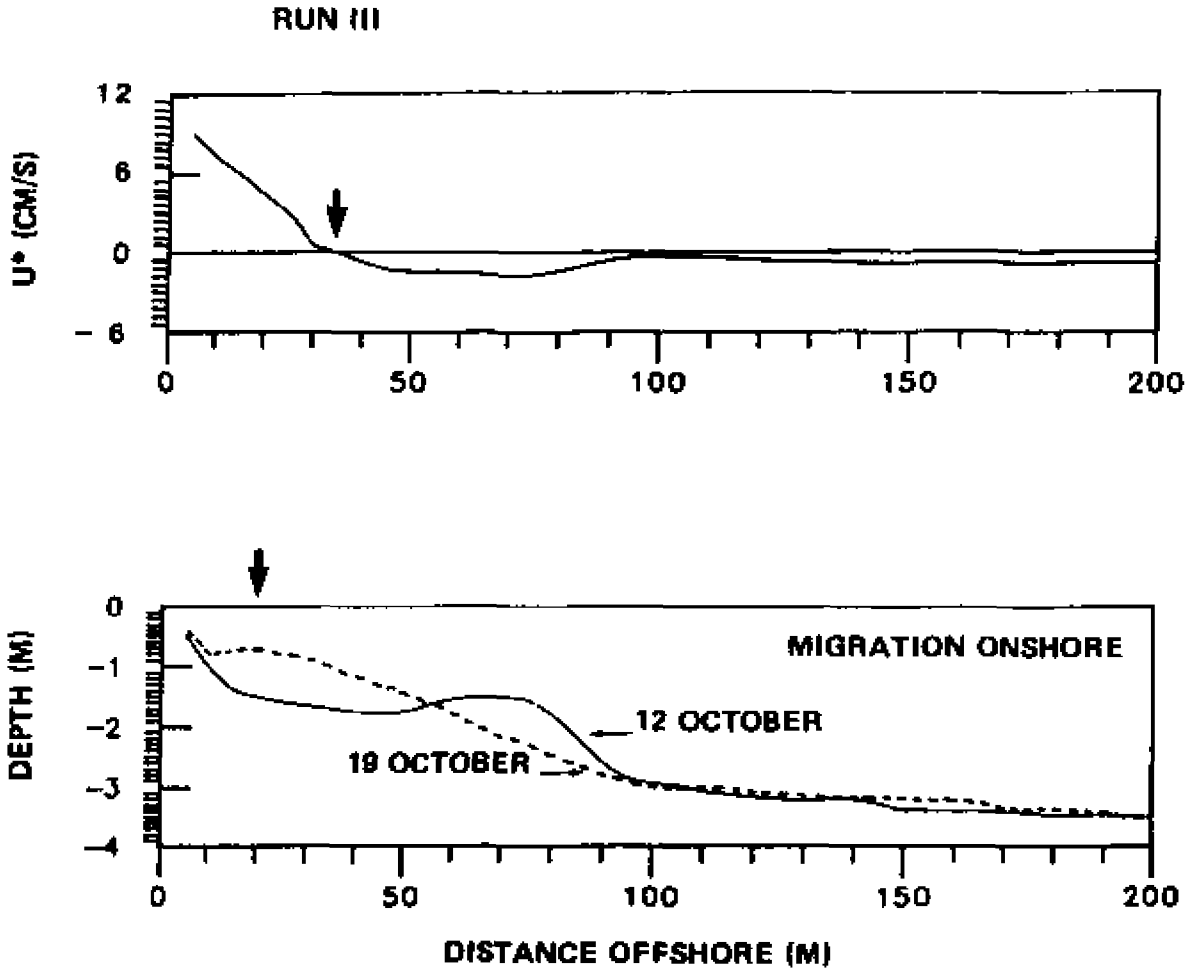

Figure 6.7: Results of running model for Run III (migration onshore), comparing the predicted node of friction velocity (+u*; offshore) and observed position of bar crest. (upper) Distribution of the friction velocity in the bottom boundary layer on 15 October when the storm was waning out. The node of the friction velocity was predicted at about 35 m offshore on 16 October; (lower) the initial profile (solid) on 12 October changed to the pre-storm profile by 19 October (dotted) showing bar crest migrated onshore. The predicted node of the friction velocity at about 35 m offshore on 16 October (upper) is consistent with observed trend of bar-crest movement shoreward, ending up at about 20 m offshore on 19 October.

Run IV: To support the predictability of the model for a persisting bar system, Run IV was selected. If we assume a steady wave condition on a given bar profile created by the given waves, we would expect no change in the bottom configuration. The first case of Run IV is given with a wave condition on 10 October assuming that this wave condition exerted steadily on the profile 10 October. The node of the friction velocity was predicted at around 40 m offshore which is the same with the location of bar crest observed on 10 October (Figure 6.8 a). In fact the wave condition of 10 October lasted until 11 October, and little change in bottom configuration was observed between 10-11 October, resulting a persisting bar system.

The second case of a persisting bar system is presented in Figure 6.8b. The wave condition on 12 October was assumed steadily to exert on the profile on a prominent bar system on 12 October. The friction velocity node for this case was observed at around 70 m offshore and the bar crest was also observed at the same location. The section with very weak velocity between 60-70 m offshore might yield a relatively flat bar crest as shown in the lower panel in Figure 6.8b, perhaps due to the friction velocities lower than the critical threshold velocity of the local sediments.

In summary the model predictions of the bar migration offshore or landward based on the position of the friction velocity node in the bottom boundary layer are consistent with the field observations. In such ways, the model provides unambiguously a mechanism of bar migration with an emphasis on the important role of the friction velocity in the bottom boundary layer induced by the mass transport velocity associated with the wave field superposed with incident waves and long waves at surf beat periods.

Figure 6.8: Results of running model for Run IV (persisting bar system), comparing predicted nodes of the friction velocity (+u*: offshore) and observed positions of bar crests (arrows).
(a) Running with wave condition on 10 October and profile on 10 October, assuming that the waves were in steady state. The predicted node of the friction velocity is coincident with the position of bar crest.
(b) Running with wave condition on 12 October and profile on 12 October, assuming that the storm was in the same intensity through the day. The predicted region of nil friction velocity is in a good agreement with the flat-top bar profile (lower).

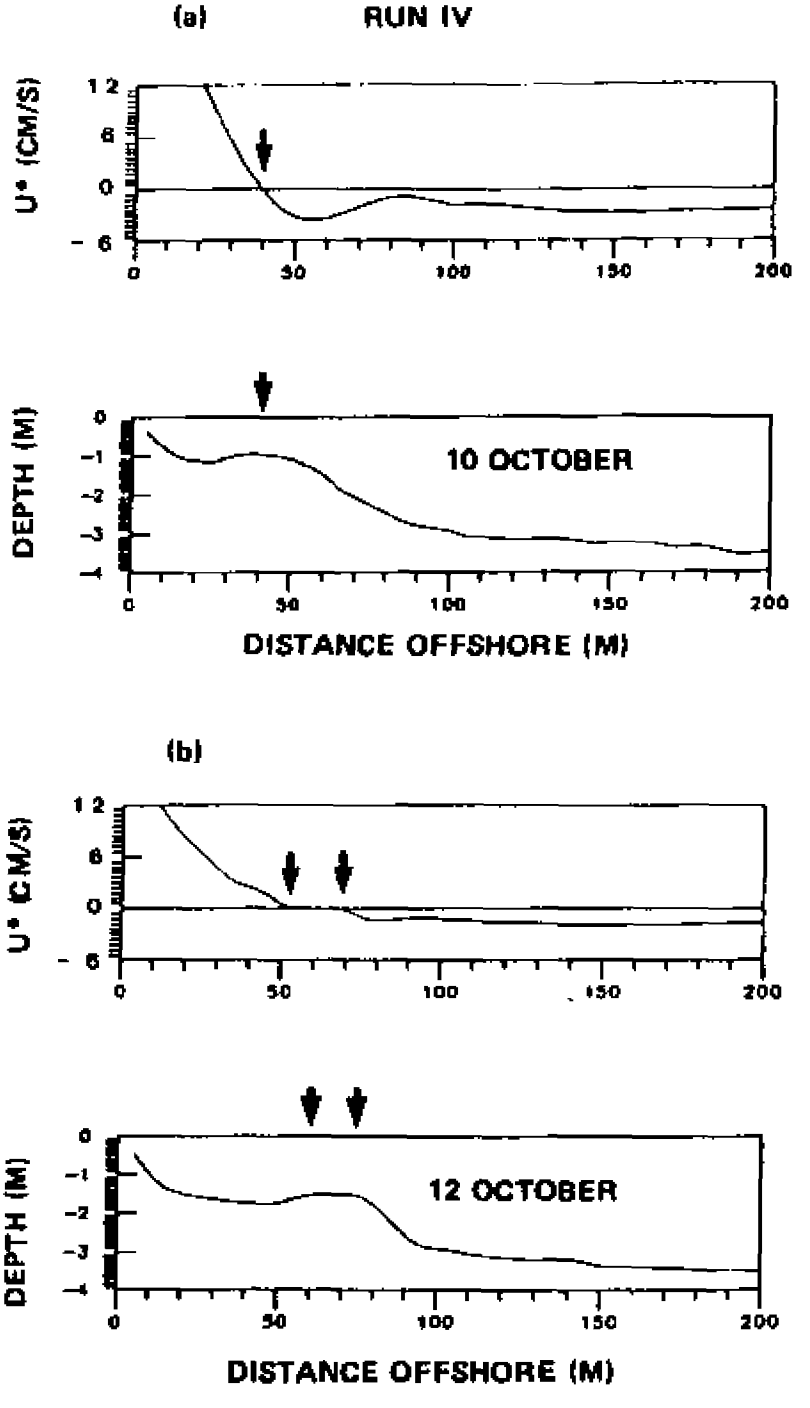
(a)
RUN IV
U* (CM/S)
12
6
0
-6
0
50
100
150
200
DEPTH (M)
0
-1
-2
-3
-4
10 OCTOBER
DISTANCE OFFSHORE (M)
(b)
U* (CM/S)
12
6
0
-6
0
50
100
150
200
DEPTH (M)
0
-1
-2
-3
-4
12 OCTOBER
DISTANCE OFFSHORE (M)

Also the model prediction is in excellent agreement with the case of persisting bar systems. The present study has examined a mechanism of bar migration that, until now, has not been considered formally. The model predicts characteristics of the mass transport velocity and the friction velocity node induced by a superposition of wind waves and long waves, and it has been verified with field observations, yielding an excellent agreement. In the present study, the long wave energy is not necessarily to be at a predominant frequency (Table 6.1), allowing a nearly-white energy spectrum consisting of multi-frequency. More important factor is turned out to be the energy level of waves rather than the presence of a predominant frequency. However some analyses on the same experiment such as the report by Sallenger and Holman (1987) postulate that there was no clear evidence for infragravity waves to form or force the offshore migration of nearshore bars, in which they simply sought the nodal position of infragravity waves with a predominant frequency colocating the position of a bar crest. The discrepancy between the present study and the analysis by Sallenger and Holman (1987) is discussed in the next section.

6.4 Discussion

By investigating the mass transport velocity in the bottom boundary layer due to the wave field combined with wind waves and long waves, it is attempted to compare the model results with field observed data. The observed wave conditions and geomorphologic configurations are divided into distinct groups according to the stages of storm (pre- , developing, fully developed and post- storm) and bar development (bar formation, migration offshore, migration onshore and persisting bar system). The basic assumptions are such that the observed wave parameters used as inputs in the model are steady until the next stage of storm, and the beach profiles are changing from procedent profile to a new one associated with varying wave conditions.

Based on the structure of the mass transport velocity in the bottom boundary layer, the present study makes use of the node of bed friction velocity to determine the position of the bar crest which is resulted from convergence of sediment transport. The structure of long waves are given by the frequency information of measured runup. With given frequencies, the positions of nodes and antinodes of standing waves are very sensitive to the beach slope as seen in Figure 2.1. Consequently the node of bed friction velocity in the bottom boundary layer is very sensitive to the beach slope as described in Chapter 4. The choice of an appropriate beach slope is not straightforward, particularly in natural beaches. The present study adopts the overall beach slope even on a barred topography. The overall beach slope is estimated by drawing a best-fitting line which follows the sloping trend from the foot of foreshore to the position where little change in vertical profile is expected. The foreshore slope at Duck is

approximated at 0.1, the slope at bar developing region is about 0.02 and the slope farther offshore is about 0.006 (Figure 6.3). As Holman and Sallenger (1985) noted, for low-frequency waves whose dynamics occur over a large scale, using the large-scale beach slope instead of using the foreshore slope seems reasonable to reduce the observed data scatter in their runup study. For low-frequency waves, the foreshore would act as a reflector rather than the bottom to be felt. Also long waves with wave length on the order of several hundred meters would feel the relatively steep slope around the bar as a small bump. Hence it seems sensible to use the overall beach slope which would determine the long wave structure over a complicated topography. In the present study, the overall slope in Figure 6.3 is estimated as about 0.01. The results obtained through the numerical investigationusing the estimated overall slope are in good agreement with the observed behavior of bar profiles during the different stage of the storm.

Many investigators have attempted to correlate the velocity nodes of standing waves with the positions of bar crests. The conventional approach is such that the velocity node of a long wave at a predominant frequency would fall over bar crest of a persisting bar system. Critical to the bar formation theories is the presence of a dominant infragravity wave at a discrete frequency (Sallenger and Holman, 1987). However in most field studies, the infragravity band has been found to be very broad (Guza and Thornton, 1982), consequently the nodes and antinodes of each frquency would float around the surf zone. It is not surprising to say that no bar would form under broad-band infragravity waves if one would try to match the bar position with nonexisting predominant node of infragravity wave as done in Sallenger and Holman (1987). At this point, we have two problems to be solved; One

is that under broad-band infragravity waves (e.g., Run II on 12 October in Table 6.1) more prominant bar system was observed; the other is that bar migration can not be explained by the conventional approach.

Being different from the classical approach, the present study allows us to incorporate the contributions of wind wave as well as of long waves. As seen in the earlier part of this Chapter, the more important factor to form a bar is the strength of the steady current induced by long waves rather than the presence of a predominant frequency. The node of bed friction velocity is given by the linear summation of component of each frequency including the wind waves. The present approach provides bar formation even under wide-band infragravity waves during storms, which is consistent with the field studies. Also this study provides the insight into the mechanism of bar migration during different stage of storm, and narrows down the gap between our understanding and field observation on this subject.

CHAPTER 7

SUMMARY AND CONCLUSIONS

The dynamics of nearshore processes are complicated due to the presence of the shoreline and variable topography, consequently due to the surf zone, wave deformation and bottom changes. The nearshore zone is a region of potentially important variability in hydrodynamic and geomorphologic processes, since this region is subject to major threats of storms such as erosion, flooding and property damage. For this reason, understanding and prediction of appropriate physical aspects of waves and their impact should be addressed.

On sloping beaches, it is clear from recent field studies that wave energy at frequencies much lower than incident waves takes a substantial part of total wave energy (e.g., Guza and Thornton, 1985). These low-frequency motions (infragravity waves), particularly with periods of 30 - 300 s (surf beat) increase their amplitude shoreward, eventually are reflected to form standing waves, while the incident waves which dominate the visible wave field are much steeper and therefore are dissipated by breaking rather than reflected.

In many locations where submarine bars are observed, some bar positions often remain reasonably fixed for extended periods of time while some bars migrate onshore during post-storm phase and offshore during storms with migration rate up to 2.1 m/hr (Sallenger et al., 1985). The dynamic aspects of bar migration shoreward or seaward suggest the importance of interaction between the response of loose bottoms and wave motion, which have direct implications for sediment tranport by means of erosion or deposition of sediment in the nearshore. Although many attempts have been made to link the possible role of infragravity

waves with the large scale geomorphologic features in the nearshore (e.g., for a review, Bowen and Huntley, 1984), the mechanism controlling longshore bar formation and migration are not well understood.

The present study has examined a possible mechanism for bar formation and migration during varying wave conditions, based on mass transport velocity in bottom boundary layer. A possible modification of long wave characteristics by the barred profile is also investigated. The forcing wave field in the present study is a superposition of incident wind waves and infragravity waves. Associated bed friction velocities are estimated at a bed of hydraulic roughness in the bottom boundary layer, while existing approaches consider mass transport velocities at the outer edge of boundary layer due to only infragravity waves. The numerical investigations have revealed an important influence of the incident wind waves in determining the positions of friction velocity nodes at which the bar crests would colocate.

The numerical approach was tested against the DUCK82 data and found to be in good agreement, lending credence to the present hypothesis.

The general problem of interaction of infragravity waves and nearshore geomorphologic features has been reviewed in Chapter 2. Previous observations of characteristics of long waves on sloping beaches, and their kinematics and generation mechanisms are presented. Basic concept of mass transport velocity consisting of Stokes drift and Eulerian streaming in the bottom boundary layer is addressed. Considering the temporal and spatial scales of nearshore geomorphologic features, it is clear that nearshore topographic responses are likely controlled by the drift velocity structure of long waves. However previous results are only as good as the assumptions upon which they are

based, and none of them provides the dynamic mechanism for bar migration under varying wave conditions.

Based on a knowledge of nearshore long waves and resultant mass transport velocity in the bottom boundary layer, Chapter 3 developed a simple model for initiation of bar formation. The wave field is modeled as a superposition of incident wind waves and long waves. The mass transport velocities of the model wave field are derived. The characteristic boundary layer due to these two waves at different frequencies shows how one component incorporates with the other (Figure 3.6). Numerical studies on sample cases show that the bottom flows are characterized by bidirectional flows; shoreward outside the surf zone and seaward well inside the surf zone. Strikingly, the position of convergence of two flows is determined by relative strength of mass transport velocities of wind waves and long waves, rather than by predicted velocity node of long wave itself. The intensity of mass transport velocity is sensitive to the beach slope as well as wave conditions. An apparent tendency of bar formation is on mild-slope beaches under moderately high wave energy (e.g., Ho > 1m on a beach of $\beta < 0.02$).

Chapter 4 examined the bar migration on a given barred-topography under varying wave conditions. Deepwater wave heights 0.3m, 1.0m and 2.0m and period 10s, and long wave period 50s, 75s and 100s were used for example calculations on a barred topography with an overall slope $\bar{\beta} = 0.02$. The bar crest was located at 100m offshore. The energy of long wave is assumed to be proportional to the wind wave energy according to Figure 3.7 which is due to Guza and Thornton (1985). For incident wave conditions with wave height less than 1.0m, the mass transport velocities over the bar crest directed shoreward and the

velocity nodes were predicted close to the shoreline, leading the bar to migrate onshore. Under these fair wave conditions, the bottom flow field is not very sensitive to long wave periods. When deepwater wind wave height is about 2.0m during a storm, the long wave period is important in determining the position of velocity node. The natural period of the bar system considered here was 75s. The velocity node predicted with long wave period 75s occurred at 80m offshore instead of the bar crest located 100m offshore at which a node of infragravity wave was expected. It should be pointed out that the offshore positions of the mass transport nodes are determined by relative strength of streaming velocities of wind waves and long waves rather than solely determined by the frequency of long wave and its nodal position. By increasing the long wave period to 100s, the mass transport velocities were directed offshore over the bar, implying a possible forcing for bar migration offshore. Generally there are enhanced bottom flows in the offshore direction over the bar when the long wave period is longer than the natural period of the bar system under a severe wave condition.

As a diagnostic parameter to determine the behavior of a bar under varying wave conditions, the bed friction velocity at a bed of hydraulic roughness (Section 4.3) was introduced. The sediment movement was assumed to follow the predicted magnitude and direction of the friction velocity, which seems to be reasonable for the mesoscale processes with time and space scales of hours and several tens of meter respectively. Figure 4.11 provides a comprehensive behavior of bar system under varying wave conditions, showing bar migration shoreward under fair wave conditions (Ho = 0.3 and 1.0m) regardless of long wave periods, and bar migration offshore under severe wave condition with long wave period 100s (solid line in Figure 4.11a). In chapter 6, the

model was tested against the field data and found to be good, lending credence to the present approach developed in Chapter 3 and Chapter 4.

Chapter 5 considered the influence of bar and bottom stress on modification of long waves. Being different from existing approaches in which the choice of beach slope at the onshore boundary is critical, the present study solved the shallow water-wave equation using the finite different scheme with boundary conditions such that the elevations at the onshore boundary and at the next grid point are the same with those on a plane beach. The increment between the grids was 5m which gave the accuracy within 1% of the analytically predicted solution. The long wave profiles on a barred topography show the trapping tendency toward the bar crest with amplitude amplification as noted by Kirby et al. (1981) and Symonds and Bowen (1984). This trapping of antinode over the bar would lead the existing bar system to persist over an extended time scale. When the long waves are of broad-band frequencies, the bar system will select a modal frequency (resonant response) when the bottom flow is very weak, or the bar will be forced to move by strongly interacting bottom flows.

Chapter 6 describes the field observations and some results of numerical tests against field data obtained during the DUCK82. The wave and bathymetric data were collected before, during and after a three-day storm which lasted for 10-12 October, 1982. On 10 October when the storm was developing, a predominant bar was developed at about 40m offshore, and the bar was stable at the position until 11 October. As the storm center moved east, high swells with long period approached the shore, moving the bar farther offshore at a rate of 1.4 m/hr. By 19 October, the prominant bar observed on 12 October was moved onshore, recovering a featureless profile as on 7 October. Using the profiles and wave conditions obtained during the storm as inputs, the numerical model

described in Chapter 4 was run for 4 different cases of wave and profiles (Figure 6.4). The long waves are of a single predominant frequency or broad-band frequencies. As noted in Chapter 4, this model can be run even for broad-band waves, which is an advantage over existing approaches. The numerical results were consistent with observed data for bar formation, migration offshore, migration onshore, and even for persisting bar system, lending credence to the present model - that the mass transport velocity in bottom boundary layer due to wind waves and long waves would determine the behavior of submarine bars.

Due to the lack of field evidence on long wave growth under very severe storms with height in excess of 3.0m, the model must be applied with caution or require an adjustment in long wave amplitude at the shoreline.

In the bottom boundary layer, the present study assumed that the lower-most layer was scaled to be merged into the oscillatory wave boundary, hence the effect of the very thin layer was treated as being forgotton for the rest of boundary layer considered here. The oscillatory boundary layer was assumed to pump up the bed materials into the steady-flow boundary layer, and the streaming velocity would carry those materials to its destination. At this point, it is not clear how the oscillatory boundary process at higher frequencies would interact with the steady-streaming flows at low frequencies. At least this problem would be important locally at a fixed position or instantaneously over short time scales, say, a couple of wind wave periods. This nonlinear and transient problem would require a time-dependent approach on the oscillatory boundary layer which is incorporated with the thicker boundary layer considered in this study.

This model can be extended to three dimensional cases by including alongshore variation in wave field and topography, or by

including effect of edge waves. Also it would be worthwhile to make a link the bed friction velocity estimated from the Eulerian streaming velocity with the sediment transport rate. A quantitative relation between these two aspects would give quantitative estimations of bottom change and sediment volume change associated with the profile change under varying wave conditions.

REFERENCES

Bagnold, R. A., Sand movement by waves: some small scale experiments with sand of very low density, J. Inst. Civ. Eng., 447-469, 1947.

Ball, F. K., Edge waves in an ocean of finite depth, Deep Sea Res., 14, 79-88, 1967.

Battjes, J. A., Surf similarity, Proc. 14th Coast. Conf., ASCE, 466-480, 1974.

Benjamin, T. B. and J. E. Feir, The disintegration of wave trians on deep water, Part 1. Theory, J. Fluid Mech., 27, 417-430, 1967.

Berkhoff, J. C. W., Mathematical models for simple harmonic linear water waves, wave diffraction and refraction, Publication No. 1963, Delft Hydraulics Lab., Delft, The Netherlands, 1976.

Bijker, E. W., J. P. Th. Kalkwijk and T. Pieters, Mass transport in gravity waves on a sloping bottom, Proc. 14th Coastal Conf., ASCE, 447-465, 1974.

Birkemeier, W. A., Time scales of nearshore profile changes, Proc. 19th Coast. Conf., ASCE, 1507-1521, 1984.

Birkemeier, W. A., N. C. Kraus, N. W. Scheffner and S. C. Knowles, Feasibitlity study of quantitative erosion models for use by the Federal Emergency Management Agency in the prediction of coastal flooding, Technical Report CERC-87-8, US Army Engineer Waterways Experiment Station, Coastal Engiennring Research Center, Vicksburg, Miss., 1987.

Bowen, A, J., On-offshore sand transport on a beach (abstract), Eos Trans. AGU., 56, 83, 1975.

Bowen, A. J., Simple models of nearshore sedimentation; Beach profiles and longshore bars; in The Coastline of Canada, S.B. McCann, editor; Geological Survey of Canada, paper 80-10, 1-11, 1980.

Bowen, A. J. and D. A. Huntley, Waves, long waves and nearshore morphology, Mar. Geology, 60, 1-13, 1984.

Bowen, A. J. and D. L. Inman, Rip currents.2, Laboratory and field observations, J. Geophys. Res., 74, 5479-5490, 1969.

Bowen, A. J. and D. L. Inman, Edge waves and crescentic bars, J. Geophys. Res., 76,8662-8671, 1971.

Bowen, A. J., D. L. Inman and V. P. Simmons, Wave 'set-down' and 'set-up', J. Geophys. Res., 73, 2569-2577, 1968.

Brebner, A., J. A. Askew and S. W. Law, The effect of roughness on the mass transport of progressive gravity waves, Proc. 10th Coast. Conf., ASCE, 175-184, 1966.

Carrier, G. F. and H. P. Greenspan, Water waves of finite amplitude on a sloping beach, J. Fluid. Mech. 4, 97-109, 1958.

Carter, T. G., P. L. Liu and C. C. Mei, Mass transport by waves and offshore sand bedforms, J. Waterways, Harbours, Coast. Eng. Div., ASCE, ww2, 165-184, 1973.

Christoffersen, J. B. and I. G. Jonsson, Bed friction and dissipation in a combined current and wave motion, Ocean Engng, 12, 387-423, 1985.

Collins, J. I., Effect of currents on mass transport of progressive water waves, J. Geophys. Res., 69, 1051-1056, 1964.

Dally, W. R., R. G. Dean and R. A. Dalrymple, Wave height variation across beaches of arbitrary profile, J. Geophys. Res., 90, 11917-11927, 1985.

Dean, R. G., Equilibrium beach profiles: U.S. Atlantic and Gulf Coasts. Dept. Civil Eng., Univ. Delaware, Newark, Delaware, Ocean Eng. Tech. Rept. 12, 46 pp, 1977.

Deguchi, I and T. Sawaragi, Calculation of the rate of net on-offshore sediment transport on the basis of flux concept, Proc. 19th. Conf. Coastal Eng., 1325-1341, ASCE, 1984.

Ebersole, B. A., M. A. Cialone and M. D. Prater, Regional coastal processes numerical modeling system, T.R.CERC-86-3, US Army Corps of Engineers, Vicksburg, Miss, pp 160, 1986.

Eckart, C., Surface waves in water of variable depth, Wave Rep.100, Scripps Inst. Oceanogr., Ref. 51-12, La Jolla, Calif., 1951.

Elgar, S. and R. T. Guza, Shoaling gravity waves: comparisons between field observations, linear theory, and a nonlinear model, J. Fluid Mech., 158, 47-70, 1985.

Gallagher, B., Generation of surf beat by non-linear wave interactions, J. Fluid Mech., 49, 1-20, 1971.

Grant, W. D. and O. S. Madsen, The continental-shelf bottom boundary layer, Ann. Rev. Fluid Mech., 18, 265-305, 1986.

Guza, R. T. and A. J. Bowen, Finite amplitude edge waves, J. Mar. Res., 34, 269-293, 1976.

Guza, R. T. and R. E. Davis, Excitation of edge waves by waves incident on a beach, J. Geophys. Res., 79, 1285-1291, 1974.

Guza, R. T. and D. L. Inman, Edge waves and beach cusps, J. Geophys. Res., 80, 2997-3012, 1975.

Guza, R. T. and E. B. Thornton, Swash oscillations on a natural beach, J. Geophys. Res., 87, 483-491, 1982.

Guza, R. T. and E. B. Thornton, Observations of surf beat, J. Geophys. Res., 90, 3161-3172, 1985.

Guza, R. T., E. B. Thornton and R. A. Holman, Swash on steep and shallow beaches, Proc. 19th Coastal Eng. Conf., 708-723, ASCE, 1984.

Holman, R. A. and A. J. Bowen, Edge waves on complex beach profile. J. Geophy. Res., 84, 6369-6346, 1979.

Holman, R. A. and A. J. Bowen, Bars, bumps and holes: Models for the generation of complex beach topography, J. Geophys. Res., 87, 457-468, 1982.

Holman, R. A. and A. H. Sallenger, Setup and swash on a natural beach, J. Geophys. Res., 90, 945-953, 1985.

Horikawa, K., Coastal sediment processes, Ann. Rev. Fluid Mech., 13, 9-32, 1981.

Hunt, J. N. and B. Johns, Currents produced by tides and gravity waves, Tellus, 15, 343-351, 1963.

Huntley, D. A., Long period waves on a natural beach, J. Geophys., Res., 81, 6441-6449, 1976.

Huntley, D. A., Edge waves in a crescentic bar system, in The coastline of Canada, S.B.McCann (ed), Geological survey of Canada, paper 80-10, 111-121, 1980.

Huntley D. A. and C. S. Kim, Is surf beat forced or free ?, Proc. 19th Coast. Conf., ASCE, 871-885, 1985.

Huntley, D. A., R. T. Guza and A. J. Bowen, A universal form for shoreline run-up spectra ?, J. Geophys. Res., 82, 2577-2581, 1977.

Johns, B., On the mass transport induced by oscillatory flow in a turbulent boundary layer, J. Fluid Mech., 43, 177-185, 1970.

Johnson, D. W., Shore processes and shoreline development, Hafner Publ. Co., pp 348-395, 1965.

Jonsson, I. G., Measurements in the turbulent wave boundary., Proc. 10th Congr. IAHR., London, 85-92, 1963.

Jonsson, I. G., A new approach to oscillatory rough turbulent boundary layers, Ocean Eng., 7, 109-152, 1980.

Kajiura, K., A model of the bottom boundary layer in water waves, Bull. Earthquake Res. Inst., Univ. Tokyo, 46, 75-123, 1968.

Keulegan, G. H., An experimental study of submarine sand bars, US Beach Erosion Board, Tech, Rept. 3, 1948.

Kim, C. S., Field observations of wave groups and long waves on sloping beaches, Master's Thesis, Dalhousie Univ., Halifax, Canada, pp151, 1985.

Kim, C. S.and D. A. Huntley, Long waves in the nearshore zone, Proc. of Can. Coastal Conf. 37-51, St.John's, NFDL, 1985.

King, C. A. M. and W. W. Williams, The formation and movement of sand bars by wave action, Geographical J., 113, 70-85, 1949.

Kirby, J. T., Jr., R. A. Dalrymple and P. L. F. Liu, Modification of edge waves by barred-beach topography. Coastal Engineering, 5, 35-49, 1981.

Komar, P. D., Beach processes and sedimentation, Prentice-Hall, Englewood, N.J., 429pp, 1976.

Komar, P. D., Selective grain entrainment by a current from a bed of mixed sizes: A reanalysis, J. Sed. Petrology, 57, 203-211, 1987.

Kostense, J. K., Measurements of surf beat and set-down beneath wave groups, Proc. 19th Coast. Conf., ASCE, 724-740, 1984.

Lau, J. and B. Travis, Slowly varying Stokes waves and submarine longshore bars, J. Geophys. Res., 78, 4489-4497, 1973.

Longuet-Higgins, M. S., Mass transport in water waves, Phil. Trans.of Roy. Soc. Lond. A, 245, 535-581, 1953.

Longuet-Higgins, M. S. and R. W. Stewart, Radiation stress and mass transport in gravity waves, with application to 'surf beat', J. Fluid Mech., 13, 481-504, 1962.

Longuet-Higgins, M. S. and R. W. Stewart, Radiation stresses in water waves, a physical discussion with applications, Deep SEa Res., 11, 529-562, 1964.

Mason, C., A. H. Sallenger, R. A. Holman and W. A. Birkemeier, DUCK82 - A coastal storm processes experiments, Proc. 19th Coast. Conf., ASCE, 1913-1928, 1984.

Miller, H. C., M. W. Leffler, W. E. Grogg,Jr., S. C. Wheeler and C. R. Townsend III, Annual data summary for 1982 CERC Field Research Vicksburg, Miss., 1984.

Munk, W. H., Surf beats. EOS, Trans. Am. Geophys. Union, 30, 849-854, 1949.

Murray, M., Control of grain dispersion by particle size and wave state, J. of Geology, 75, 612-634, 1967.

Noda, H., A study on mass transport in boundary layers in standng waves, Proc. 11th Coast. Conf., ASCE, 227-247, 1968.

Peregrine, D. H., Long waves on a beach, J. Fluid Mech., 27, 815-827, 1967.

Phillips, O. M., Dynamics of the upper ocean, Cambridge Univ. Press, N.Y., 336pp, 1966.

Richmond, B. M. and A. H. Sallenger, Jr., Cross-shore transport of bimodal sands, Proc. 19th Conf. Coastal Eng., 1997-2008, ASCE, 1984.

Russell, R. C. H. and J. D. C. Osorio, An experimental investigation of drift profiles in a closed channel, Proc. 6th Coast. Conf., ASCE, 171-193, 1957.

Sallenger, A. H. and R. A. Holman, Wave energy saturation on a natural beach of variable slope, J. Geophys. Res., 90, 11939-11944, 1985.

Sallenger, A. H. and R. A. Holman, Infragravity waves over a natural barred profile, J. Geophys. Res., 92, 9531-9540, 1987.

Sallenger, A. H., R. A. Holman and W.A.Birkemeier, Storm-induced response of a nearsore-bar system, Marine Geol., 64, 237-257, 1985.

Saylor, J. H. and E. B. Hands, Properties of longshore bars in the Great Lakes, Proc. 12th Coast. Conf., ASCE, 839-853, 1970.

Schlichting, H., Boundary-layer theory, McGraw-Hill, 817pp, 1979.

Shepard, F. P., Beach cycles in Southern California, US Army Corps of Engineers, Beach Erosion Board, Technical Memorandum 15, 32pp, 1950.

Short, A. D., Multiple offshore bars and standing waves, J. Geophys. Res., 80,3838-3840, 1975.

Sleath, J. F. A., Mass transport over a rough bed, J. Mar. Res., 32, 13-24, 1974.

Sleath, J. F. A., Sea bed mechanics, John Wiley, pp 335, 1984.

Suhayda,J. N., Standing waves on beaches, J. Geophys. Res.,79, 3065-3071, 1974.

Symonds, G., D. A. Huntley and A. J. Bowen, Two-dimensional surf beat: long wave generation by a time-varying breakpoint, J. Geophys. Res , 87, 492-498, 1982.

Symonds, G. and A. J. Bowen, Interactions of nearshore bars with incoming wave groups, J. Geophys. Res., 89, 1953-1959, 1984.

Trowbridge, J. and O. S. Madsen, Turbulent wave boundary layers, 2, Second- order theory and mass transport, J. Geophys. Res., 89, 7999-8007, 1984.

Tucker, M. J., Surf beat: Sea waves of 1 to 5 minutes period, Proc. R. Soc., A, 202, 565-573, 1950.

Ursell, F., Edge waves on a sloping beach, Proc. R. Soc., Series A, 214, 70-97, 1952.

Weggel, J. R., Maximum breaker height, J. of Waterways, Harbors and Coast. Engng. Div., 78, WW4, 529-548, 1972.

Whitford, D. J. and E. B. Thornton, Measuring wind and wave forcing of longshore currents during SuperDuck, Proc. ASCE Specialty Conf. on Coastal Hydrodynamics / ASCE, June 1987, Newark, DE., 589-602.

Whitham, G. B., Lectures on wave propagation, Springer for Tata Institute, Bombay, 1979.

Wright, L. D., Field observations of long-period, surf-zone standing waves in relation to contrasting beach morphologies, Aust. J. Mar. Freshwater Res., 33, 181-201, 1982.

Wright, L. D., P. Nielson, A. D. Short, F. C. Coffey and M. O. Green, Nearsore and surf zone morphodynamics of a storm wave environment: Eastern bass strait, Australia, Coastal studies unit tech. report No.82/3, The University of Sydney, Australia, pp 154, 1982.

Wright, L. D., S. K. May, A. D. Short and M. O. Green, Beach and surf zone equilibria and response times, Proc. 19th Coast. Conf., ASCE, 2150-2164, 1984.

Wright, L. D., P. Nielsen, N. C. Shi and J. H. List, Morphodynamics of a bar-trough surf zone, Marine Geology, 70, 251-285, 1986.

Yuen, H. C. and B. M. Lake, Instabilities of waves on deep water, Ann. Rev. of Fluid Mech., 12, 303-334, 1980.

Zenkovitch, V. P., On the study of shore dynamics, Akademiya nauk U.S.S.R., Institut Okeonologi, Trudy, 1, 99-112, 1946.

Zenkovich, V. P., Submarine sand bars and related formations, in Processes of Coastal Development, Interscience, pp219-236, 1967.

VITA

CHANG SHIK KIM

The author was born in Kyungbook, Korea, on 15 August, 1951. He grew up in Seoul, where he attended Seoul National University, receiving B.Sc. in Oceanography in 1974. After completing the military service in 1977, he worked with Korea Ocean Research & Development Institute / Korea Advanced Institute of Science and Technology, Seoul, until 1981 as a physical oceanographer. Earned M.Sc. in physical oceanography from Dalhousie University Halifax, Canada in 1985 and immediately entered doctoral program in College of William and Mary, School of Marine Science, Virginia, U.S.A.

Publications:

Refereed

Huntley, D. A. and C. S. Kim, 1984.
Is surf beat forced or free?. Proc. 19th International Coastal Engineering Conference, ASCE/ September 1984, Houston, TX, U.S.A., p871-885.

Kim, C. S. and D. A. Huntley, 1985.
Long waves in the nearshore zone, Proc. Canadian Coastal Conference, NRC Canada/ August 1985, St. Johns, Newfoundland, Canada, p37-51.

Kim, C. S. and D. A. Huntley, 1986.
On the time delays in the nearshore between onshore and longshore currents at incident wave frequencies, Journal of Geophysical Research, v91, p3967-3977.

Kim, C. S. and L. D. Wright, 1986.
Interaction of long waves and barred nearshore topography (abstract), EOS, p1026, Nov.,4, 1986.

Kim, C. S. and L. D. Wright, 1987.
Longshore bars and mass transport induced by long waves, Proc. of ASCE Specialty Conference on Coastal Hydrodynamics/ ASCE, June 1987, Newark, DE, (Robert A. Dalrymple, editor), p564-578.

Thesis

Kim, C. S., 1985.
Field observations of wave groups and long waves on sloping beaches, 151pp, Master's Thesis, Dalhousie University, Halifax, N.S., Canada.

Technical Report

Wright, L. D., C. S. Kim, C. S. Hardaway, S. M. Kimball, and M. O. Green, 1987.
Shoreface and beach dynamics of the coastal region from Cape Henry to False Cape, Virginia, Technical Report prepared for The Virginia Department of Conservation and Historic Resources by Virginia Institute of Marine Science, Gloucester Point, Virginia, 116pp.